FACULTEIT GENEESKUNDE EN GEZONDHEIDSWETENSCHAPPEN

UNIVERSITEIT GENT

Application of Optical Genome Mapping for detection of Structural Variants in Sarcomas

MASTERTHESIS

Jason Legein

Academic year: 2025 – 2026

Promotor: Prof. N. Van Roy
Co-promotor: Prof. K. Durinck
Mentor: Dr. S. Loontiens

Table of Contents

1. Abstract

Sarcomas are rare malignancies arising from connective tissues such as bone, muscle, and fat. Their genomic complexity makes accurate diagnosis challenging and currently requires a combination of histology and a combination of various molecular techniques like fluorescence in situ hybridization (FISH), copy number analysis, and RNA sequencing. Although effective, this multi-step workflow is time-consuming and fails to capture all structural variants in a single assay.

In this study, Optical Genome Mapping (OGM) using the Bionano Saphyr system was evaluated as an alternative molecular workflow. OGM was applied to rhabdomyosarcoma (RMS) cell lines and patient-derived tumoroids. In parallel, the workflow for extracting ultra-high molecular weight (UHMW) DNA from primary sarcoma tissue was optimized. The OGM results were subsequently benchmarked against standard cytogenomic techniques. UHMW DNA extraction from primary tumor samples remains challenging with success depending on tissue type, input mass, and dissociation method. Therefore, further testing and optimization steps are required before routine diagnostic implementation, including UHMW DNA extraction from frozen tissues sections, guidelines per tumor/cell type and further assessment of allowed time between tumor resection and sample freezing for optimal OGM results. In samples meeting quality thresholds, OGM showed clear diagnostic potential, where translocations, copy number variations and smaller structural variants could be identified in one molecular test. For instance, the rhabdomyosarcoma associated *PAX3::FOXO1* fusion was detected in both the RH30 cell line and a patient-derived tumoroid, while *CDK4* amplification and *CDKN2A* deletion were identified within the same assay. A malignant peripheral nerve sheath tumor (MPNST) showed a very complex genome, consistent with known tumor suppressor losses.

Overall, OGM offers a comprehensive, genome-wide view of structural variants in a single assay and represents a valuable complement to RNA sequencing in genomically complex sarcomas.

2. Societal impact

The main aim of this study was to evaluate whether the implementation of Optical Genome Mapping (OGM) could improve the current diagnostic workflow in sarcoma care. Accurate classification of sarcomas remains challenging, with diagnostic discrepancies reported in approximately 20–30% of cases, particularly upon expert review. Such misclassification may lead to delays or inappropriate treatment and can negatively impact patient outcomes. OGM offers a single, comprehensive overview of structural variants, which could make diagnostics faster, clearer, and more reliable. While this may seem like a technical improvement, its real impact lies in reducing uncertainty for patients and helping clinicians reach the right diagnosis earlier, which in turn can support better treatment decisions and improved outcomes.

On a broader level, integrating OGM into routine molecular diagnostics could also benefit the healthcare system as a whole. Patients with rare cancers like sarcomas often experience differences in diagnostic quality and access to advanced technologies. Making OGM part of standard practice could help reduce these inequalities by providing more consistent genomic information, while also lowering the need for repeated or unnecessary tests and supporting the selection of more targeted therapies. Over time, wider clinical use could yield larger and more consistent datasets, helping to refine diagnostic guidelines and support the development of new treatments. Successful implementation in sarcoma diagnostics could furthermore facilitate broader application of OGM to other solid tumors with similar diagnostic challenges.

This work primarily impacts molecular diagnostics in oncology, particularly sarcoma care. Key stakeholders include patients, clinicians, and molecular diagnostic laboratories, all of whom may benefit from faster, more accurate diagnostics.

3. Introduction

I. Clinical and Epidemiological Background of Sarcomas

Sarcomas are rare but clinically significant malignancies that originate from mesenchymal tissues, including bone, cartilage, fat, muscle, or connective tissue.[1] Although they account for less than 1% of adult cancers and roughly 15% of pediatric malignancies, their overall burden is considerable due to their aggressive biology, frequent occurrence in younger patients, and complex management.[2] In Europe, the age-standardized incidence of sarcomas is estimated at approximately 5 cases per 100,000 inhabitants per year, with the majority arising from soft tissue and visceral sites.[3] The biological heterogeneity of sarcomas can be partly explained by the mesenchymal origin of sarcomas and the stage at which malignant transformation occurs. Sarcomas may arise either from early mesenchymal stem cells that acquire multiple oncogenic hits (*Theory 1*) or from more committed progenitor cells that undergo malignant transformation after fewer, later events during differentiation (*Theory 2*) (**Figure 1**).[2]

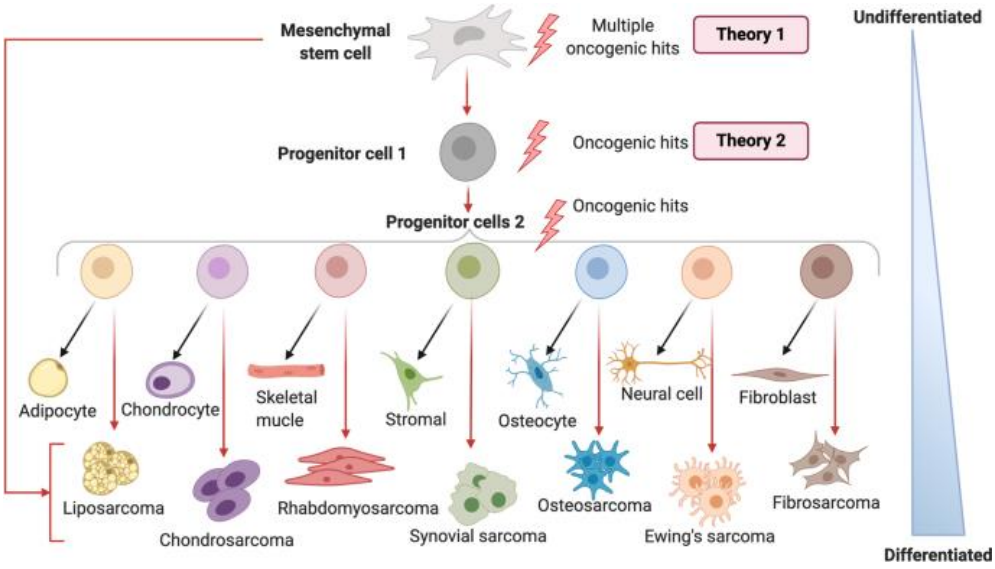

Figure 1. Mesenchymal Origin and Classification of Sarcoma Subtypes. *Sarcomas can arise from mesenchymal stem cells or from more differentiated progenitor cells following the accumulation of oncogenic events. The figure illustrates two proposed models of tumorigenesis: Theory 1, in which transformation occurs at the level of mesenchymal stem cells after multiple oncogenic hits, and Theory 2, in which transformation arises in more committed progenitor cells during differentiation. The diagram further shows the relationship between cell lineage and the development of specific sarcoma subtypes (e.g. liposarcoma, rhabdomyosarcoma, osteosarcoma). The vertical axis represents the degree of cellular differentiation, which is often associated with increasing genomic complexity (Adapted from [2]).*

Up to now, more than 70 distinct sarcoma subtypes have been recognized, each defined by unique histologic, immunohistochemical, and molecular features.[1] In adults, common subtypes include liposarcoma (well- and dedifferentiated), leiomyosarcoma, and osteosarcoma, whereas Ewing sarcoma and rhabdomyosarcoma are among the most prevalent entities in children and adolescents.[4] These tumors differ substantially in their biological behavior, metastatic potential, and treatment sensitivity.[1] Given this diversity, accurate classification is essential for guiding therapy and predicting patient outcomes.[4] Despite advances in sarcoma pathology, diagnostic uncertainty remains a significant challenge.

International guidelines, including those from ESMO-EURACAN-GENTURIS, emphasize the importance of diagnosis and treatment in specialized referral centers.[5] In Belgium, multidisciplinary expertise for the diagnosis and treatment of sarcomas is concentrated in academic hospitals, including Ghent, Antwerp, and Leuven. These centres provide specialised, multidisciplinary oncology care for these rare and complex tumors and are involved in national and European collaborative networks aimed at improving outcomes for patients with rare cancers.[5,6]

Despite advances in multimodal therapy, survival outcomes for sarcoma patients remain poor and are strongly determined by histologic subtype, anatomical location, and stage at diagnosis.[1,5] Overall, the 5-year survival for soft-tissue sarcomas is approximately 57%, with stage I and II patients showing a markedly favorable prognosis compared to stage III and IV patients, who achieve a median overall survival of 56 and 16 months, respectively.[7] Survival also differs considerably between subtypes: dermatofibrosarcoma shows 5-year survival rates up to 97%, whereas angiosarcoma has one of the worst prognoses at only 22%.[7] Localized Ewing sarcoma achieves survival rates near 70–75%, whereas metastatic disease remains largely incurable, with less than 30% of patients surviving past 5 years and relapsed patients facing a 5-year event-free survival of only 10%.[8] Aggressive entities such as leiomyosarcoma and undifferentiated pleomorphic sarcoma show similarly poor outcomes compared to low-grade subtypes.[1,5] Beyond subtype and stage, patient age at diagnosis is an important determinant of survival, with children and adolescents/young adults generally showing better outcomes than older adults across bone sarcoma subtypes, including osteosarcoma, chondrosarcoma, and Ewing sarcoma (**Figure 2**).[9]

Prognosis in sarcoma is determined by a combination of clinical and pathological factors. The most established predictors include tumor grade, size, anatomical location, and surgical margin status.[5] High-grade and large (>5 cm) tumors are associated with an increased risk of local recurrence and distant metastasis.[5] In addition, sarcomas arising from deep anatomical locations or complex locations, such as the retroperitoneum, generally carry a poorer outlook due to their challenging surgical removal.[10] Complete surgical resection with negative margins remains the single most important factor for long-term survival with localized disease.[11]

Beyond clinical parameters, molecular and immune features increasingly inform prognosis. Gene-expression signatures such as CINSARC, which reflect genomic complexity, have been associated with aggressive clinical behavior and increased metastatic risk.[12–14] Independently, characterization of the tumor immune microenvironment has emerged as a prognostic factor, with sarcomas showing high cytotoxic T-cell infiltration or tertiary lymphoid structures generally demonstrating more favorable outcomes.[15]

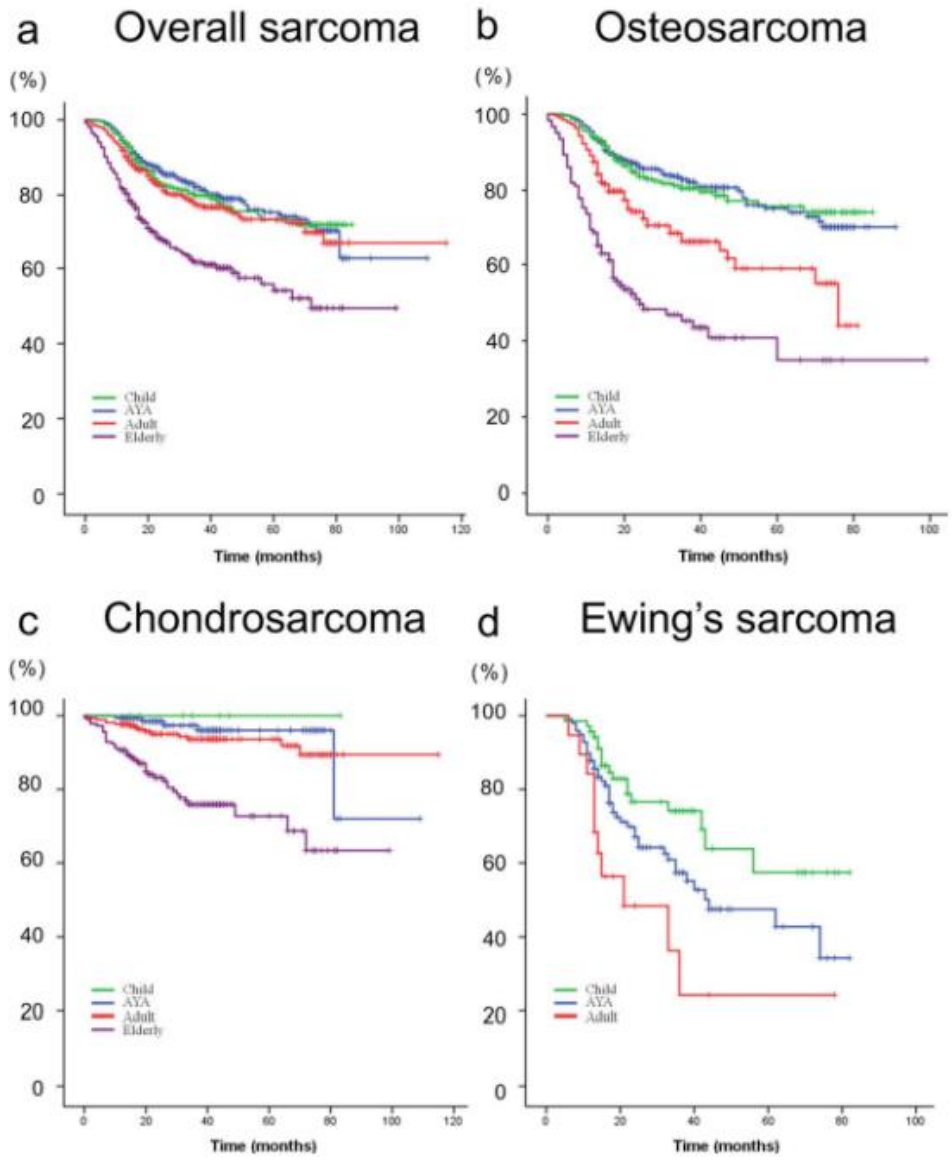

Figure 2. *Kaplan-Meier survival curves showing disease-specific survival for overall sarcoma (a), osteosarcoma (b), chondrosarcoma (c), and Ewing sarcoma (d), stratified by age. Child: ≤14 years, adolescent and young adult (AYA): 15-39 years, adult: 40-64 years, and elderly: ≥65 years (Adapted from [9]).*

II. Molecular classification of Sarcoma Subtypes

At the molecular level, sarcomas are broadly divided into fusion-driven and genomically complex types, reflecting fundamental differences in tumor biology, genomic stability, and clinical behaviour.[16] Fusion-driven sarcomas are genetically simple tumors defined by a single, recurrent chromosomal translocation that creates an oncogenic fusion gene, such as *EWSR1::FLI1* in Ewing sarcoma, *SS18::SSX* in synovial sarcoma, and *PAX3::FOXO1* in alveolar rhabdomyosarcoma.[2,16]

The PAX3::FOXO1 fusion is the key genetic driver in approximately 60% of cases of alveolar rhabdomyosarcoma (ARMS).[17,18] It arises from a recurrent chromosomal translocation, t(2;13)(q36.1;q14.11), which fuses the 5' region of *PAX3* on chromosome 2 with the 3' region of *FOXO1* on chromosome 13, resulting in a chimeric transcription factor that is not present in normal cells.[19] The oncogenic activity of this fusion protein is driven by the combination of the DNA-binding domains of *PAX3* with the potent transactivation domain of *FOXO1*, leading to a transcription factor with enhanced regulatory activity.[20] The resulting fusion protein retains the DNA-binding domains of *PAX3* while acquiring the transactivation domain of *FOXO1*, thereby altering its transcriptional function.[20] Once expressed, *PAX3::FOXO1* reprograms myogenic cells by activating genes involved in proliferation and invasion while inhibiting normal muscle differentiation pathways. This leads to the maintenance of an immature, highly proliferative cellular state and contributes to the aggressive clinical behavior of fusion-positive ARMS. The fusion protein can therefore be considered a key regulator of aberrant developmental programs in these tumors (**Figure 3**).[20]

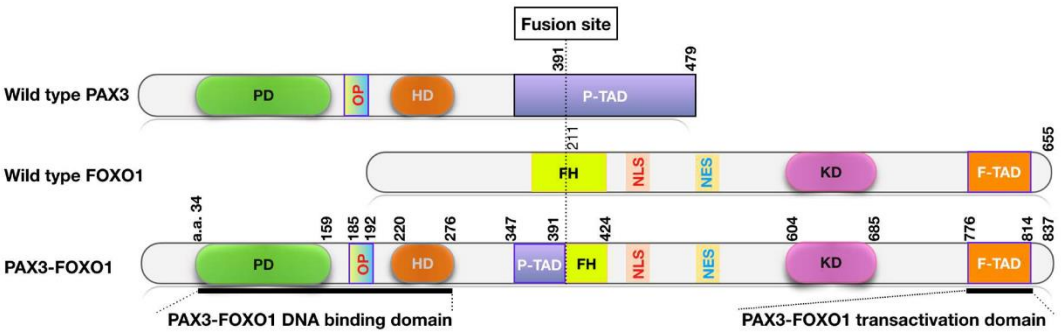

Figure 3. PAX3::FOXO1 fusion in alveolar rhabdomyosarcoma*. Schematic overview of the recurrent chromosomal translocation t(2;13)(q36.1;q14.11) that generated the oncogenic PAX3::FOXO1 fusion gene in alveolar rhabdomyosarcoma (ARMS). The figure illustrates the genomic organization of the wild-type PAX3 and FOXO1 genes and the resulting fusion protein after translocation, combining the DNA-binding domains of PAX3 with the potent transactivation domain of FOXO1. This chimeric transcription factor promotes tumorigenesis by dysregulating myogenic differentiation and enhancing cellular proliferation and invasion (Adapted from [17]).*

Because these rearrangements are highly specific, they serve as powerful diagnostic and sometimes prognostic biomarkers, and in some cases offer opportunities for targeted therapy.[16] For example, the *EWSR1::FLI1* fusion protein in Ewing sarcoma is currently being investigated as a therapeutic target, with research efforts focused on developing drugs that disrupt its function or downstream signaling pathways, although direct clinical translation remains challenging.[8] These therapeutic implications will be discussed further in a later section.

By contrast, genomically complex sarcomas such as osteosarcoma, leiomyosarcoma, undifferentiated pleomorphic sarcoma (UPS), and pleomorphic liposarcoma are characterized by extensive chromosomal instability, numerous copy-number alterations, and structural rearrangements. [2,16,21] This genomic complexity is frequently driven by the inactivation of key tumor suppressor genes, including *TP53* and *RB1*, and is often accompanied by catastrophic events such as chromothripsis, in which chromosomes undergo massive fragmentation and aberrant reassembly, contributing to ongoing genomic instability and intra-tumoral heterogeneity.[22–24] This molecular distinction has important diagnostic relevance and underpins the ongoing shift towards precision oncology in sarcoma care.[5] In summary, fusion-driven sarcomas are typically characterized by a single defining genetic event and a relatively low level of additional genomic alterations, whereas genomically complex sarcomas accumulate damage over time through defective DNA repair and chromosomal instability. This contrast underlies the broad biological and clinical diversity that makes sarcomas particularly challenging to classify and treat. [16,21]

III. Treatment of Sarcomas

Effective treatment of sarcomas requires close collaboration between multiple specialists, including surgeons, medical oncologists, radiologists, and pathologists. Due to their rarity and biological complexity, patients should ideally be managed in specialized centers by multidisciplinary teams (MDTs) experienced in sarcoma care.[5,25,26] Surgery remains the cornerstone of curative treatment for localized soft-tissue sarcomas, with the primary goal of achieving complete tumor resection with microscopically negative margins (R0).[25,27] Adequate surgical margins are a key determinant of local control and are strongly associated with improved clinical outcomes, although overall survival is also influenced by factors such as tumor grade, subtype, and metastatic spread.[27] However, wide margins are often difficult to achieve due to tumor size, anatomical location, or proximity to critical structures. In these cases, radiotherapy is frequently combined with surgery to improve local disease control. Radiotherapy plays an important adjunctive role, particularly in patients with large, high-grade, or deeply located tumors, and has been shown to significantly reduce the risk of local recurrence.[28,29] It may be administered either preoperatively or postoperatively. Preoperative radiotherapy is generally associated with better sparing of surrounding healthy tissues and reduced late toxicity, but carries a higher risk of wound-healing complications, whereas postoperative radiotherapy is typically used in cases with close or positive margins and is associated with increased long-term fibrosis and functional impairment. [28,30]

For patients with large, aggressive, or metastatic sarcomas, systemic therapy is often combined with local treatment. Conventional chemotherapy with anthracyclines, with or without ifosfamide, remains the standard first-line treatment for advanced disease, despite modest response rates.[25,31] In recent years, treatment strategies have increasingly shifted toward a more personalized approach guided by molecular tumor profiling, reflecting the growing influence of precision oncology in sarcoma management.[5]

Finally, immunotherapy and other molecularly targeted strategies are under active investigation. Although current evidence remains limited, these approaches highlight an ongoing transition away from a "one-size-fits-all" model toward tailored, biology-driven therapies. This shift is largely driven by the pronounced biological and immunological heterogeneity observed across sarcoma subtypes.

Sarcomas show substantial genomic and cellular heterogeneity that strongly influences their immune landscape and response to immunotherapy (**Figure 4**). Tumors with complex genomes, often characterized by extensive copy number alterations and structural variants, may exhibit more immunogenic features, including increased immune cell infiltration and activation of immune-related pathways. [15] However, many of these tumors still display an immunologically "cold" phenotype, and immune activation varies considerably between and within subtypes. In contrast, fusion-positive sarcomas, generally exhibit an "immune-cold" or immune-excluded microenvironment, characterized by limited T-cell infiltration and the presence of immunosuppressive mechanisms.[15] The figure further highlights how different therapeutic strategies are being explored to overcome these immune barriers, including modulation of the tumor microenvironment to convert immune-cold tumors into more immunogenic states, as well as antigen-directed approaches such as CAR-T cell therapy, T-cell receptor-based therapies, and cancer vaccines. [15]

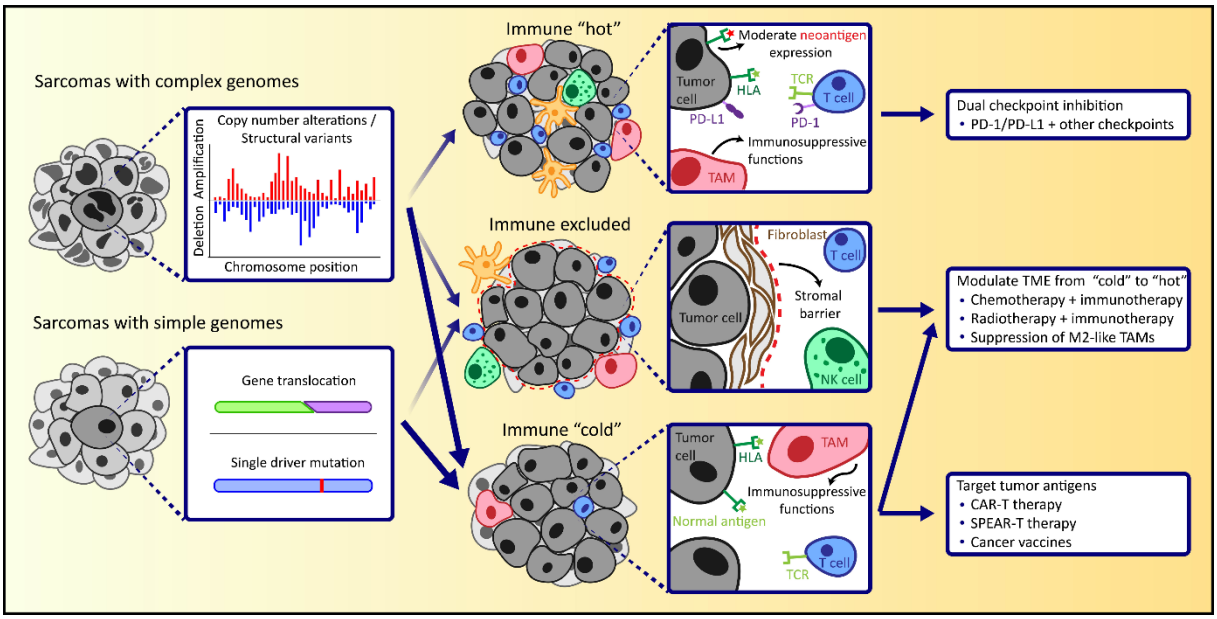

Figure 4. Genetic complexity shapes the immune microenvironment of sarcomas and guides therapeutic strategies. *Schematic overview showing how genomic complexity in sarcomas influences immune phenotypes ("hot", "excluded", and "cold"). Tumors with complex genomes are often associated with higher neoantigen load and T-cell infiltration, whereas simple-genome sarcomas tend to be immunologically "cold". These immune contexts inform therapeutic approaches, including checkpoint inhibition, combination strategies to convert "cold" to "hot" tumors, and antigen-targeted therapies (Adapted from [15]).*

Together, these observations underscore that immunotherapeutic efficacy in sarcomas is closely associated with underlying genomic features and the tumor microenvironment, rather than histological classification alone.

In addition to immunotherapy, targeted therapies are gaining importance, particularly in tumors driven by specific genetic alterations. One of the most established examples involves the use of tyrosine kinase inhibitors (TKIs) in sarcomas characterized by oncogenic fusions or activating mutations. Although the overall repertoire of effective targeted therapies in sarcomas remains relatively limited, TKIs have demonstrated clear clinical benefit in selected subtypes.[22] For instance, imatinib has shown remarkable efficacy in tumors harboring *COL1A1::PDGFB* rearrangements, such as dermatofibrosarcoma protuberans (DFSP), as well as in gastrointestinal stromal tumors (GIST) driven by *KIT* or *PDGFRA* mutations.[5,22] In addition, kinase gene fusions involving *ALK* or the *NTRK* gene family (*NTRK*1–3) represent critical oncogenic drivers across multiple sarcoma subtypes.[32] The development of highly selective *TRK* inhibitors, particularly larotrectinib, has enabled tumor-agnostic treatment strategies for patients with advanced NTRK-rearranged solid tumors, including sarcomas.[5,32]

In contrast to these fusion-driven tumors, genomically complex sarcomas often lack a single dominant driver but instead exhibit widespread chromosomal instability and recurrent copy number alterations.[2,21] In this context, amplifications of key cell cycle regulators such as *CDK4* and *MDM2*, particularly in well-differentiated and dedifferentiated liposarcomas, represent biologically relevant and potentially targetable alterations.[22,33] These alterations may create therapeutic vulnerabilities that can be explored using *CDK4/6* inhibitors (e.g., palbociclib) or *MDM2* inhibitors, although clinical efficacy remains variable and context-dependent.[22] For example, loss of the tumor suppressor *RB1* may confer resistance to *CDK4* inhibition, while alterations in *TP53* can limit the effectiveness of *MDM2*-targeted therapies.[34,35] This underscores the importance of comprehensive genomic profiling, as co-occurring structural alterations may critically influence therapeutic response.

IV. Current Diagnostic Workflow

Imaging plays a central role in both diagnosis and staging.[5] For extremity and trunk lesions, magnetic resonance imaging (MRI) is preferred for its superior soft-tissue contrast and ability to define tumor relationships to neurovascular and fascial structures.[5,36] Computed tomography (CT) is typically used for retroperitoneal or visceral sarcomas or when MRI is contraindicated [5]. A CT scan of the chest is recommended as part of standard staging, as the lungs represent the most common site of metastases.[7,37] Although PET-CT is not routinely recommended, it can be useful in selected cases, for example to clarify inconclusive findings or to help identify the most metabolically active areas for biopsy.[5,36]

Once imaging suggests the possibility of sarcoma, tissue sampling becomes critical. Core-needle biopsy is the standard method for tissue sampling, providing sufficient material for histopathology and molecular analysis while minimizing contamination of surrounding structures.[18] If core biopsy results are inconclusive, an incisional biopsy may be performed, whereas excisional biopsy is reserved for small, superficial, and easily resectable tumors.[18]

In recent years, molecular testing has become an increasingly essential component of sarcoma pathology. In fusion-driven sarcomas (e.g., *EWSR1::FLI1* in Ewing sarcoma, *SS18::SSX* in synovial sarcoma), detection of recurrent gene rearrangements provides diagnostic confirmation. Methods such as FISH and RNA sequencing for fusion detection are routinely applied.[38] For genomically complex sarcomas, detection of copy-number alterations through FISH or CNV sequencing (e.g., *MDM2* amplification in well- and dedifferentiated liposarcoma) can serve as an important diagnostic marker. In addition, advanced molecular profiling using broad DNA NGS panels is increasingly employed to identify diagnostic and prognostic markers in fusion-negative or genomically complex sarcomas, such as mutations in *TP53*, *RB1*, and *ATRX*.[39] These approaches align with the principles of precision oncology, guiding both diagnosis and potential targeted therapies. Finally, all diagnostic data must be reviewed by a multidisciplinary sarcoma team. This collaborative approach ensures diagnostic accuracy, appropriate staging, and optimal treatment planning.[5]

V. Conventional Cytogenetic and Molecular Techniques

The diagnosis of sarcomas currently relies on a combination of conventional cytogenetic and molecular methods. Each technique offers unique strengths but also important limitations, making it difficult to capture the full genomic complexity of these tumors (**Table 1**). Historically, karyotyping has long served as the cornerstone of cytogenetic diagnostics, offering a genome-wide overview of large chromosomal abnormalities, including translocations, deletions, duplications, and aneuploidy, at a relatively low resolution of approximately 5–10 Mb. The technique is relatively cost-effective, with indicative costs ranging from €100-380 per sample, and a turnaround time of approximately 7-21 days from sample to result.[40] Its main limitation includes the requirement for viable, dividing cells and a restricted sensitivity for detection of smaller structural variants. These constraints are particularly problematic in solid tumors such as sarcomas, where necrosis and low mitotic indices are common, and where successful analysis depends heavily on access to fresh tissue and cell culture conditions.[2,41,42] As a result, the routine use of karyotyping in sarcoma diagnostics has steadily declined in favor of higher-resolution molecular techniques.

Among these, fluorescence in situ hybridization (FISH) remains a valuable targeted approach in sarcoma diagnostics, particularly for confirming known gene rearrangements such as the *EWSR1::FLI1* fusion resulting from the t(11;22)(q24;q12) translocation in Ewing sarcoma, or the *SS18::SSX* fusion associated with the t(X;18)(p11;q11) translocation in synovial sarcoma. With a typical resolution of approximately 100 kb, FISH enables the detection of gene amplifications, deletions, and translocations, but only within predefined genomic regions. The technique is relatively rapid, with a turnaround time of approximately 1–3 days, and has an indicative cost of €200–400 per target.[43] In addition, FISH can be applied to interphase nuclei and formalin-fixed, paraffin-embedded (FFPE) tissue samples, making it broadly applicable in routine diagnostics. Nevertheless, because FISH requires prior knowledge of the target locus, it cannot detect novel or complex rearrangements outside its probe set, offering only a partial view of the tumor its genomic architecture.[44] Therefore, although FISH remains highly useful for specific diagnostic purposes, it does not provide a comprehensive assessment of the tumor genome. Moreover, the type of FISH assay used determines how much information can be obtained. Break-apart FISH probes can confirm that a genomic rearrangement has occurred at a specific locus, but they do not identify the fusion partner. In contrast, fusion-specific (dual-color, dual-fusion) FISH probes can detect a known recurrent fusion and its partner gene, but only when the exact fusion is already suspected. Break-apart probes generate a split signal in the presence of a rearrangement, whereas fusion-specific probes produce a combined signal only when a predefined gene fusion is present (**Figure 5**). As a result, both methods are inherently limited: break-apart FISH lacks partner resolution, and fusion-specific FISH cannot detect novel or atypical rearrangements.[44–46]

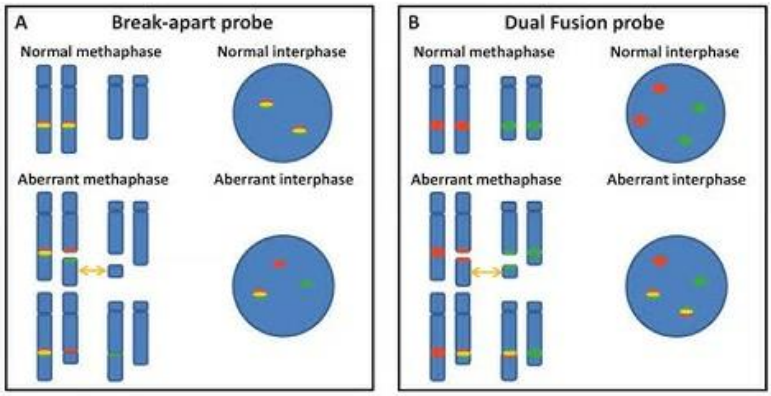

***Figure 5. Schematic overview of break-apart and fusion-specific FISH assays**. Break-apart FISH probes target regions flanking a gene of interest and generate a split fluorescent signal when a genomic rearrangement occurs at that locus, without identifying the fusion partner. In contrast, fusion-specific (dual-color, dual-fusion) FISH probes are designed to detect a known gene fusion by producing a combined signal when two predefined gene regions are brought together through a chromosomal translocation. While break-apart probes allow detection of unknown rearrangements at a given locus, fusion-specific probes are limited to the identification of known and expected fusion events (Adapted from [46]).*

In addition, genome-wide copy number profiling using SNP arrays or shallow whole genome sequencing (sWGS) has improved the detection of chromosomal gains, losses, and oncogenic amplifications in sarcomas with complex karyotypes.[47] However, CNV-based assays cannot detect balanced structural variants such as inversions or reciprocal translocations, as these do not result in changes in DNA copy number. This limitation is particularly relevant in fusion-driven sarcomas, where balanced rearrangements often represent the key oncogenic event.[16]

Furthermore, CNV-based techniques, as well as Optical Genome Mapping (OGM), rely on bulk DNA analysis and therefore require a sufficient tumor cell fraction typically around 20%, to reliably detect genomic alterations. In contrast, techniques such as FISH and karyotyping enable analysis at the single-cell level, allowing the detection of subclonal alterations even in samples with low tumor cellularity.[42]

In parallel, RNA sequencing has emerged as an important tool in sarcoma diagnostics, particularly for the detection of gene fusions. In routine clinical practice, targeted RNA sequencing panels are most commonly used, focusing on a predefined set of genes of interest. These assays enable sensitive detection of gene fusions and splice variants, which are key diagnostic features in many sarcoma subtypes.[48] While whole-transcriptome RNA sequencing can provide a more comprehensive view of the transcriptome, including gene expression changes and novel fusion events, it is less commonly applied in routine diagnostics due to higher costs, longer turnaround times, and increased data complexity.[45] In addition, interpretation of gene expression data in a diagnostic setting remains challenging due to the lack of standardized reference frameworks. Despite their advantages, RNA-based approaches are restricted to actively transcribed alterations and may fail to identify structural variants that are not expressed at the RNA level. Furthermore, RNA degradation in formalin-fixed, paraffin-embedded (FFPE) samples can significantly compromise assay sensitivity and reproducibility.[49]

In addition to genome-wide copy number profiling, short-read DNA next-generation sequencing (NGS) is widely used in molecular diagnostics for the detection of sequence-level alterations such as single-nucleotide variants and small insertions or deletions.[50] In routine clinical practice, this is typically performed using targeted gene panels rather than whole-genome sequencing, as accurate mutation detection requires substantially higher sequencing depth.[51] While shallow whole-genome sequencing (sWGS) is sufficient for copy number analysis at low coverage, reliable detection of somatic mutations generally requires deep sequencing, often exceeding 300x coverage.[52] As a result, whole-genome sequencing is not routinely applied for mutation detection in diagnostic settings.[52] Targeted short-read DNA NGS therefore represents a practical and cost-effective approach for identifying clinically relevant mutations.[53] However, this approach is inherently limited to predefined genomic regions and has reduced sensitivity for detecting balanced or complex structural variants, particularly in repetitive regions or when breakpoint architecture is intricate.[45]

Taken together, the technical characteristics that are summarized illustrate why no single conventional diagnostic method is sufficient to capture the genomic heterogeneity of sarcomas (**Table 1**). As a result, diagnosis often requires a multimodal workflow combining FISH, CNV analysis, and RNA sequencing.[2,47] While effective, this multiplatform strategy increases diagnostic cost, lengthens turnaround time, and fragments genomic data across different assays.

METHOD	RESOLUTION	DETECTABLE ALTERATIONS	LIMITATIONS	COST (€)	TURNAROUND TIME
Karyotyping (classical)	~5–10 Mb	Large structural abnormalities (translocations, deletions, duplications, aneuploidy)	Low resolution; requires dividing cells	100–380	7–21 days
FISH	~100 kb	Gene amplifications, deletions, translocations (targeted regions)	Limited to predefined loci	200–400 per target	1–3 days
SNP array/sWGS	~50 kb – 1 Mb	Copy number alterations, aneuploidy	Cannot detect balanced SVs (e.g. inversions, reciprocal translocations)	200–500	3–7 days
Targeted DNA NGS (gene panels)	~1 bp	SNVs, indels, selected CNVs; limited structural variant detection	Restricted to predefined regions; reduced sensitivity for complex/balanced SVs	300–600	1–2 weeks
Optical Genome Mapping (OGM)	~5 kb (practical)	Large and medium SVs (insertions, deletions, inversions, translocations), CNVs, aneuploidy	Cannot detect SNVs/indels; requires sufficient tumor fraction (~20%)	400–800	4–5 days
RNA sequencing (targeted/whole transcriptome)	~1 bp (transcript level)	Gene fusions, splice variants, gene expression, expressed SVs	Limited to expressed alterations; sensitive to RNA quality (e.g. FFPE degradation)	600–1200	1–2 weeks

Table 1. Overview of genomic techniques used in sarcoma diagnostics. *Comparison of commonly used cytogenetic and molecular methods, including their resolution, types of detectable genomic alterations, key limitations, approximate costs, and turnaround times. The table highlights complementary strengths of each technique in detecting copy number alterations, sequence variants, and structural variants (Adapted from [40,41,48,49,51]).*

Given the fundamental differences in genomic architecture, diagnostic approaches that can comprehensively detect both balanced and unbalanced SVs across the genome are essential. Optical Genome Mapping (OGM) has recently emerged as a powerful complementary approach that addresses many of these gaps. By analyzing ultra-high molecular weight DNA molecules, OGM generates unbiased, genome-wide maps capable of detecting translocations, inversions, insertions, deletions, and complex rearrangements with high resolution. Recent studies in both soft-tissue and bone sarcomas demonstrate that OGM can uncover genomic complexity overlooked by conventional assays, refining tumor classification and optimizing the diagnostic workflow.[3] As such, OGM represents a critical bridge between traditional cytogenetic methods and the true genomic diversity observed in sarcomas, paving the way for more accurate and comprehensive molecular diagnostics.

VI. Optical Genome Mapping: Principles and Applications

Optical Genome Mapping (OGM) represents a transformative technology for detecting structural variants (SVs), addressing many of the limitations of conventional cytogenetic and sequencing-based methods. This rapidly advancing approach enables high-resolution, genome-wide identification of SVs in an unbiased manner, offering particular promise for the characterization of complex malignancies such as sarcomas.[33]

The principle of OGM lies in the direct visualization of ultra-long DNA molecules, rather than sequencing their nucleotide composition.[37] The process begins with the isolation of ultra-high molecular weight (UHMW) DNA (N50 > 250 kbp) from fresh or cryopreserved tissue samples. The quality, length, and integrity of these DNA molecules are critical for accurate detection of large genomic rearrangements.

After isolation, DNA is labeled using Direct Labeling Enzyme (DLE-1). Fluorescent markers are enzymatically incorporated at specific six-base recognition motifs (CTTAAG) throughout the genome by the DLE-1 enzyme. These motifs occur approximately 14–17 times per 100 kbp, producing a unique sequence-specific labeling pattern along each molecule.[33] The labeled DNA is then linearized and imaged within nanochannels on the Bionano Saphyr platform. Electrophoretic flow guides each molecule through micro- and nanostructured channels, stretching it uniformly to prevent folding or entanglement. A high-resolution camera captures the fluorescent signal pattern, which is subsequently converted into digital genome maps. These maps are then aligned to a reference genome (e.g., GRCh38), and deviations in the labeling pattern or spacing reveal the presence of structural variants (**Figure 6**).[3] Representative examples of insertions, deletions, inversions, and repeat expansions as detected by Optical Genome Mapping (**Figure 7**).[37]

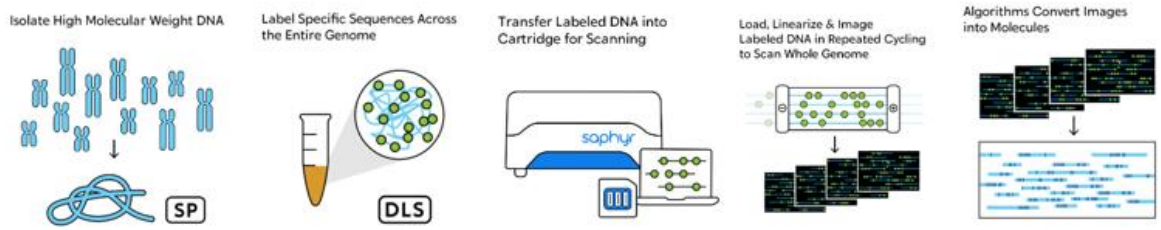

Figure 6. The 5-step process of OGM (Bionano Genomics. (n.d.). *How Optical Genome Mapping (OGM) works (Retrieved November 3, 2025, from [55]).*

By directly visualizing long DNA molecules, OGM can detect a wide spectrum of large-scale genomic alterations, including translocations, inversions, deletions, duplications, and complex rearrangements, at a resolution typically above 500 bp, which far exceeds that of conventional karyotyping (~5–10 Mb).[33,37] Because OGM examines the physical structure of DNA rather than relying on targeted probes or PCR amplification, it allows unbiased, genome-wide analysis of both known and novel SVs.

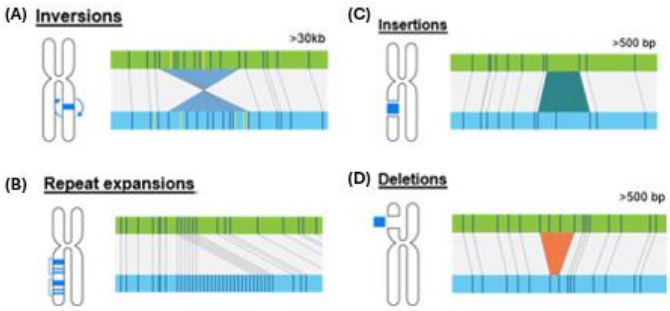

***Figure 7. Overview of the different alterations that can be detected by OGM**. (A) Inversion detection; (B) Repeat expansion detection; (C) Insertion detection and (D) Deletion detection (Adapted from [55]).*

VII. Implementation of OGM in Solid Tumors and Sarcomas

Optical Genome Mapping (OGM) has emerged as a reliable tool for detecting structural variants (SVs) in cancer, demonstrating concordance with conventional cytogenetic techniques often exceeding 95% in hematologic malignancies.[14] Its growing implementation in Belgium reflects the increasing clinical adoption. Building on this success, OGM shows strong potential in solid tumors, where genomic landscapes are frequently more complex. Early studies in breast, lung, and brain cancers indicate that OGM can detect clinically relevant SVs often missed by standard assays, suggesting improved diagnostic accuracy, refined prognostic assessment, and the identification of novel therapeutic targets.[54] In sarcomas, OGM has been applied to a diverse set of soft-tissue and bone subtypes, including Ewing sarcoma, synovial sarcoma, myxoid and dedifferentiated liposarcoma, solitary fibrous tumor, CIC-rearranged sarcoma, dermatofibrosarcoma protuberans, osteosarcoma, and other small round cell or undifferentiated sarcomas.[3,33] Extracting ultra-high molecular weight (UHMW) DNA from sarcoma tissues requires adaptations to standard protocols, particularly for bone- and fat-rich tumors such as osteosarcomas and liposarcomas, which necessitate specialized extraction kits and optimized homogenization steps. OGM is also compatible with cryopreserved tissues and snap-frozen cell pellets, making these suitable starting materials.

Clinical validation studies in sarcomas demonstrate that OGM provides high diagnostic concordance while revealing additional genomic complexity (**Table 2**). In one study, 91% of diagnostic SVs in 35 sarcoma cases were correctly identified, with missed variants mainly due to tumor heterogeneity, small inversions, or repetitive regions.[3] A second study confirmed a 97% detection rate for defining aberrations, with limitations caused by low tumor cellularity or challenging tissue types rather than technical failure.[33] Beyond identifying translocations, deletions, amplifications, and inversions, OGM also uncovered complex rearrangements such as chromoplexy and chromothripsis, and facilitated diagnostic refinement by detecting rare fusions, e.g., *POU2AF3::EWSR1*.[3]

Together, these findings highlight that OGM not only demonstrates comparable accuracy to conventional cytogenetics but also enhances the detection of previously unrecognized structural variants, enabling improved molecular subclassification, more precise treatment selection, and potential identification of novel therapeutic targets. Its integration into routine diagnostics promises a more comprehensive, biology-driven approach to sarcoma management.

Study	Total samples	Evaluable samples	Sarcoma subtypes included	Diagnostic concordance with standard-of-care	Missed diagnostic aberrations	Additional findings by OGM
Baelen et al., 2024	53	38 (72%)	20 subtypes (e.g. Ewing sarcoma, synovial sarcoma, myxoid and dedifferentiated liposarcoma, solitary fibrous tumor, osteosarcoma	32/35 cases concordant with standard-of-care cytogenetics (91%)	*CIC::DUX4* fusion; small inversion generating *STAT6::NAB2*; heterogeneous MDM2 amplification	Chromoplexy (5 cases), chromothripsis (9 cases), additional complex SVs and CNAs
Berenguer-Rubio et al., 2025	53	33 (62.3%)	Adipocytic, non-adipocytic, bone sarcomas, small round cell sarcomas, sarcomas of uncertain differentiation	97% detection of expected diagnostic alterations	*COL6A3::CSF1* fusion (malignant tenosynovial giant cell tumor) likely due to low tumor cell fraction	Additional SVs and CNAs detected by de novo analysis; increased structural complexity

Table 2. *Overview of published studies evaluating the analytical performance of Optical Genome Mapping (OGM) in soft-tissue and bone sarcomas, including diagnostic concordance with standard-of-care cytogenetic methods and additional structural findings (Adapted from [3,33]).*

VIII. Limitations and Complementary Approaches

Despite its strong potential, Optical Genome Mapping (OGM) still has several limitations that must be addressed before it can be fully implemented in clinical diagnostics. Recognizing these challenges is essential for defining how the technology can be best applied and further optimized.

A primary limitation concerns sample quality. OGM requires the extraction of ultra-high molecular weight (UHMW) DNA, which can only be obtained from fresh or frozen tissue. This poses a major obstacle, as most clinical specimens are routinely preserved as formalin-fixed, paraffin-embedded (FFPE) blocks, in which DNA is fragmented and chemically crosslinked, rendering it unsuitable for OGM analysis.[37]

In addition, tumor purity plays a critical role. As OGM is a bulk DNA-based technique, it does not provide single-cell resolution, and therefore requires a sufficient proportion of tumor cells typically at least 10–20%, to reliably detect somatic and subclonal variants. Samples with low tumor cellularity may fail to reveal clinically relevant alterations, reducing analytical sensitivity.[33]

Furthermore, the requirement for UHMW DNA places strict demands on sample collection and handling. Rapid and appropriate processing of tissue, including timely freezing, is essential to preserve DNA integrity. This introduces logistical challenges in routine diagnostics, as fresh or cryopreserved material must be obtained at the time of biopsy or surgery. In contrast to FFPE-based workflows, where tissue can be histologically evaluated by a pathologist prior to molecular testing, the use of fresh or frozen samples limits the ability to preselect tumor-rich regions, potentially affecting downstream analysis.[3,33]

OGM also has several technical blind spots. While it excels at identifying large structural variants, it cannot detect small mutations such as single-nucleotide variants (SNVs) or small insertions and deletions (indels), as it does not provide nucleotide-level sequence information.[37] In addition, breakpoint resolution is inherently limited, as OGM is based on a label-derived pattern rather than base-pair–level sequencing. For this reason, OGM should be complemented with sequencing-based methods to achieve comprehensive genomic profiling.[37] Furthermore, copy number analysis by OGM is inherently relative, which may complicate the detection of genome-wide copy number changes, such as whole-genome duplication events.[33] Although the clinical impact of this limitation may vary, it represents an important consideration when interpreting OGM data. Finally, highly repetitive regions of the genome, including centromeres and telomeres, remain challenging to resolve and may harbor undetected rearrangements.[37]

Another limitation involves cost and throughput. Although recent advances have improved efficiency and affordability, OGM remains more expensive and less high-throughput than targeted assays such as FISH or NGS panels.[14,33] This is partly due to platform-specific constraints, as the Bionano Saphyr system typically allows the processing of only a limited number of samples per run, with approximately three samples per chip and up to six samples per run. While newer platforms such as the Stratys system offer increased throughput, overall sample capacity remains lower compared to sequencing-based approaches. However, when compared with a combined diagnostic workflow integrating FISH, CNV profiling, and RNA sequencing to achieve comparable genomic coverage, overall costs may be similar. Its cost-effectiveness for routine diagnostics will need to be confirmed in larger clinical validation studies.

For these reasons, OGM should be considered a complementary rather than a replacement technology. A combined workflow integrating OGM with DNA and RNA sequencing currently provides a comprehensive genomic characterization.[3,37] While whole-genome sequencing (WGS) offers the most complete assessment of sequence-level variation, targeted DNA panels are often sufficient for mutation analysis in routine clinical practice and are more cost-effective. OGM excels in detecting large and complex structural alterations, whereas DNA sequencing identifies smaller sequence-level variants. In addition, RNA sequencing provides important complementary information by enabling the detection of expressed gene fusions and splice variants. While OGM can identify underlying structural rearrangements such as translocations, it does not always allow precise determination of the resulting fusion transcript, nor whether the rearrangement leads to an actively expressed fusion gene. RNA sequencing therefore plays a crucial role in confirming the functional relevance of structural variants at the transcript level. Together, these methods enable an integrated, high-resolution view of the tumor genome, with the choice of sequencing strategy tailored to the clinical context.[37]

IX. Aims of Current Study

The preceding chapters highlight two key insights: the need for improved genomic profiling in sarcomas and the potential of Optical Genome Mapping (OGM) to address current diagnostic limitations. This study aims to bridge the gap between the theoretical advantages of OGM and its practical implementation in clinical diagnostics.
This project is structured into four work packages that together evaluate the feasibility, performance, and clinical value of OGM in sarcoma diagnostics. The central research question is whether OGM can serve as a robust and reliable technique for detecting structural variants in sarcomas and improve upon existing diagnostic approaches.

The first work package focuses on DNA extraction and optimization, aiming to establish a standardized and reproducible workflow for isolating ultra-high molecular weight (UHMW) DNA from fresh and cryopreserved sarcoma samples (WP1). Given the technical challenges associated with solid tumor material, particular attention is paid to sample handling, DNA quality control, and protocol optimization. The second work package evaluates the diagnostic performance of OGM by comparing its ability to detect structural variants with conventional techniques such as FISH and CNV-based assays (WP2). This includes assessing concordance, sensitivity, and the detection of known genomic alterations. The third work package investigates the added clinical value of OGM by identifying additional or complex structural variants not detected by standard methods and correlating these findings with histopathological and clinical data (WP3). Finally, the fourth work package assesses the feasibility of implementing OGM in routine diagnostics, including evaluation of turnaround time, technical success rate, workflow integration, and potential bottlenecks (WP4). Together, these work packages (**Figure 8**) provide a comprehensive framework to evaluate the role of OGM within the existing diagnostic pathway of the UZ Ghent sarcoma program, with the ultimate goal of improving diagnostic accuracy, prognostic stratification, and therapeutic decision-making.

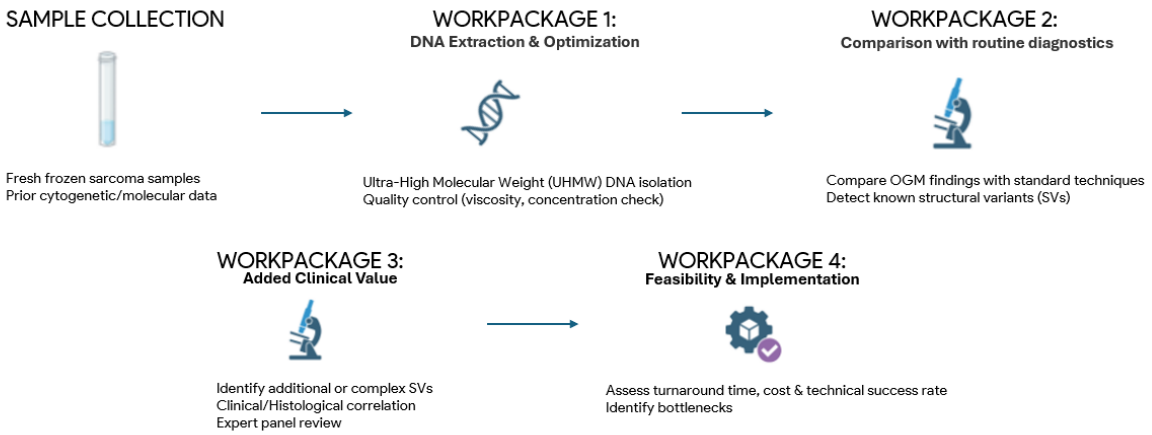

Figure 8. Overview of the study design and work packages. *Schematic representation of the study workflow, including sample collection and 4 work packages: (1) DNA extraction and quality optimization for ultra-high molecular weight DNA, (2) comparison of Optical Genome Mapping (OGM) with routine diagnostic techniques, (3) assessment of additional clinical value through identification of complex structural variants and clinical correlation, and (4) evaluation of feasibility and implementation, including turnaround time, cost, and technical performance.*

4. Material & Methods

I. RMS Cell Culture and Cryopreservation

Human rhabdomyosarcoma (RMS) cell lines (RH30, RH41, RMS-YM) were used in this study. An overview of their clinical, morphological, and molecular characteristics is provided in **Table 3**.

Cells were harvested during the logarithmic growth phase, ensuring a cell viability of at least 70%. The cell concentration was determined using a Luna II automated cell counter (10 µL sample volume). Based on the calculated cell concentration, the required volume of cell suspension was determined using the internal Freezing Cell Pellets Excel template to achieve a final concentration of 1.5 x 10^6 cells/mL. Cells were transferred to pre-labeled 1.5 mL Eppendorf tubes and centrifuged for 5 min at 500x g at 4°C. The supernatant was discarded, and the cell pellets were resuspended in 1 mL of cold Stabilization Buffer per tube. After gentle mixing, the tubes were centrifuged again for 2 min at 2,200x g at 4°C. The supernatant was carefully removed using a P1000 pipette, followed by removal of residual liquid with a P200 pipette.
Finally, the cell pellets were snap-frozen on dry ice for 5 minutes and subsequently stored at −80°C until ultra-high molecular weight (UHMW) DNA extraction for Optical Genome Mapping (OGM). Each sample was registered in the SMAPLE database, and a new aliquot identifier was assigned.

Cell line	Type	Age	Sex	Morphology	Primary/metastatic	Mutations	Post-treatment
RH30	Rhabdomyosarcoma	17y	M	Alveolar	Metastatic	Myogenin, fusion positive (PAX3-FOXO1 translocation), FGFR4/FGF8 overexpression	
RH41	Rhabdomyosarcoma	7y	F	Alveolar	Metastatic	t(2;13), TP53 mutation, FGFR4/FGF8 overexpression	After chemo
RMS-YM	Rhabdomyosarcoma	2y	M	Embryonal	Abdominal mass	Multiple chromosomal rearrangements, upregulation of MDM2, FGFR1	

Table 3. *Clinical and genomic characteristics of the rhabdomyosarcoma cell lines (RH30, RH41 & RMS-YM) included in this study.*

II. Patient-derived rhabdomyosarcoma tumoroids

Tumoroids are three-dimensional cellular structures that are generated by dissociating tumor tissue obtained from a patient. Because of their 3D organization, tumoroids mimic the behavior and characteristics of the original tumor more accurately than conventional two-dimensional cell cultures. This makes them a valuable in vitro model for studying pediatric sarcomas. In the PPOL lab, three rhabdomyosarcoma tumoroids were established and two were received from the Memorial Sloan Kettering (MSK) Cancer Center. Three were fusion-positive (FP-RMS) and two were fusion-negative (FN-RMS). Interestingly, fusion-negative (FN) rhabdomyosarcomas consistently showed adherent growth (2/2), whereas fusion-positive (FP) rhabdomyosarcomas mainly formed true spheroidal structures (2/3). The biological explanation for this difference is currently unknown. However, a research group in Australia with extensive experience in tumoroid cultures has reported similar findings, suggesting that this observation is reproducible.

One of the major challenges in pediatric oncology research is the limited amount of tumor tissue available. In children, tumor samples are usually obtained through small needle biopsies, which provide only a minimal amount of starting material. To obtain enough tissue for downstream analyses, the tumor fragments are first implanted into immunocompromised mice to establish a patient-derived xenograft (PDX) model. The timing and origin of the starting material differed between the samples. PEDSAR01 and PEDSAR03 were established from frozen tumor fragments, whereas for PEDSAR02 only 45 minutes elapsed between biopsy collection and implantation into the mice. Once the tumor in the mouse reaches a volume of approximately 500 mm^3, it is passaged into a new mouse. Although ethical regulations allow tumor growth up to 1500–2000 mm^3, earlier passaging is preferred to minimize the development of necrotic tissue. During passaging, the tumor is divided into small fragments and re-implanted into a new mouse generation (generation 2, generation 3, etc.). Part of the tumor tissue is simultaneously dissociated to generate tumoroids.

So far, attempts to establish tumoroids directly from frozen tumor tissue have been unsuccessful, indicating that fresh PDX-derived material is essential for successful initiation. The main challenge lies in maintaining these cultures long term. Adherent tumoroids are relatively easy to culture and are typically passaged once they reach 80–100% confluency. In contrast, spheroidal tumoroids are more difficult to manage, as splitting them too early can impair their ability to continue growing. Within the scope of this thesis, the tumoroids were not used for functional experiments; instead, they were analyzed using Optical Genome Mapping (OGM). In total, 5 rhabdomyosarcoma (RMS) tumoroid lines were available for characterization. Three were fusion-positive (FP-RMS) and two were fusion-negative (FN-RMS). Their characteristics are summarized below (**Table 4**).

PEDSAR01 was derived from an 18-year-old male patient with FP-RMS. Genomic analysis identified two *KMT2A* point mutations (p.A1278V and p.P3577L, both with a variant allele frequency of 0.12) as well as a frameshift insertion/deletion mutation (p.S1277fs). PEDSAR02 originated from a 16-year-old male patient with FP-RMS and was mainly characterized by trisomy 21. PEDSAR03, derived from a 14-year-old female patient with FP-RMS, did not show any specifically reported genomic alterations. MSKPED0023 is an FN-RMS tumoroid line derived from a male patient. This sample harbored two KMT2A mutations (K1364Nfs*14 and E1363D) together with an *RBM10* P245L mutation. MSKPED0087, derived from a female patient with FN-RMS, contained several notable mutations, including *NRAS* Q61L, *ALK* V1058L, *ATR* L692I, *INSR* R813Q, and *TET1* N688S.

Tumoroid name	Age patient	Gender	Type of RMS	Selected genomic events
PEDSAR01	18	M	FP-RMS	*KMT2A* mutations (p.A1278V, VAF 0.12; p.P3577L, VAF 0.12) and frameshift insertion/deletion p.S1277fs
PEDSAR02	16	M	FP-RMS	Trisomy 21
PEDSAR03	14	F	FP-RMS	Not specified
MSKPED0023	-	M	FN-RMS	*KMT2A* K1364Nfs*14, *KMT2A* E1363D, *RBM10* P245L
MSKPED0087	-	F-	FN-RMS	*NRAS Q61L, ALK V1058L, ATR L692I, INSR R813Q, TET1 N688S*

Table 4. *Overview of the rhabdomyosarcoma (RMS) tumoroid models, including patient age and sex, fusion status (FP-RMS vs. FN-RMS), and key genomic events identified in each model.*

III. Optical Genome Mapping (OGM)

i. Sample Collection & Ethics

Sarcoma samples used in this study consisted of diagnostic residual material. Tumor tissue was routinely received at the Centre for Medical Genetics Ghent for standard diagnostic workup, including CNV sequencing. When sufficient material remained after completion of the routine diagnostic workflow, a fragment was set aside to evaluate the OGM workflow. Ethical approval for the use of residual diagnostic material was obtained from the Ghent University Hospital Ethics Committee.

ii. Tissue Preparation

For each included case, a fragment of tumor tissue was snap-frozen and stored at −80 °C when sufficient diagnostic residual material remained after the routine diagnostic workflow. These frozen tissue fragments served as starting material for the different experimental setups tested in this study, including bulk frozen tissue and cryosections. Bulk frozen tissue was directly subjected to UHMW DNA extraction. Different tissue input amounts were tested to determine the minimum mass required for successful extraction (see Results, **Table 7**).

For the cryosection-based approach, tumor cell percentage was first determined by a pathologist on a hematoxylin and eosin (H&E)-stained reference slide to confirm sufficient tumor content prior to cryosectioning. Tumor tissue was subsequently embedded in OCT compound (Tissue-Tek) on a pre-cooled cryobar and sectioned on a cryostat with the specimen chamber set at −19 °C and the cryobar at approximately −26 °C. A first 50 µm section was discarded to remove surface OCT, after which 10 sections of 20 µm were collected per sample for UHMW DNA extraction. Sections were transferred directly into a pre-cooled 1.5 mL Eppendorf tube using cooled forceps and immediately placed on dry ice to preserve molecular weight. All instruments and surfaces in contact with the tissue were kept cold throughout, and forceps were decontaminated between samples through a NaOH–water–ethanol cleaning series.

In an initial comparison, bulk frozen tissue yielded sufficient DNA for downstream OGM analysis, whereas cryosections did not. However, as this comparison was performed only once, no definitive conclusions can be drawn, and further replication would be required before excluding cryosections as a viable input format.

iii. Ultra-High Molecular Weight (UHMW) DNA Extraction

Two different extraction protocols were applied depending on the sample type. For RMS cell lines and patient-derived tumoroids, UHMW DNA was extracted from cell pellets (1.5×10^6 cells /pellet) using the Bionano Prep SP Frozen Cell Pellet DNA Isolation Kit (**ADDENDUM L**) according to the manufacturer's protocol.[55] For primary sarcoma tissue samples, UHMW DNA was extracted using the Bionano Prep SP Tissue and Tumor DNA Isolation Kit (**ADDENDUM M**) according to the manufacturer's protocol, with optimizations specific to sarcoma tissue as described below.[55]

Different tissue dissociation methods were systematically evaluated to identify the conditions most compatible with UHMW DNA preservation in primary sarcoma tissue. The following approaches were tested: (i) manual pestle-based mechanical disruption (3 min), (ii) automated processing with a tissue lyser using sequential frequency steps from 15 Hz to 30 Hz (total duration approximately 4 min), and (iii) a tissue ruptor, which allows shorter and more controlled mechanical processing. In addition, the impact of post-dissociation filtration was assessed by processing tissue in parallel with and without a 40 µm cell strainer. A detailed overview of the conditions tested and their performance is provided in the Results section (**Table 7**).

iv. Direct Labeling and Staining (DLS) of UHMW DNA

UHMW DNA was labeled using the Direct Label and Stain (DLS) G2-chemistry. Fluorescent tags were enzymatically incorporated at specific CTTAAG motifs via the DLE-1 enzyme, generating a unique label pattern along each DNA molecule at a density of approximately 14–17 labels per 100 kbp. After labeling, DNA was stained for backbone visualization. The protocol included the following steps: aliquoting of gDNA, preparation of the Green Label Master Mix, DLE-1 incubation (1 h at 37°C), Proteinase K digestion (30 min at 50°C), dye removal (1 h), and staining with homogenization (30 min). Light exposure was minimized throughout to protect fluorescent molecules. The labeled DNA concentration was quantified using the Qubit Fluorometer, with a target concentration of 4–16 ng/µL required for downstream genome imaging. Sample homogeneity was confirmed by duplicate measurements, with a coefficient of variation (CV) below 0.30 considered acceptable. (**ADDENDUM N**).

v. Genome Imaging

Labeled and stained DNA was loaded onto Bionano Saphyr chips and imaged using the Bionano Saphyr system. Electrophoretic flow guided individual DNA molecules through nanochannels, linearizing them for high-resolution fluorescence imaging. The resulting fluorescent label patterns were digitized and used for genome map assembly.

vi. Data Analysis

Data analysis was performed using Bionano Access and Bionano Solve software using the Guided Assembly (rare variant) pipeline.[55] Genome maps were assembled de novo and aligned to the human reference genome (GRCh38). Structural variants were identified based on deviations in fluorescent label spacing or pattern relative to the reference, including translocations, inversions, deletions, duplications, insertions, and complex rearrangements. Copy number variants were identified through coverage analysis using the integrated CNV pipeline within Bionano Solve.

Run quality was assessed using seven standard Bionano metrics. Molecule N50 (≥ 150 kbp) reflects the length distribution of the imaged ultra-high molecular weight DNA molecules and is reported in kilobase pairs (kbp); longer molecules enable more reliable detection of large structural variants, with a recommended threshold of ≥ 250 kbp. The N50 (≥ 20 kbp) provides a complementary measure of overall DNA integrity by including shorter fragments alongside the UHMW molecules, with a recommended threshold of > 150 kbp; substantially lower values indicate the presence of a large fraction of degraded DNA and negatively affect downstream mapping. Label density indicates the average number of DLE-1 fluorescent labels per 100 kbp of DNA and determines the resolution of the resulting genome map; values between 14 and 17 labels per 100 kbp are considered optimal, as both under- and over-labeling reduce mapping accuracy. Map rate represents the fraction of molecules that could be successfully aligned to the reference genome (GRCh38) and should exceed 70%; lower values typically reflect DNA fragmentation, suboptimal labeling, or insufficient molecule integrity. Effective coverage corresponds to the average sequencing depth across the genome and should reach at least 300x to ensure reliable variant calling, particularly for subclonal events. Finally, two label variance metrics describe the accuracy of the labeling pattern relative to the reference: the positive label variance (PLV) represents the percentage of labels present in the molecules but absent in the reference and should remain below 10%, while the negative label variance (NLV) represents the percentage of reference labels missing from the molecules and should remain below 15%; elevated values typically point to suboptimal labeling efficiency. Samples not meeting these thresholds were flagged as suboptimal and the corresponding variant calls were interpreted with caution.

To distinguish high-confidence somatic variants from background noise and germline polymorphisms, a multi-step filtering strategy was applied. First, a variant allele frequency (VAF) threshold was used. The RMS cell lines RH30, RH41, and RMS-YM showed extensive subclonal copy number and structural heterogeneity, with many low-VAF calls likely representing late-arising subclonal alterations or technical background rather than the dominant tumor clone. To focus the analysis on the major clonal events, a stricter cutoff of VAF ≥ 0.40 was applied. In contrast, patient-derived tumoroids and primary sarcoma tissue samples were analyzed using a lower threshold of VAF ≥ 0.10. This lower cutoff was deliberately chosen to preserve biologically relevant intra-tumoral heterogeneity and to account for the mixed cellular composition of primary tumor material, which contains stromal, vascular, and immune cells in addition to tumor cells. Second, a minimum molecule support threshold of more than five molecules was required for a structural variant to be retained, ensuring that reported events were supported by sufficient independent DNA molecules. For translocations, a minimum of 10 molecules was required to limit the risk of false-positive calls. Third, variants present in the Bionano rare variant control database of healthy individuals were filtered out to exclude common germline polymorphisms and technical artefacts. Only variants passing all three criteria were considered for downstream interpretation.

To prioritize variants with potential diagnostic or biological relevance, both copy number variant (CNV) and structural variant (SV) calls were filtered against a custom cancer-related gene panel compiled specifically for this study. This panel was constructed using two clinical NGS panels currently implemented at the Centre for Medical Genetics Ghent. The first source was the DNA NGS SOLID TUMOR panel (112 genes), routinely used for the detection of clinically relevant somatic mutations in solid tumors and sarcomas, including oncogenes and tumor suppressor genes with established diagnostic, prognostic, or therapeutic significance. The second source was the RNA NGS PANCANCER Fusion Panel (175 genes), which targets genes recurrently involved in fusion events associated with solid tumors, including well-known fusion partners such as *EWSR1*, *SS18*, *FUS*, and *PAX3*/*PAX7*. Altogether, the final custom cancer-related gene panel consisted of 260 genes (**ADDENDUM A**).

The downstream analysis followed a workflow adapted to the type of structural variant. First, genome-wide CNV analysis was performed, after which only CNVs overlapping genes from the cancer-related gene panel were retained for further evaluation. These retained CNVs were manually curated to confirm true copy number events and to annotate the involvement of clinically relevant genes. Genome-wide translocation analysis was subsequently performed, with all retained translocations manually reviewed to exclude false-positive calls and to assess the involvement of known fusion partners or sarcoma-associated genes. Finally, other structural variants, including deletions, insertions, duplications, and inversions detected at the default size thresholds of the Rare Variant Pipeline, were evaluated. Variants overlapping genes from the cancer-related panel were retained and each event was individually reviewed for potential diagnostic or biological relevance.

IV. FISH – Fluorescence in situ hybridization

Fluorescence in situ hybridization (FISH) was performed on rhabdomyosarcoma cell lines and patient-derived tumoroids following the validated clinical protocol of the Centre for Medical Genetics Ghent. A *FOXO1* break-apart probe was used to assess the presence of *FOXO1* rearrangements, which are diagnostic for fusion-positive rhabdomyosarcoma. Break-apart probes consist of two differentially labeled fluorescent probes flanking the *FOXO1* locus on chromosome 13q14. In the absence of a rearrangement, the two signals remain in close proximity and appear as a fused (co-localized) signal. When a translocation disrupts the *FOXO1* locus, the two probes are physically separated, producing a clearly split signal pattern that indicates a *FOXO1* rearrangement.

Prior to hybridization, slides were pre-treated by fixation in a methanol/acetic acid mixture (3:1) for 5 minutes under agitation, followed by enzymatic digestion with 0.05% pepsin in 0.01 M HCl at 37 °C for 30 minutes to improve probe accessibility by removing surrounding proteins. Slides were then rinsed in 1× PBS, post-fixed in PBS containing $MgCl_2$ for 5 minutes, followed by fixation in 1% formaldehyde buffer for 10 minutes, and washed again in PBS. Subsequently, slides were dehydrated through a graded ethanol series (70%, 90%, 95%) for 3 minutes each and allowed to air-dry. Probe mixtures (5 µL per slide) were prepared according to the manufacturer's instructions, vortexed, briefly centrifuged, and denatured at 70 °C for 5 minutes in a thermomixer, then immediately placed on ice for at least 3 minutes. In parallel, slides were denatured in 70% formamide/2× SSCP at 80 °C for 5 minutes, rapidly transferred to ice-cold 70% ethanol, and dehydrated again through a graded ethanol series (70%, 90%, 95%) for 5 minutes each at room temperature. The denatured probe was applied to the dried slide and covered with a coverslip using a flip-over technique to minimize air bubbles. Hybridization was carried out overnight at 37 °C in a chamber containing 60% formamide/2× SSCP.

Post-hybridization washes were performed the following day to remove non-specifically bound probe. Slides were washed three times for 5 minutes in 50% formamide/2× SSC at 42 °C with agitation, followed by five washes of 2 minutes each in 0.1× SSC at 42 °C, a wash in 2× SSC for 5 minutes at room temperature, and a final wash in 1× PBS. Slides were then dehydrated through ethanol, dried in the dark, and mounted with 25 µL DAPI/Vectashield (100 ng/mL) under a 24×60 mm coverslip. Fluorescence signals were visualized using a Zeiss fluorescence microscope and captured with Metafer-ISIS software.

V. CNV - Copy Number Variation Sequencing

Copy number variation sequencing (CNV-seq) was performed using shallow whole genome sequencing (sWGS) in accordance with the validated clinical protocols of the Centre for Medical Genetics Ghent. DNA concentration was measured fluorometrically using a Fluoroskan Microplate Fluorometer (Thermo Scientific), after which samples were normalized to 100 ng of input DNA in a total volume of 30 µL with Milli-Q water. Library preparation was carried out using a PCR-free Illumina protocol on a Hamilton Star automated liquid handling system. During this process, each sample was assigned a unique molecular barcode, allowing multiple samples to be sequenced simultaneously. Library concentrations were subsequently quantified by qPCR using a LightCycler 480, and libraries were pooled in equimolar amounts prior to sequencing.

Sequencing was performed on an Illumina NovaSeq 6000 platform using a 100-cycle kit, targeting a minimum of 15 million reads per tumor sample to achieve the low-resolution coverage applied to malignant samples at CMGG (50 kb bin size, with a minimum reportable aberration size of 400 kb). After sequencing, raw data were demultiplexed and FASTQ files were generated for each sample. Reads were aligned to the human reference genome (GRCh38) using Bowtie, producing BAM files for downstream analysis. Copy number analysis was then performed using the WisecondorX algorithm, which divides the genome into equal windows, counts reads per window, and applies normalization and correction steps. Segmentation was carried out using the Circular Binary Segmentation (CBS) algorithm to identify regions with consistent copy number states.

Copy number alterations were determined based on log2 ratios of observed versus reference read counts, using thresholds of +0.33 for gains and −0.33 for losses, in line with CMGG clinical standards for tumor samples. Final results were visualized and interpreted using VIVAR software.[56]

5. Results

To evaluate the performance of OGM across different sample types, analyses were performed on cell lines, tumoroids, and primary sarcoma samples.

I. Data analysis workflow

The Optical Genome Mapping (OGM) data of each sample were processed and analyzed according to the workflow described in Material & Methods (Section III.vi — Data Analysis). For every OGM run, quality control (QC) metrics were first evaluated to determine whether the sample was suitable for downstream variant calling. Samples meeting the recommended Bionano thresholds were processed through the standard filtering strategy combining a sample-specific variant allele frequency (VAF) cutoff (≥ 0.40 for cell lines, ≥ 0.10 for tumoroids and primary tissue), a minimum molecule support requirement, and exclusion of variants present in the Bionano control database of healthy individuals. Retained CNV and SV calls were subsequently filtered against the 260-gene cancer-related panel (**ADDENDUM A**) and manually curated. Samples not meeting the recommended QC thresholds were flagged as suboptimal and the corresponding variant calls were interpreted with appropriate caution, as further detailed in the relevant Results sections below.

II. Implementation of Optical Genome Mapping in RMS Cell Lines

UHMW DNA was extracted from cell pellets ($1.5x10^6$ cells/pellet) using the Bionano Prep SP Frozen Cell Pellet DNA Isolation Kit.[55] Extraction was consistently successful across both RMS cell lines, yielding UHMW DNA of sufficient quality and quantity for OGM analysis.

Quality control metrics for all three RMS cell lines (RH30, RH41, and RMS-YM) met or exceeded the manufacturer's recommended thresholds, confirming that the data were of sufficient quality for reliable downstream structural variant and copy number analysis (**Table 5**).

QC metric	RH30	RH41	RMS-YM	Recommended treshold
Molecule N50 (≥ 150kbp)	339	355.88	318	≥ 250
Molecule N50 (≥ 20kbp)	305.25	319.88	242.25	≥ 150
Label density (/100 kbp)	15.46	14.48	16.51	14-17
Map rate (%)	89.3	85.7	81.1	≥ 70
Effective coverage (x)	422.87	409.44	367.78	≥ 300
Positive label variance (PLV)(%)	3.35	3.3	3.86	< 10
Negative label variance (NLV)(%)	9.15	14.78	12.6	< 15

Table 5. Quality control metrics of Optical Genome Mapping runs for the RMS cell lines RH30, RH41, and RMS-YM. *Metric definitions and recommended thresholds are described in the Data analysis workflow section. All three samples met or exceeded the manufacturer's recommended thresholds, confirming that the data were of sufficient quality for downstream analysis.*

i. Genomic characterization of RH30

The RH30 cell line was derived from a metastatic lesion of a 17-year-old male patient with fusion-positive alveolar rhabdomyosarcoma (FP-ARMS) and harbors the canonical t(2;13)(q36.1;q14.11) translocation, resulting in the characteristic *PAX3::FOXO1* fusion gene, alongside *FGFR4* and *FGF8* overexpression (**Table 3**). Because this fusion is considered the molecular hallmark of FP-ARMS, RH30 served as an ideal positive control to evaluate the ability of Optical Genome Mapping (OGM) to detect both the diagnostic rearrangement and additional genomic abnormalities associated with this sarcoma subtype. The expected balanced translocation between chromosomes 2 and 13, corresponding to the canonical t(2;13)(q36.1;q14.11) rearrangement, was clearly identified by OGM. To confirm this finding, break-apart FISH analysis targeting FOXO1 was performed (**Figure 10**). In normal cells, the 5'-*FOXO1* (red) and 3'-*FOXO1* (green) signals are located together and appear as a fused signal. In RH30 cells, however, the red and green signals were separated, indicating disruption of the *FOXO1* locus due to the translocation. This break-apart pattern was also observed on metaphase spreads, where the separated *FOXO1* fragments could be visualized on different chromosomes. In addition, an increased number of 3'-*FOXO1* (green) signals was observed in both interphase nuclei and metaphase spreads, consistent with amplification of the derivative chromosome carrying the *PAX3::FOXO1* fusion. Together, these findings confirmed the presence of the *PAX3::FOXO1* fusion and demonstrated complete concordance between OGM and FISH for detecting this defining rearrangement.

Beyond the fusion event itself, OGM revealed a highly complex genomic landscape with widespread copy number alterations across nearly all chromosomes (**Figure 9**). Several regions showed high-level amplifications involving oncogenes from the cancer-related gene panel. The most prominent amplification was located at chromosome 12q13.3-q14.1 and included the oncogenes *CDK4* and *GLI1*, together with the co-amplified *STAT6*. In addition, amplification of the *FOXO1* locus on chromosome 13q14 was observed, consistent with amplification of the derivative chromosome carrying the *PAX3::FOXO1* fusion. Additional chromosomal gains involved several other oncogenes, including *ALK*, *EGFR*, *CDK6*, *KRAS*, and *ERBB2*, as well as *PAX3*, the partner gene of the defining fusion.

Widespread copy number losses were also observed. Most notably, a deletion at chromosome 9p24.3-p21.3 involved the tumor suppressor genes *CDKN2A* and *CDKN2B*, together with the co-deleted *MTAP*. Additional losses affected the tumor suppressor genes *CDH1* and *BCOR*. Several other copy number alterations involved genes whose direction of alteration is not consistent with their canonical role in tumorigenesis (e.g., gain of tumor suppressors or loss of oncogenes) and were therefore considered likely passenger events within larger chromosomal segments; a complete overview is provided in **ADDENDUM B**.

Structural variant analysis identified multiple additional rearrangements besides the defining *PAX3::FOXO1* fusion. A total of 13 inter-chromosomal translocations were detected. Of these, the majority did not give rise to a putative fusion gene and likely represent passenger alterations associated with the genomic instability of the RH30 cell line. Two translocations were flagged by the Bionano Access software as resulting in putative fusion transcripts, even though the genes involved were not part of the cancer-related gene panel applied during filtering: a t(1;7) producing a *MROH3P::MAD1L1* fusion and a t(3;X) producing a *PCDH19::GRM7* fusion. Neither of these fusions has been previously described, and their biological and clinical significance therefore remains unclear. In addition, 24 intrachromosomal structural variants, including deletions, duplications, and insertions, were detected across multiple chromosomes.

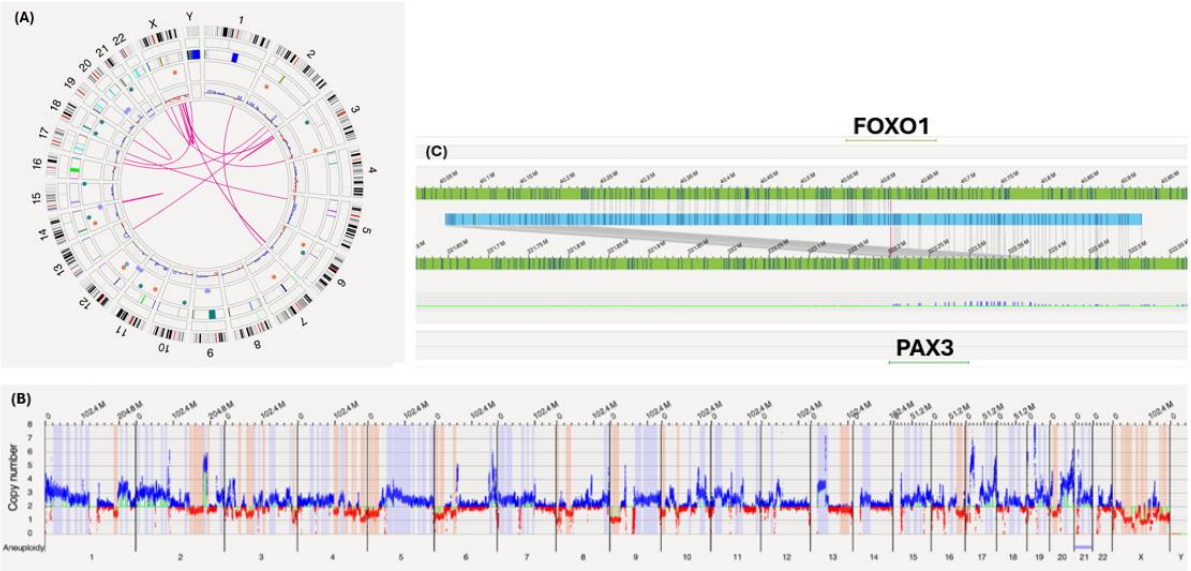

Figure 9. Optical Genome Mapping (OGM) analysis of the RH30 cell line. *(A) Circos plot representing the genome-wide structural variant landscape of the RH30 cell line. Translocations are visualized as connecting lines, including the balanced translocation between chromosomes 2 and 13 corresponding the PAX3::FOXO1 fusion. (B) Genome-wide copy number variation (CNV) profile of RH30. Copy number gains (blue) and losses (red) are shown across all chromosomes, illustrating multiple genomic imbalances. (C) Detailed view of the PAX3 and FOXO1 loci, confirming the presence of the PAX3::FOXO1 fusion detected by OGM.*

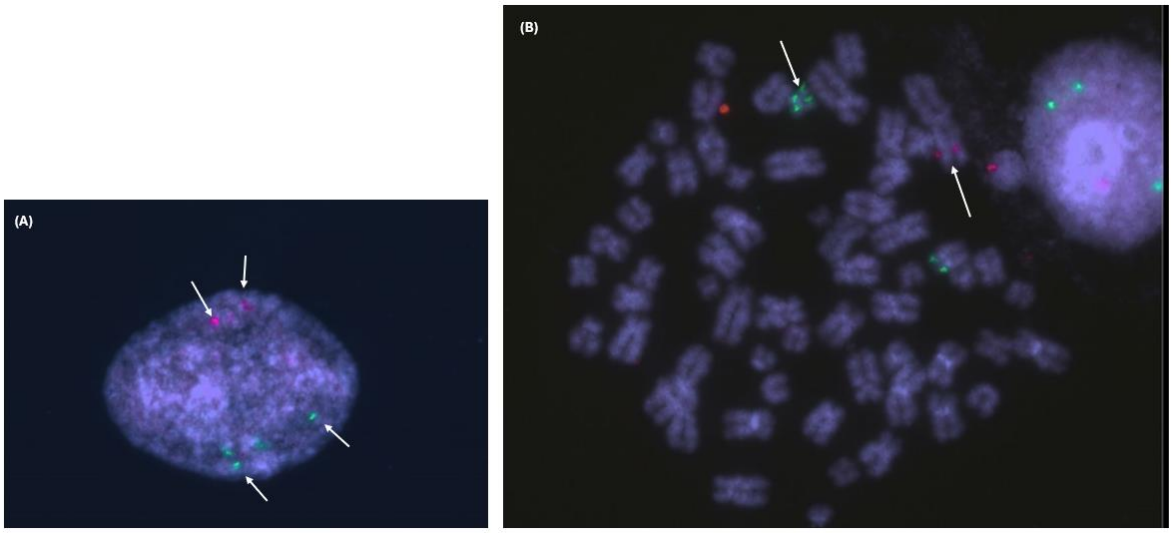

Figure 10. Break-apart FISH analysis of the RH30 cell line using a FOXO1 break-apart probe (3'-FOXO1 in green, 5'-FOXO1 in red). *(A) Interphase nucleus showing separated red and green signals (arrows), the characteristic break-apart pattern indicating disruption of the FOXO1 gene as a result of the t(2;13)(q36.1;q14.11) translocation. In an intact FOXO1 locus, the red and green signals would be co-localized. (B) Metaphase spread confirming the break-apart pattern at the chromosomal level. The isolated green signal (arrow) marks the 3'-FOXO1 fragment retained on chromosome 13, while the isolated red signal (arrow) represents the 5'-FOXO1 fragment translocated together with PAX3 onto chromosome 2, generating the PAX3::FOXO1 fusion. These results confirm the fusion-positive status of RH30.*

To compare the OGM-derived copy number profile of RH30 against an established diagnostic reference, shallow whole-genome CNV sequencing (CNV-seq) was performed in parallel (**Figure 11**). CNV-seq is part of the validated diagnostic workflow at CMGG and is therefore used here as a reference to benchmark the OGM CNV output. Both techniques rely on a coverage-based approach to detect copy number changes. CNV-seq from short-read sequencing depth, OGM from the density of fluorescently labeled DNA molecules, and were applied to the same sample to evaluate concordance.

The two profiles showed good agreement in the major copy number events that define the genomic landscape of RH30, including the high-level *CDK4* amplification at 12q13.3-q14.1, the *FOXO1* gain at 13q14 consistent with amplification of the derivative chromosome carrying the *PAX3::FOXO1* fusion, and the *CDKN2A/CDKN2B/MTAP* deletion at 9p21. Additional concordant events included gains on 1p, 1q32, 2q32, 10q24, 11p, 17q, 18q, and 20q, and losses on 5p15, 7p22, 8p23, 16q, and 17p13. Several OGM calls, mostly low-level gains and losses on chromosomes 3, 4, 6, 9q, 11q, and X, were not clearly visible on the CNV-seq profile. Both OGM and CNV-seq are relative techniques in which copy number is inferred from coverage deviations against an assumed diploid baseline, and the absolute ploidy of the sample cannot be directly determined. In a highly rearranged genome such as that of RH30, this makes ploidy calling, and consequently the precise positioning of the diploid (two-chromosome) reference line, particularly challenging, which complicates the interpretation of low-level copy number changes regardless of the technique used. The discordant calls between OGM and CNV-seq are therefore most likely a reflection of this shared limitation rather than of a true difference in accuracy between the two methods. As expected, balanced rearrangements such as the *PAX3::FOXO1* fusion were not visible on CNV-seq, since they do not alter DNA copy number.

Overall, OGM and CNV-seq showed good concordance for the principal copy number alterations in RH30, with the remaining differences confined to low-level events for which baseline definition is inherently difficult in a complex genome

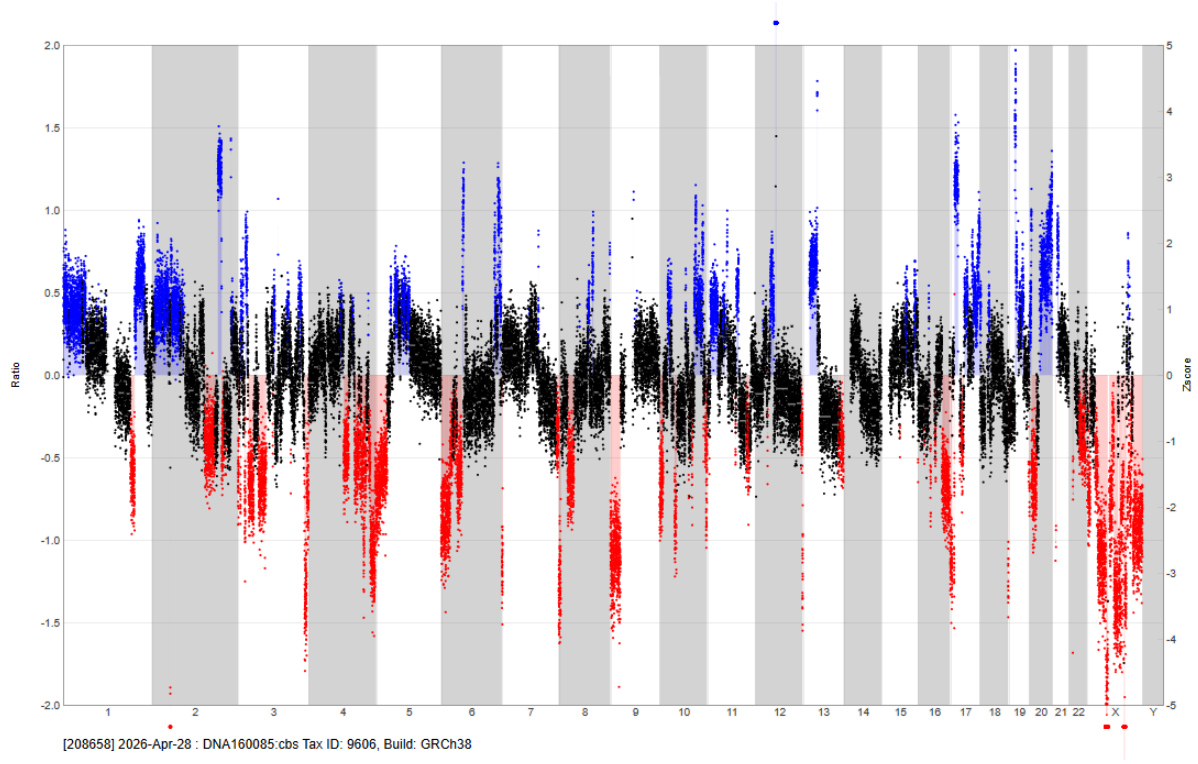

Figure 11. Shallow whole-genome CNV sequencing (sWGS) profile of the RH30 cell line. *Genome-wide copy number profile of RH30, performed as validation of the OGM-derived CNV calls.*

ii. Genomic characterization of RH41

The RH41 cell line was derived from a metastatic alveolar rhabdomyosarcoma in a 7-year-old female patient and was established after chemotherapy treatment (**Table 3**). It has previously been reported to harbor the canonical t(2;13)(q36.1;q14.11) translocation resulting in the *PAX3::FOXO1* fusion gene, alongside a *TP53* mutation and *FGFR4*/*FGF8* overexpression. The post-chemotherapy origin of this cell line is notable, as it may have contributed to the highly rearranged genomic background described below. Surprisingly, however, the expected *PAX3::FOXO1* fusion was not detected. Even after lowering the variant allele frequency (VAF) threshold to 0.10 to capture possible subclonal events, no balanced t(2;13)(q36.1;q14.11) translocation could be identified. To further investigate this finding, break-apart FISH analysis targeting *FOXO1* was performed (**Figure 13**). In contrast to RH30, where a clear break-apart pattern was observed, RH41 showed co-localized red and green *FOXO1* signals in both interphase nuclei and metaphase spreads, consistent with an apparently intact *FOXO1* locus. The fact that both OGM and FISH failed to detect the expected rearrangement suggests that this was unlikely to be due to a technical issue alone and instead may reflect a more complex or non-canonical genomic architecture in this cell line. This observation is further discussed in the Discussion section.

Despite the absence of the canonical fusion, OGM revealed a highly complex genomic landscape characterized by widespread copy number alterations, predominantly gains (**Figure 12**). Several chromosomal arm gains were identified, including 2q, which contains *PAX3* as well as *SF3B1*, *IDH1*, together with gains involving regions containing *CDK6*, *MET*, *BRAF*, *MYC*, and *NCOA2*. The most prominent amplification was a focal high-level gain at chromosome 8p11.23-p11.21 involving *FGFR1*, a receptor tyrosine kinase frequently implicated in cancer and considered a potentially actionable target. Another major finding was a broad gain at chromosome 12q, encompassing the well-known sarcoma-associated 12q amplicon containing *CDK4*, *MDM2*, *HMGA2*, *STAT6*, *GLI1*, and *ERBB3*. Additional gains affecting cancer-related genes included regions containing *KRAS*, *CIC*, *FOSB*, *CHEK1*, *PTCH1*, *NR4A3*, and SS18. Copy number losses were less frequent but involved several biologically relevant regions. Most notably, a homozygous deletion at chromosome 9p21.3 encompassed the tumor suppressor genes *CDKN2A*, *CDKN2B*, and *MTAP*. This alteration was also observed in RH30 and represents a recurrent event in alveolar rhabdomyosarcoma associated with cell cycle dysregulation. Additional losses affected regions containing *SMAD4*, *GATA3*, and *EPC1*.

Structural variant analysis identified seven inter-chromosomal translocations. One of these, a t(11;20), was flagged by the Bionano Access software as resulting in a putative *DHX35::PPP6R3* fusion, even though the genes involved were not part of the cancer-related gene panel applied during filtering. This fusion is not part of the sarcoma-associated fusion repertoire and has, to our knowledge, not been described as a recurrent driver in alveolar rhabdomyosarcoma. Most other rearrangements did not involve genes from the cancer-related gene panel either and likely represent passenger events associated with the genomic instability of the cell line. In addition, 3 intrachromosomal structural variants, including deletions, duplications, insertions, and inversions, were identified throughout the genome. Of particular interest was an inversion involving *MDM2* within the amplified 12q region, which may further affect regulation of this oncogene. A complete overview of all detected CNVs and SVs is provided in **ADDENDUM C**.

Overall, OGM characterized RH41 as a genomically highly unstable cell line with extensive copy number alterations and structural rearrangements. Recurrent sarcoma-associated alterations such as the *CDKN2A/CDKN2B/MTAP* deletion and amplification of the 12q region containing *CDK4*, *MDM2*, and *HMGA2* were readily detected. However, despite the documented fusion-positive status of RH41, neither OGM or break-apart FISH identified the expected *PAX3::FOXO1* fusion. Possible biological explanations for this unexpected finding are discussed further in the Discussion section.

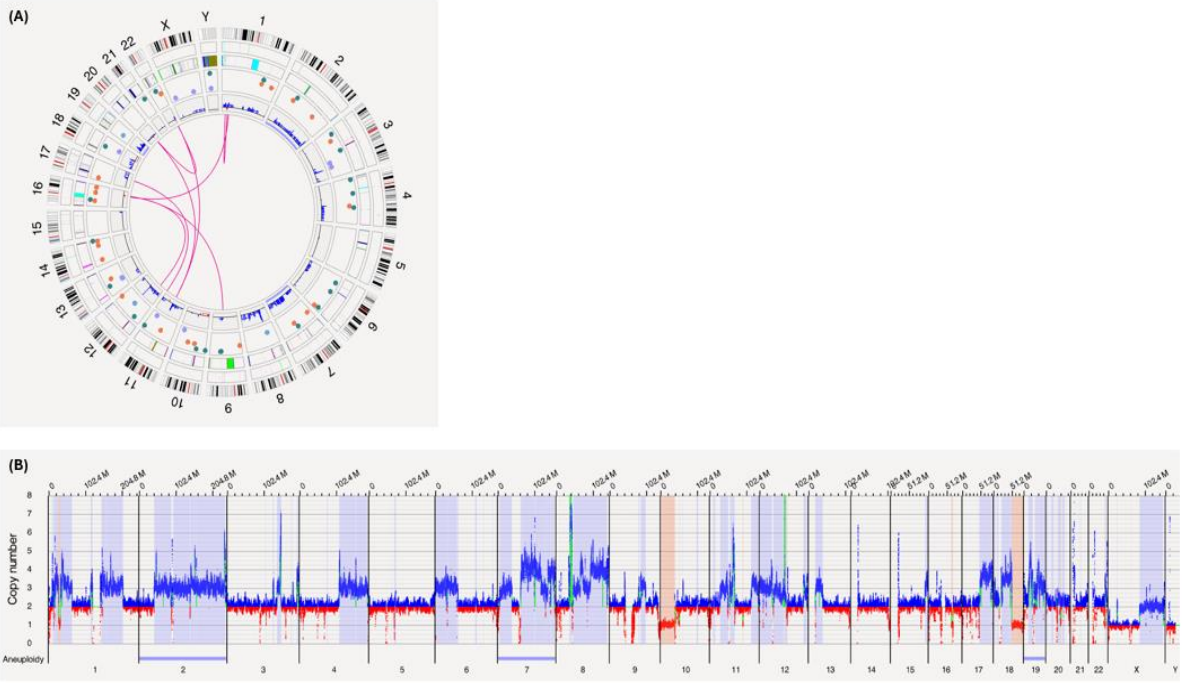

Figure 12. Optical Genome Mapping (OGM) analysis of the RH41 cell line. *(A) Circos plot representing the genome-wide structural variant landscape of the RH41 cell line. Numerous inter-chromosomal rearrangements are visualized as connecting lines, indicating a complex pattern of structural variation across multiple chromosomes. (B) Genome-wide copy number variation (CNV) profile of RH41. Copy number gains (blue) and losses (red) are distributed across the genome, illustrating widespread genomic imbalances affecting multiple chromosomal regions.*

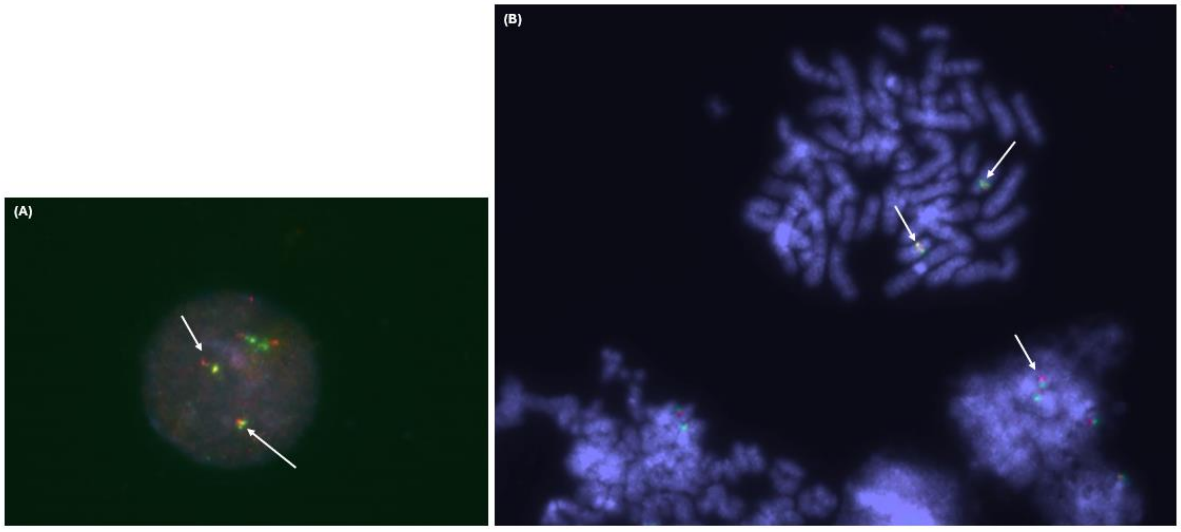

Figure 13. Break-apart FISH analysis of the RH41 cell line using a FOXO1 break-apart probe (3'-FOXO1 in green, 5'-FOXO1 in red). *(A) Interphase nucleus and (B) metaphase spread showing co-localized red-green signals (arrows), resembling an intact FOXO1 locus. Although RH41 is a known PAX3::FOXO1 fusion-positive cell line, the expected break-apart pattern is not detected.*

iii. Genomic characterization of RMS-YM

The RMS-YM cell line was established from an abdominal mass of a 2-year-old male patient with embryonal rhabdomyosarcoma (ERMS) and is reported to harbor multiple chromosomal rearrangements together with upregulation of *MDM2* and *FGFR1* (**Table 3**). RMS-YM was therefore included in this study as a third reference cell line alongside the fusion-positive ARMS cell lines RH30 and RH41, allowing further evaluation of OGM in a genetically distinct, fusion-negative rhabdomyosarcoma background. No inter-chromosomal translocations were detected after filtering, including the canonical t(2;13)(q36.1;q14.11) translocation responsible for the *PAX3::FOXO1* fusion. This finding was independently confirmed by break-apart FISH analysis targeting *FOXO1* (**Figure 15**). Both interphase nuclei and metaphase spreads showed co-localized red and green signals, consistent with an intact *FOXO1* locus and the absence of a break-apart pattern. Together, the OGM and FISH findings consistently classified RMS-YM as fusion-negative for *PAX3::FOXO1*. Despite the absence of a defining fusion event, RMS-YM displayed a highly complex genomic landscape characterized by widespread copy number alterations, predominantly gains (**Figure 14**). The most prominent finding was a focal high-level amplification at chromosome 12q15 (copy number 8) involving *MDM2*. In addition to this amplification, four independent structural variants affecting *MDM2* were identified within the same region, including one insertion, two deletions, and one inversion. This combination of amplification and multiple intragenic rearrangements suggests extensive structural remodeling of the 12q15 locus that may further alter *MDM2* regulation or expression.

Several broad chromosomal gains were also detected, including gains of 6p, 7q, and 8q, involving genes such as *CDK6*, *MET*, *BRAF*, *MYBL1*, *NCOA2*. Notably, a gain of nearly the entire chromosome 19 was observed, encompassing multiple cancer-related genes including *CCNE1*, and *FOSB*. A focal amplification at chromosome 8p12p11.21 involving *FGFR1* (copy number 6) was also identified, similar to the *FGFR1* amplification observed in RH41. Additional gains affected regions containing *PAX3*, *NR4A3*, and *SS18*. Copy number losses were less frequent but included several biologically relevant regions. Most notably, a focal deletion at chromosome 9p21.3 involving *CDKN2A*, *CDKN2B*, and *MTAP* was identified. This same deletion was also observed in both *RH30* and *RH41*, highlighting it as a recurrent shared alteration across all three RMS cell lines analyzed in this study. Additional losses involved regions containing *SMAD4*. Although no inter-chromosomal translocations were identified, structural variant analysis revealed 16 intrachromosomal rearrangements distributed throughout the genome. Several of these involved genes from the cancer-related gene panel, including alterations affecting *RAF1*, *EGFR*, *NRG1*, *CDK6*, *NOTCH1*, *RAD51B*, *AKT1*, *NUTM1*, *PRKCA*, *STK11*, and *KEAP1*. A complete overview of all detected CNVs and SVs is provided in **ADDENDUM D**.

Overall, OGM characterized RMS-YM as a fusion-negative rhabdomyosarcoma cell line with a highly complex and unstable genome. The genomic profile was dominated by widespread chromosomal gains, a focal high-level *MDM2* amplification accompanied by multiple structural rearrangements, amplification of *FGFR1*, and gain of nearly the entire chromosome 19. Several alterations overlapped with those observed in RH30 and RH41, particularly the recurrent *CDKN2A/CDKN2B/MTAP* deletion and shared gain patterns involving chromosomes 7q, 8q, and 17q. Importantly, both OGM and FISH consistently confirmed the absence of the *PAX3::FOXO1* fusion, demonstrating the ability of OGM to distinguish fusion-positive from fusion-negative RMS cell lines within a single genome-wide assay.

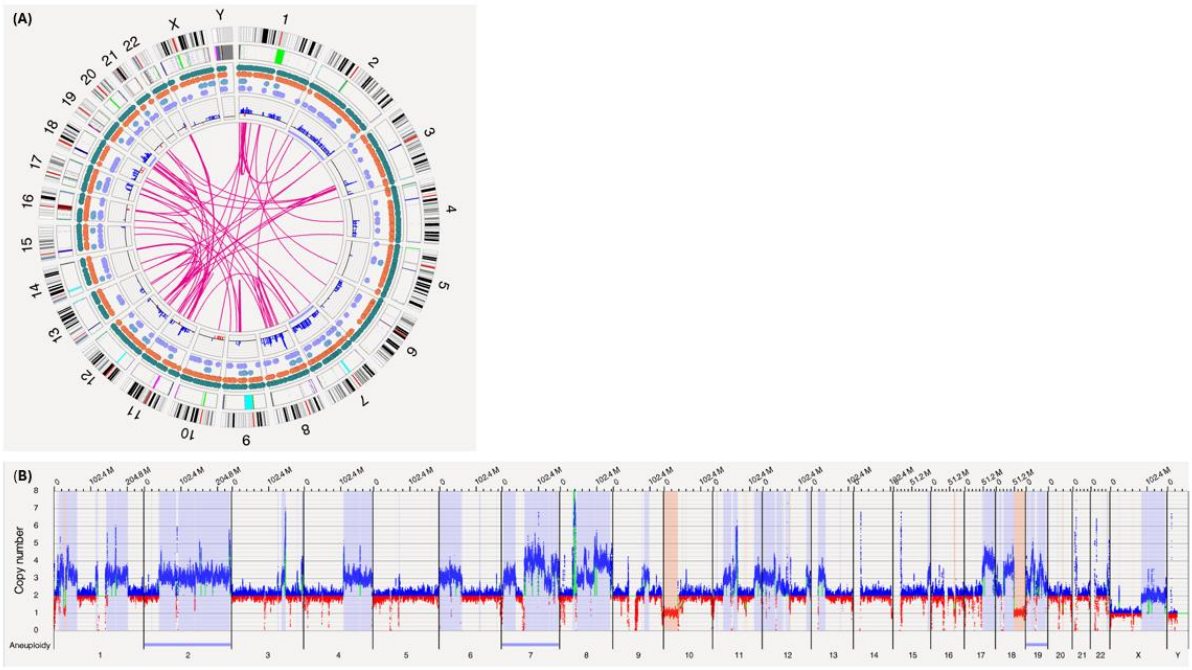

Figure 14. Optical Genome Mapping (OGM) analysis of the RMS-YM cell line*. (A) Circos plot representing the genome-wide structural variant landscape of RMS-YM. The absence of inter-chromosomal connecting lines reflects the lack of detected translocations, consistent with the fusion-negative status of this cell line. (B) Genome-wide copy number variation (CNV) profile of RMS-YM. Copy number gains (blue) and losses (red) are shown across all chromosomes, illustrating widespread genomic imbalances.*

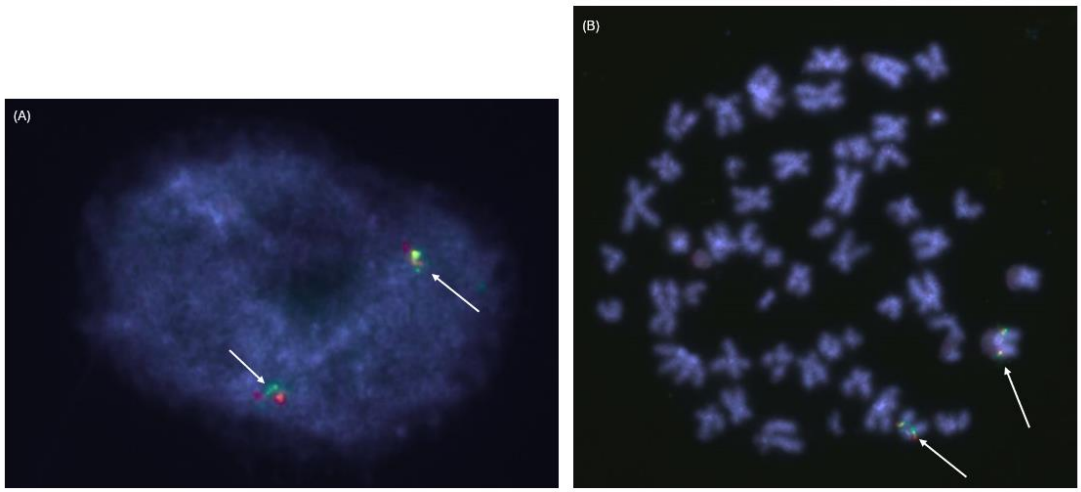

Figure 15. Break-apart FISH analysis of the RMS-YM cell line using a FOXO1 break-apart probe. *The 3'-FOXO1 segment is labeled in green and the 5'-FOXO1 segment in red. (A) Interphase nucleus showing two co-localized red-green signals (arrows), resembling an intact FOXO1 locus. (B) Metaphase spread confirming the co-localized signal pattern at the chromosomal level (arrows), with no evidence of a break-apart pattern. The absence of separated red and green signals indicates an intact FOXO1 gene, consistent with the fusion-negative status of RMS-YM and in line with the absence of t(2;13)(q36.1;q14.11) detected by OGM.*

III. Implementation of Optical Genome Mapping in Patient-derived rhabdomyosarcoma tumoroids

In addition to the established RMS cell lines, four patient-derived rhabdomyosarcoma tumoroids (PEDSAR02, PEDSAR03, MSKPED0023 and MSKPED0087) were analyzed by OGM. As these are recently established models with only limited prior molecular characterization, a comprehensive genome-wide profile is essential to define their genomic background and to assess their suitability as preclinical models for rhabdomyosarcoma. OGM was therefore applied to confirm any previously reported diagnostic rearrangements and to provide a broad characterization of additional copy number and structural alterations across each genome.

Quality control metrics for all four patient-derived rhabdomyosarcoma tumoroids (PEDSAR02, PEDSAR03, MSKPED0023 and MSKPED0087) met or approached the manufacturer's recommended thresholds (**Table 6**). MSKPED0023 met all recommended criteria, while PEDSAR02, PEDSAR03 and MSKPED0087 displayed slightly reduced label density values, and PEDSAR03 additionally showed a molecule N50 and map rate (69.4%) slightly below the recommended thresholds. As only single metrics deviated by less than 10% from the recommended ranges, and effective coverage exceeded 300x in all four samples, the data were considered of sufficient quality for downstream structural variant and copy number analysis.

PEDSAR01 was ultimately excluded from further analysis because the sample quality did not meet the required quality control standards. Consequently, OGM analysis was performed only on PEDSAR02, PEDSAR03, MSKPED0023, and MSKPED0087.

QC metric	PEDSAR01	PEDSAR02	PEDSAR03	MSKPED0023	MSKPED0087	Recommended treshold
Molecule N50 (≥ 150kbp)	393	322.5	229.13	278.25	412.4	≥ 250
Molecule N50 (≥ 20kbp)	67.13	261	157.13	202.5	370.5	≥ 150
Label density (/100 kbp)	24.43	13.02	12.72	15.78	13.48	14-17
Map rate (%)	16.7	71.7	69.4	88.4	83.7	≥ 70
Effective coverage (x)	28.99	237.52	323.97	419	394.37	≥ 300
Positive label variance (PLV)(%)	6.39	2.2	2.32	3.92	2.42	< 10
Negative label variance (NLV)(%)	3.59	23.27	22.15	8.82	20.75	< 15

Table 6. Quality control metrics of Optical Genome Mapping runs for the patient-derived rhabdomyosarcoma tumoroids PEDSAR01, PEDSAR02, PEDSAR03, MSKPED0023, and MSKPED0087. ***Metric*** *definitions and recommended thresholds are described in the Data analysis workflow section. Values below the recommended thresholds are highlighted in red.*

i. Genomic characterization of PEDSAR02

The PEDSAR02 tumoroid was derived from a 16-year-old male patient diagnosed with fusion-positive alveolar rhabdomyosarcoma (FP-ARMS) and is reported to harbor trisomy 21 as its most prominent previously characterized genomic feature (**Table 4**). The expected balanced translocation between chromosomes 2 and 13, corresponding to the canonical t(2;13)(q36.1;q14.11) rearrangement, was clearly identified by OGM, confirming the fusion-positive status of this tumoroid. In addition, an intrachromosomal *FOXO1::WDFY2* event was detected on chromosome 13, with a breakpoint at 13q14.11, identical to the *FOXO1* breakpoint involved in the canonical t(2;13)(q36.1;q14.11) translocation. This indicates that the *FOXO1* locus is recurrently rearranged in PEDSAR02, with both the canonical *PAX3::FOXO1* fusion and a secondary intrachromosomal *FOXO1::WDFY2* event sharing the same *FOXO1* breakpoint at 13q14.11. The biological and clinical relevance of this secondary rearrangement remains unclear.

Beyond the fusion event itself, OGM revealed a complex genomic landscape with multiple copy number alterations involving genes from the cancer-related gene panel (**Figure 16**). A gain of chromosome 21 was observed, consistent with the previously reported trisomy 21 in this tumor and encompassing the oncogene *ERG* together with the fusion partner gene *TMPRSS2*. A broad gain of chromosome 17q was also identified, encompassing the oncogenes *ERBB2*, *CDK12*, *STAT3*, and *PRKCA*. Gain of 17q is a recurrent feature in fusion-positive alveolar rhabdomyosarcoma. An additional gain was observed on chromosome 1q, involving the oncogene *NTRK1*. Widespread copy number losses were also detected. Most notably, a hemizygous loss of chromosome 17p13.3-p11.2 was observed, encompassing the tumor suppressor gene *TP53*. A loss of chromosome 13q14 affected the tumor suppressor gene *RB1*. In addition, a loss at chromosome 10q22.3-q26.3 affected the tumor suppressor genes *PTEN* and *SUFU*, and a loss at chromosome 5q12.1-q23.1 involved the tumor suppressor gene *APC*. Several other copy number alterations involved genes whose direction of alteration is not consistent with their canonical role in tumorigenesis (e.g., gain of tumor suppressors or loss of oncogenes) and were therefore considered likely passenger events within larger chromosomal segments; a complete overview is provided in **ADDENDUM E.**

Structural variant analysis further identified multiple rearrangements besides the defining *PAX3::FOXO1* fusion. In total, 12 inter-chromosomal translocations were detected. Given the limited number of translocations, all were screened for putative fusion gene formation without restricting the analysis to the cancer-related gene panel. The majority did not give rise to a putative fusion gene and likely represent passenger alterations associated with the genomic instability of the tumor. Three translocations resulted in putative fusion transcripts: a t(2;3) producing an *ST3GAL5::CACNA2D3* fusion, a t(4;8) producing a *LINC02509::CSPP1* fusion, and a t(7;X) producing an *RBM10::ABCB1* fusion, none of which have been previously described and whose clinical relevance therefore remains unclear. In addition, four intrachromosomal insertions were identified, affecting *RAD51B* (14q24.1), *DICER1* (14q32.13), *TCF12* (15q21.3), and *TP53* (17p13.1). To independently validate the *PAX3::FOXO1* fusion detected by OGM, break-apart FISH analysis was performed on PEDSAR02 using a *FOXO1* break-apart probe (**Figure 17**).

Overall, these findings demonstrate that OGM successfully identified the diagnostic *PAX3::FOXO1* fusion, independently confirmed by break-apart FISH, while simultaneously providing a genome-wide overview of the secondary genomic complexity present in PEDSAR02. Recurrent co-alterations such as trisomy 21, gain of 17q, and combined loss of *TP53*, *RB1*, and *PTEN* were detected within the same experiment, illustrating the added value of OGM as a comprehensive genomic profiling technique compared with targeted methods such as FISH or targeted RNA sequencing alone, which would each capture only a fraction of this genomic landscape.

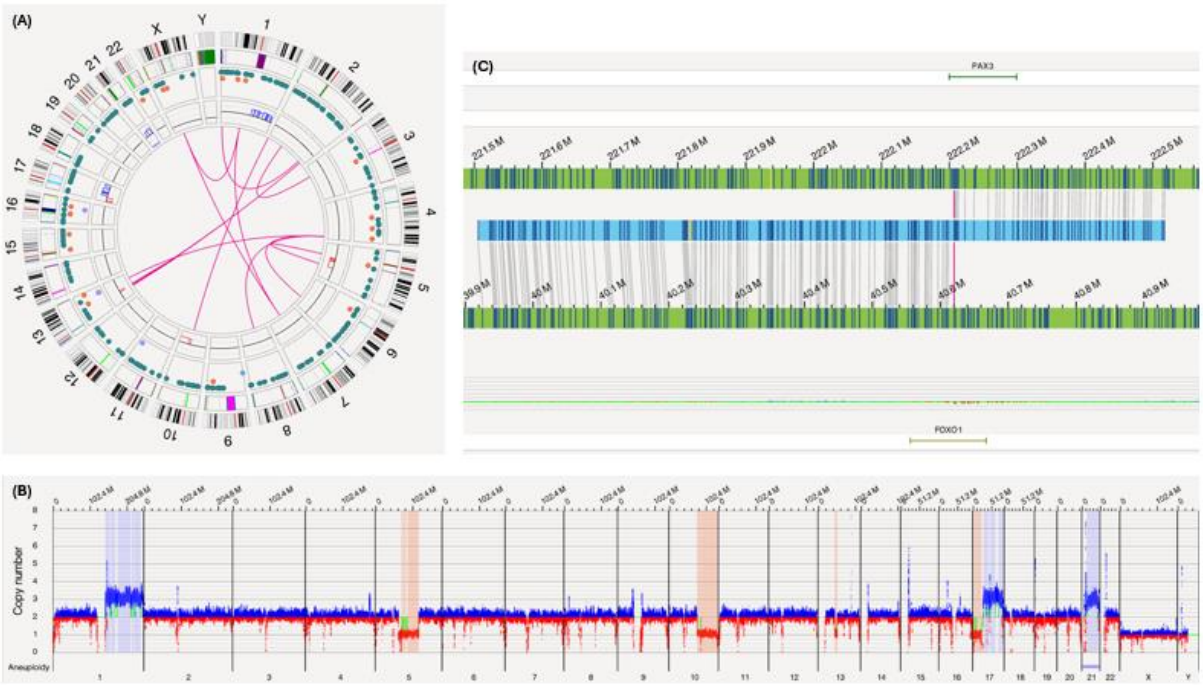

Figure 16. Optical Genome Mapping (OGM) analysis of tumoroid sample PEDSAR02. *(A) Circos plot showing genome-wide structural variants detected by OGM. (B) Copy number variation (CNV) profile derived from OGM data, illustrating genome-wide gains and losses. (C) detailed view of the translocation t(2;13)(q36.1;q14.11) PAX3::FOXO1*

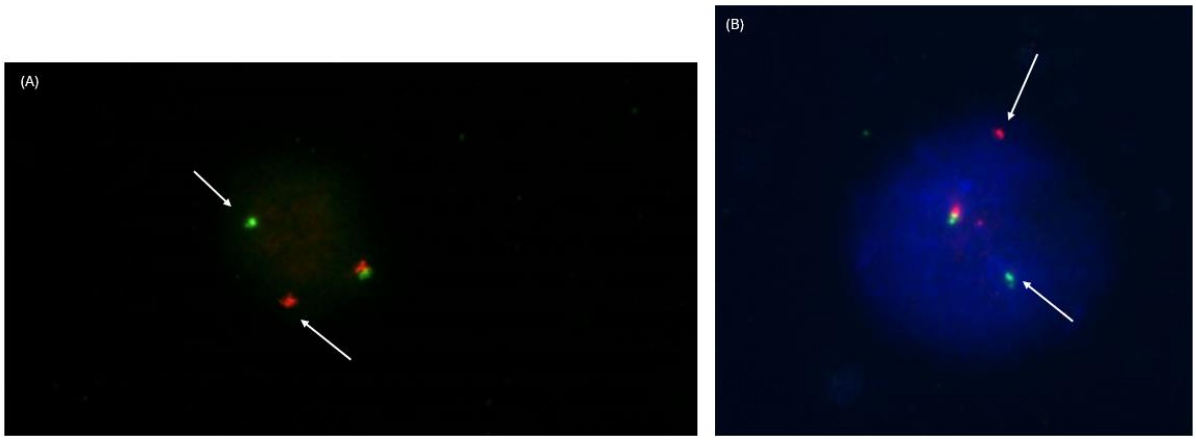

Figure 17. Break-apart FISH analysis of the PEDSAR02 tumoroid using a FOXO1 break-apart probe. *The 3'-FOXO1 segment is labeled in green and the 5'-FOXO1 segment in red.* ***(A, B)*** *Two representative interphase nuclei showing separated red and green signals (arrows), confirming disruption of the FOXO1 gene. This break-apart pattern is consistent with the fusion-positive status of PEDSAR02 and the t(2;13)(q36.1;q14.11) translocation detected by OGM.*

ii. Genomic characterization of PEDSAR03

The PEDSAR03 tumoroid was derived from a 14-year-old female patient diagnosed with fusion-positive alveolar rhabdomyosarcoma (FP-ARMS) and did not have any specifically reported genomic alterations from previous molecular characterization (**Table 4**). PEDSAR03 was established from frozen tumor fragments, in contrast to PEDSAR02, which was implanted directly from fresh biopsy material. The expected balanced translocation between chromosomes 2 and 13, corresponding to the canonical t(2;13)(q36.1;q14.11) rearrangement, was clearly identified by OGM, confirming the fusion-positive status of this tumoroid. In addition, a second t(2;13) event with an alternative *FOXO1* breakpoint was detected, suggesting additional structural complexity at the *FOXO1* locus.

To independently validate the *PAX3::FOXO1* fusion detected by OGM, break-apart FISH analysis was performed on PEDSAR03 using a *FOXO1* break-apart probe (**Figure 19**). Interphase nuclei displayed clearly separated red (5'-*FOXO1*) and green (3'-*FOXO1*) signals, in contrast to the co-localized signal pattern expected from an intact *FOXO1* locus. This break-apart pattern confirms disruption of the *FOXO1* gene and is fully consistent with the t(2;13)(q36.1;q14.11) rearrangement identified by OGM, thereby providing validation of the fusion-positive status of PEDSAR03.

Beyond the fusion event itself, OGM revealed an extremely complex genomic landscape characterized by widespread chromosomal gains affecting nearly every chromosome (**Figure 18**). Whole-chromosome gains were observed for chromosomes 1 and 2, with the gain of chromosome 2 encompassing the oncogenes *PAX3*, *NCOA1*, and *ALK*. Additional broad gains were identified involving chromosomes 5, 7, 11, 16, 17, 18, 20, 21, and 22, as well as gains affecting parts of chromosomes 4, 13, 14, and X. Numerous oncogenes were involved across these regions, including *KIT* and *PDGFRA* on 4q12, *EGFR*, *CDK6*, *MET*, and *BRAF* on chromosome 7, *YAP1* on chromosome 11, *FOXO1* on chromosome 13, *SS18* on chromosome 18, *ERG* and *TMPRSS2* on chromosome 21, and *EWSR1* and *PDGFB* on chromosome 22. Particularly notable were several focal high-level gains on chromosome 9, including amplification of *NR4A3* at 9q31.1 (CN 4) and *JAK2* at 9p24.1 (CN 4). Importantly, no copy number losses were detected in PEDSAR03, distinguishing this tumor from the other RMS samples analyzed in this study. Several other regions of gain involved tumor suppressor genes (e.g., *BARD1*, *ATM*, *CHEK1*, *BRCA2*, *CDH1*, *TP53*, *SMAD4*, *SMARCB1*, *CHEK2*, *NF2*, *PTCH1*); as gain of tumor suppressors is not expected to confer a functional driver effect, these are considered likely passenger events within larger chromosomal segments, and a complete overview is provided in **ADDENDUM F**.

Structural variant analysis further identified multiple rearrangements besides the defining *PAX3::FOXO1* fusion. In total, 11 intrachromosomal structural variants were detected, including insertions affecting *RAF1* (3p25.2), *AKT1* (14q32.33), *NUTM1* (15q14), *NF1* (17q11.2), and *STK11* (19p13.3), as well as deletions involving *ESR1* (6q25.2), *NRG1* (8p12), and *PRKCA* (17q24.2). Two additional deletions were identified adjacent to *SDHA* (5p15.33) and *NF2* (22q12.2), and a duplication was detected at 9q31.1.

Overall, these findings demonstrate that OGM successfully identified the diagnostic *PAX3::FOXO1* fusion, independently confirmed by break-apart FISH, while simultaneously providing a genome-wide overview of the extensive structural complexity present in PEDSAR03. The genomic profile was dominated by widespread chromosomal gains, multiple focal high-level amplifications on chromosome 9, and an absence of detectable copy number losses. Together, these alterations were detected within the same experiment, illustrating the added value of OGM as a comprehensive genomic profiling technique compared with targeted methods such as FISH or targeted RNA sequencing alone.

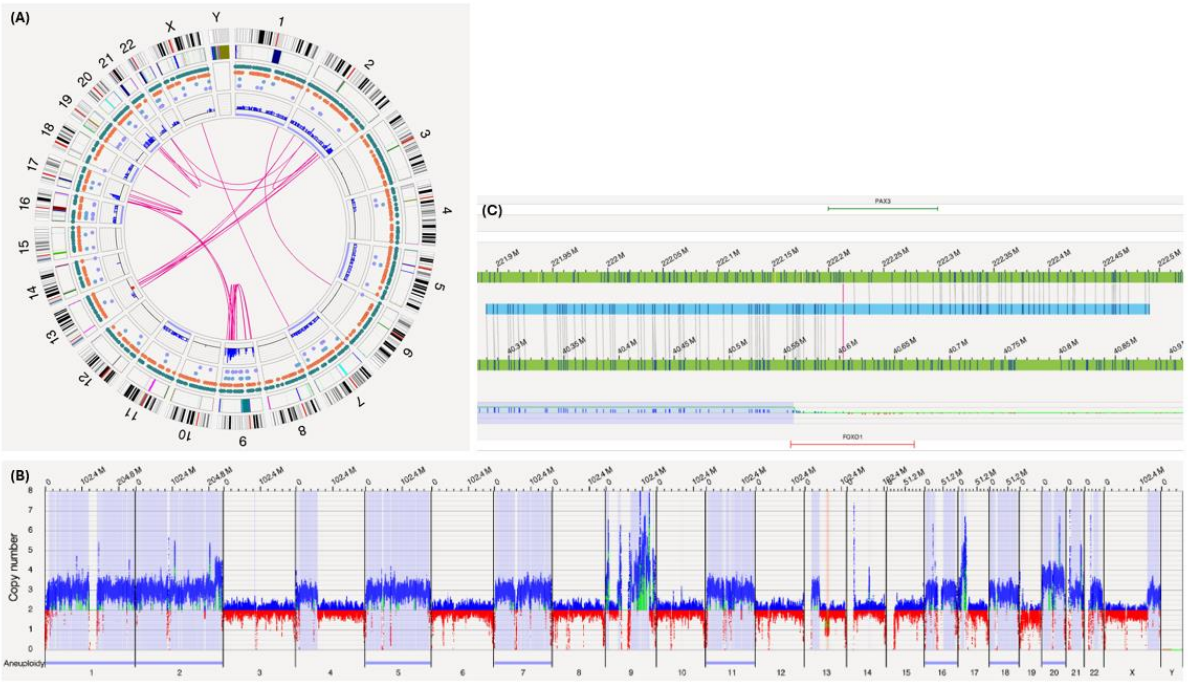

Figure 18. Optical Genome Mapping (OGM) analysis of tumoroid sample PEDSAR03. *(A) Circos plot showing genome-wide structural variants detected by OGM, including multiple chromosomal rearrangements. (B) Copy number variation (CNV) profile derived from OGM data, illustrating genome-wide gains and losses across chromosomes. (C) Detailed view of a structural variant involving the PAX3 gene on chromosome 2 and the FOXO1 gene on chromosome 13, consistent with a PAX3::FOXO1 fusion, characteristic of alveolar rhabdomyosarcoma.*

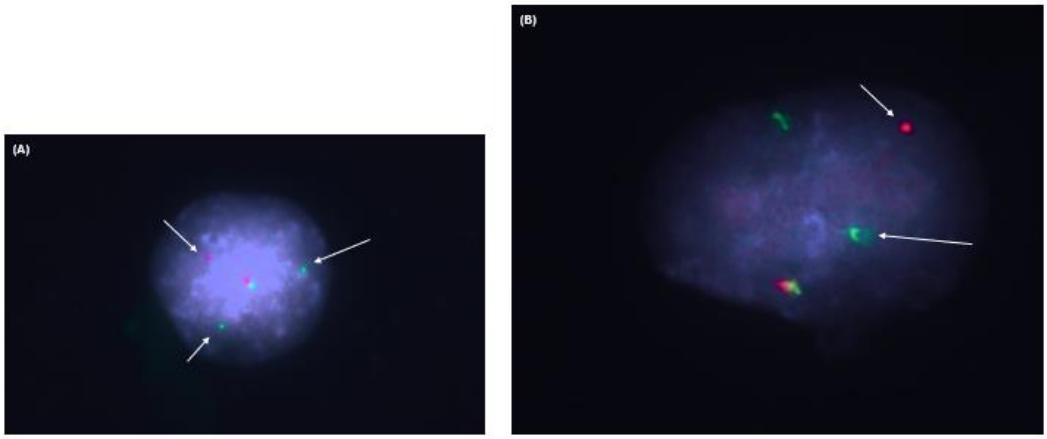

Figure 19. Break-apart FISH analysis of the PEDSAR03 tumoroid using a FOXO1 break-apart probe (3' in green, 5' in red). *(A) Interphase nucleus showing separated red and green signals (arrows), the characteristic break-apart pattern indicating disruption of FOXO1 as a result of the t(2;13)(q36.1;q14.11) translocation. In an intact FOXO1 locus, both signals would be co-localized. (B) A second interphase nucleus confirming the break-apart pattern, with isolated red and green signals (arrows) at distinct nuclear locations. A co-localized red–green signal corresponding to the retained wild-type FOXO1 allele is also visible, together with an additional isolated 3'-FOXO1 (green) signal, consistent with duplication of the 3'-FOXO1 segment on the derivative chromosome. These findings confirm disruption of FOXO1 and are consistent with the fusion-positive status of PEDSAR03 and the t(2;13)(q36.1;q14.11) detected by OGM.*

iii. Genomic characterization of MSKPED0023

The MSKPED0023 tumoroid was derived from a male patient diagnosed with fusion-negative rhabdomyosarcoma (FN-RMS) and was previously reported to harbor *KMT2A* K1364Nfs*14, *KMT2A* E1363D, and *RBM10* P245L mutations (**Table 4**). Consistent with the reported fusion-negative status, no t(2;13)(q36.1;q14.11) translocation, nor any other inter-chromosomal translocation involving panel fusion genes, was detected by OGM. A single intra-chromosomal translocation event was identified involving the *MDM2* region on chromosome 12.

To independently validate the fusion-negative status of MSKPED0023, break-apart FISH analysis was performed using a *FOXO1* break-apart probe (**Figure 21**). Both interphase nuclei examined displayed co-localized red (5'-*FOXO1*) and green (3'-*FOXO1*) signals, consistent with an intact *FOXO1* locus and the absence of a break-apart pattern. Notably, approximately four paired red–green signals were observed per nucleus instead of the expected two, suggestive of an increased copy number of the *FOXO1* locus. No corresponding gain or amplification of the 13q14 region was detected in the CNV-seq data derived from OGM. Overall, the FISH results confirm an intact *FOXO1* gene and are fully concordant with the absence of a t(2;13)(q36.1;q14.11) translocation detected by OGM, providing confirmation of the fusion-negative classification of MSKPED0023. Beyond the absence of a defining fusion event, OGM revealed a highly complex genomic landscape characterized by widespread copy number alterations affecting nearly every chromosome, with both gains and losses contributing to the overall imbalance (**Figure 20**). Broad gains were detected on chromosomes 2, 5, 11, 17q, 20, and 21q. These regions encompassed multiple oncogenes, including *MYCN*, *NCOA1*, *ALK*, and *PAX3* on chromosome 2; *TERT*, *PDGFRB*, and *FGFR4* on chromosome 5; *RELA*, *CCND1*, and *YAP1* on chromosome 11; *PRKCA* on 17q21.33-q25.3; and *GNAS* on chromosome 20. Particularly notable was a focal high-level amplification at 12q15 involving the oncogene *MDM2* (CN 7/8), accompanied by three independent intragenic structural variants in the same region (one insertion, one deletion, and one duplication), as well as a translocation event nearby, indicating extensive structural remodeling of the *MDM2* locus. An additional focal gain was identified at 9q22.32-q32, encompassing the oncogene *NR4A3*.

Copy number losses were equally widespread. Most notably, a deletion at 9p was detected encompassing the tumor suppressor genes *CDKN2A*, *CDKN2B*, and *MTAP*, mirroring the recurrent 9p21.3 deletion observed across the rhabdomyosarcoma cell lines RH30, RH41, and RMS-YM analyzed in this study. Additional losses involved the tumor suppressor genes *TP53* on 17p; *NF1*, *RAD51D*, and *BRCA1* on 17q11.2-q21.32; and *SMAD4* on 18q. Several other copy number alterations involved genes whose direction of alteration is not consistent with their canonical role in tumorigenesis (e.g., gain of tumor suppressors or loss of oncogenes) and were therefore considered likely passenger events within larger chromosomal segments. Structural variant analysis identified eleven additional intra-chromosomal rearrangements beyond the *MDM2*-associated events, including insertions affecting *RAF1* (3p25.2), *AKT1* (14q32.33), *NUTM1* (15q14), and *STK11* (19p13.3), as well as deletions involving *NRG1* (8p12), *NOTCH1* (9q34.3), and *SMAD4* (18q21.2). A complete overview of all identified CNVs and SVs is provided in **ADDENDUM G**.

Overall, these findings demonstrate that OGM provided a comprehensive genome-wide profile of MSKPED0023, identifying the absence of a *PAX3::FOXO1* fusion together with extensive copy number imbalances and multiple structural rearrangements within the same experiment. The genomic profile was dominated by a focal high-level *MDM2* amplification accompanied by intragenic structural variants, recurrent 9p loss involving *CDKN2A/CDKN2B/MTAP*, broad gains across multiple chromosomes encompassing several oncogenes, and concurrent losses affecting key tumor suppressor regions including *TP53*, *NF1*, *BRCA1*, and *SMAD4*. Together with the orthogonal FISH validation, these results illustrate the added value of OGM as a single-assay comprehensive genomic profiling technique compared with targeted methods such as FISH or RNA sequencing alone.

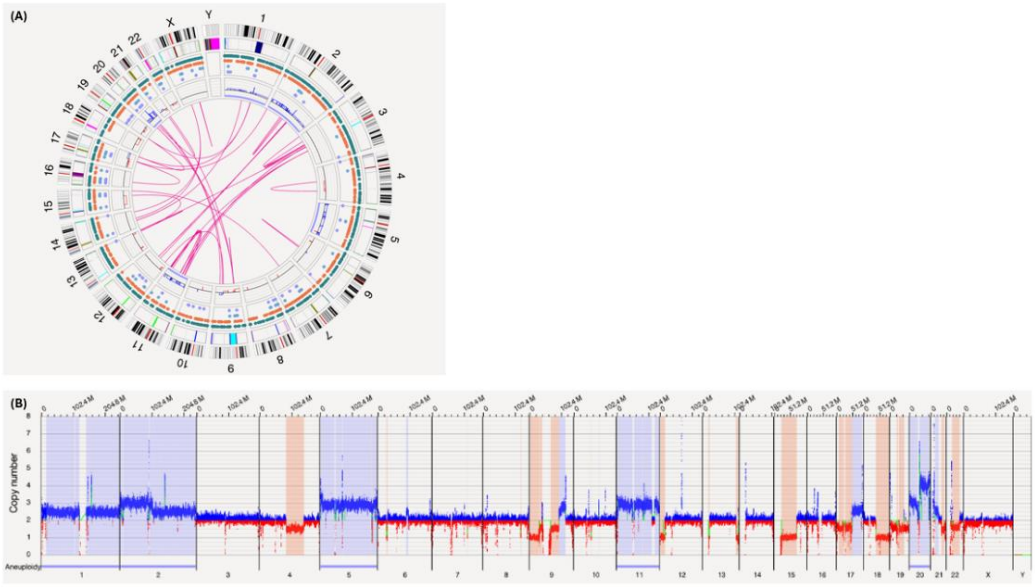

Figure 20. Optical Genome Mapping (OGM) analysis of tumoroid sample MSKPED0023. *(A) Circos plot showing genome-wide structural variants detected by OGM, including numerous intra- and inter-chromosomal rearrangements (pink lines) distributed across multiple chromosomes. (B) Copy number variation (CNV) profile derived from OGM data, illustrating genome-wide gains (blue) and losses (red) across chromosomes, with notable copy number alterations on chromosomes 1, 2, 4, 5, 8, 9, 15, 17, 20, and X.*

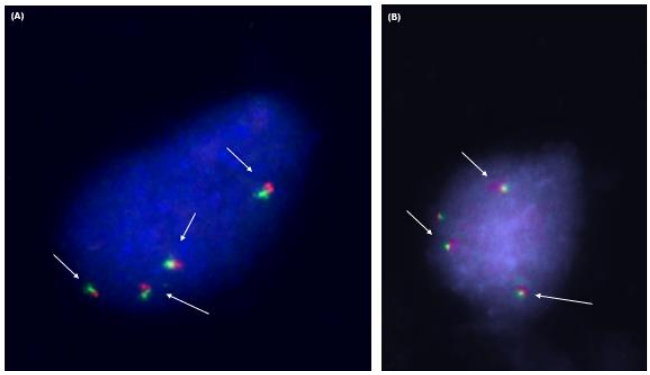

Figure 21. Break-apart FISH analysis of the MSKPED0023 tumoroid using a FOXO1 break-apart probe (3' in green, 5' in red). *(A) Interphase nucleus showing multiple co-localized red–green signals (arrows), resembling intact FOXO1 loci. (B) A second interphase nucleus confirming the co-localized signal pattern (arrows), with no evidence of a break-apart configuration. Both nuclei display approximately four paired red–green signals instead of the expected two, indicating amplification of the FOXO1 locus in the absence of rearrangement. The retained co-localization of 3'- and 5'-FOXO1 signals confirms an intact FOXO1 gene, consistent with the fusion-negative status of MSKPED0023 and in line with the absence of t(2;13)(q36.1;q14.11) detected by OGM.*

iv. Genomic characterization of MSKPED0087

The MSKPED0087 tumoroid was derived from a female patient diagnosed with fusion-negative rhabdomyosarcoma (FN-RMS) and is reported to harbor multiple point mutations, including *NRAS* Q61L, *ALK* V1058L, *ATR* L692I, *INSR* R813Q, and *TET1* N688S (**Table 4**). No inter-chromosomal translocation between chromosomes 2 and 13 was identified, confirming the absence of the *PAX3::FOXO1* fusion and consistent with the fusion-negative status of this tumoroid. To independently validate the fusion-negative status of MSKPED0087, break-apart FISH analysis was performed using a *FOXO1* break-apart probe (**Figure 23**). Interphase nuclei displayed co-localized red (5'-*FOXO1*) and green (3'-*FOXO1*) signals, consistent with an intact *FOXO1* locus, and no break-apart pattern was observed, confirming the absence of a *FOXO1* rearrangement. Notably, only a single fusion signal was detected per nucleus instead of the expected two, indicating loss of one *FOXO1* allele. This finding is consistent with the partial loss of chromosome 13 observed in the CNV-seq data derived from OGM (see below), and together these results provide validation of the fusion-negative status established by OGM.

Beyond the absence of a defining fusion event, OGM revealed an extremely complex genomic landscape characterized by widespread copy number alterations affecting nearly every chromosome (**Figure 22**). Broad chromosomal gains were observed involving chromosomes 1q, 2p/q, 5, 7, 8, 11, 12, 17q21-q25, 18p, 20, and Xq. The most prominent gain was a focal high-level amplification at chromosome 12q12q21.31 encompassing the oncogenes *CDK4*, *MDM2*, *HMGA2*, *GLI1*, and *ERBB3*, together with the co-amplified *STAT6*. Amplification of this 12q region is a recurrent event in rhabdomyosarcoma. Additional gains affected regions containing the oncogenes *ALK* and *PAX3* on chromosome 2; *FGFR4* and *PDGFRB* on 5q; *EGFR* and *CDK6* on chromosome 7; *FGFR1* and *NRG1* on chromosome 8; *RELA* and *CCND1* on 11q; *KRAS* on 12p; STAT3 and PRKCA on 17q21-q25; SS18 on chromosome 18; and GNAS on 20q. Several biologically important copy number losses were also detected. Most notably, a loss at chromosome 9p24.3-p21.1 affected the tumor suppressor gene *CDKN2A*, and an additional homozygous focal deletion at 9p21.3 involved the tumor suppressor genes *CDKN2A* and CDKN2B, together with the co-deleted *MTAP*. Loss of *CDKN2A/CDKN2B* is a recurrent alteration in genomically complex sarcomas. A loss at chromosome 13q11-q31.2 affected the tumor suppressor genes *BRCA2* and *RB1*, while losses on chromosome 17 involved the tumor suppressor gene *TP53* at 17p13.1-p11.2 and NF1 and RAD51D at 17q11.1-q21.2. An additional loss was identified at 9q22.32-q31.1 affecting the tumor suppressor gene PTCH1, and a loss was detected at 18q21.2-q23. Several other copy number alterations involved genes whose direction of alteration is not consistent with their canonical role in tumorigenesis (e.g., gain of tumor suppressors or loss of oncogenes) and were therefore considered likely passenger events within larger chromosomal segments; a complete overview is provided in **ADDENDUM H**. After filtering against the cancer-related gene panel, none of the translocations involved panel-relevant genes, and Bionano Access did not flag any of them as resulting in a putative fusion transcript. These rearrangements therefore most likely represent passenger events associated with the genomic instability of the tumor. In addition, two intrachromosomal structural variants involving panel-relevant genes were identified: a deletion involving *FGFR4* at 5q35.3 and a deletion involving *MTAP*, *CDKN2A*, and *CDKN2B* at 9p21.3. The *CDKN2A*/*CDKN2B* deletion was supported by both copy number analysis and structural variant detection, consistent with biallelic inactivation of these tumor suppressors.

Overall, these findings demonstrate that OGM characterized MSKPED0087 as a fusion-negative rhabdomyosarcoma with a highly complex and unstable genome. The genomic profile was dominated by widespread copy number alterations, including the focal 12q amplicon involving *CDK4* and *MDM2*, the recurrent 9p21.3 *CDKN2A/CDKN2B/MTAP* deletion, and combined loss of *TP53*, *RB1*, and *NF1*. Importantly, OGM also confirmed the absence of the *PAX3::FOXO1* fusion within the same assay, independently verified by break-apart FISH, demonstrating its ability to distinguish fusion-positive from fusion-negative rhabdomyosarcoma in a single genome-wide experiment.

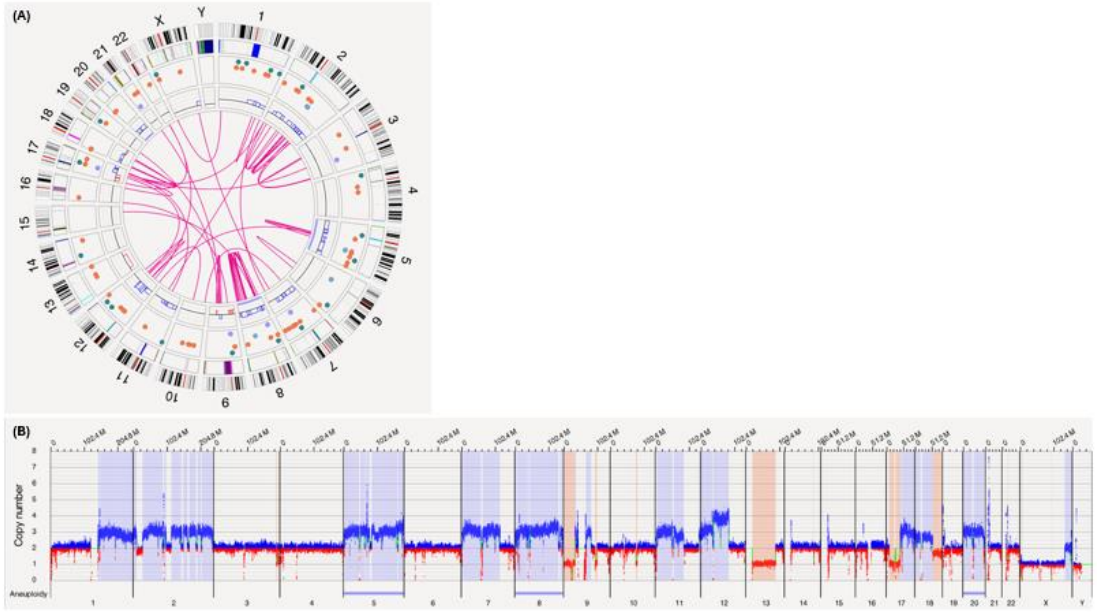

Figure 22. Optical Genome Mapping (OGM) analysis of tumoroid sample MSKPED0087*. (A) Circos plot showing genome-wide structural variants detected by OGM, including multiple inter-chromosomal rearrangements. (B) Copy number variation (CNV) profile derived from OGM data, illustrating genome-wide gains and losses across chromosomes*

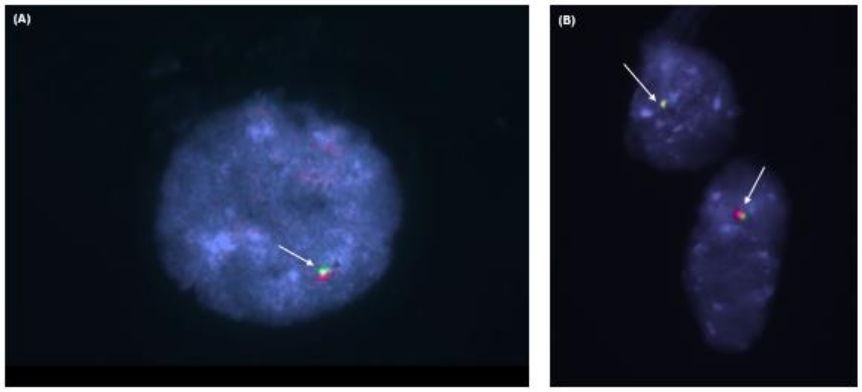

Figure 23. Break-apart FISH analysis of the MSKPED0087 tumoroid using a FOXO1 break-apart probe (3' in green, 5' in red). *(A) Interphase nucleus showing a single co-localized red–green signal (arrow), resembling an intact FOXO1 locus. (B) Two interphase nuclei each displaying a single co-localized signal (arrows), with no evidence of a break-apart pattern. The presence of only one fusion signal per nucleus instead of the expected two, indicates loss of one FOXO1 allele. The retained co-localization of 3'- and 5'-FOXO1 signals confirms an intact FOXO1 gene, consistent with the fusion-negative status of MSKPED0087 and in line with the absence of t(2;13)(q36.1;q14.11) detected by OGM.*

IV. Optical Genome Mapping of Sarcoma Tissue Samples

To establish a robust workflow for UHMW DNA extraction from primary sarcoma tissue, a stepwise optimization was performed across multiple tumor types, varying tissue dissociation methods (pestle vs tissue ruptor), tissue input mass, and processing conditions such as cryosectioning vs bulk frozen input and the use of a cell strainer (**Table 7**). Each step yielded specific lessons that informed adjustments to the protocol, ultimately defining the conditions under which UHMW DNA could be obtained. The individual steps and their outcomes are described in detail below.

Step	Sample type	Input (mg)	Method/condition	DNA yield (ng/µL)	OGM N50 (kbp)	Map rate (%)	Outcome/lesson learned
1	Leiomyosarcoma	~8–9	Pestle + tissue lyser (alternative; tissue ruptor not available)	0	-	-	No DNA recovered; both low input and non-optimal dissociation flagged as limitations
2	Myxoid mesenchymal tumor	~11	Tissue ruptor (manufacturer-recommended)	0	-	-	Failure persists with recommended equipment; low input mass identified as a critical limiting factor
3a	Chondrosarcoma	~18	Tissue ruptor + cell strainer (per protocol)	7.3	-	-	Standard protocol; lower yield in this single comparison
3b	Chondrosarcoma	~25	Tissue ruptor, no cell strainer (one-off comparison)	101.6	317.63	17.8	Higher yield but elevated PLV/NLV; cell strainer flagged for future optimization but retained per protocol
4a	Ewing sarcoma	20 sections	Cryosection input	0	-	-	No DNA detected; multiple possible causes (cell number, OCT, transfer loss
4b	Ewing sarcoma	20	Bulk frozen tissue input	72.8	250.5	30.1	
5a	MPNST (early frozen)	~43.8	Bulk frozen, ~40 min freezing delay	241	254.63	82.3	First high-quality OGM data from primary tissue; workflow validated
5b	MPNST (routine)	~39.5	Bulk frozen, ~2h freezing delay	120.3	243.75	84.2	Reduced yield but still suitable for OGM; encouraging for clinical workflows
6a	Synovial chondromatosis (early frozen)	~50	Validated workflow	0	-	-	Workflow does not generalize to ECM-rich tissues
6b	Synovial chondromatosis (routine)	~46	Validated workflow; ~4h freezing delay	0	-	-	Confirms ECM as a barrier independent of input mass

Table 7. Step-by-step optimization of UHMW DNA extraction from primary sarcoma tissue. *For each experiment, the sample type, input mass, applied method or condition, DNA yield, OGM molecule N50, map rate, and the corresponding outcome are listed in chronological order of execution. ECM, extracellular matrix; MPNST, malignant peripheral nerve sheath tumor; OCT, optimal cutting temperature compound; PLV, positive label variation; NLV, negative label variation. A (–) indicates that the metric was not determined.*

1) Pestle and tissue lyser dissociation

The Bionano Prep SP Tissue and Tumor DNA Isolation Kit recommends mechanical dissociation of frozen tissue using a tissue ruptor, with a minimum input of approximately 10 mg of tissue. As the tissue ruptor was not available in the laboratory at the start of the optimization experiments, initial extractions were performed using the most comparable alternatives accessible at the time. A single leiomyosarcoma tumor was divided into two small fragments (~8–9 mg each), one processed by manual dissociation with a pestle and the other by mechanical disruption with a tissue lyser, to directly compare both methods on matched material. No DNA was recovered from either sample (0 ng/µL for both the pestle- and tissue lyser-processed fragments), indicating that neither alternative dissociation strategy was compatible with the limited tissue input available. The combination of low starting material, which was already below the recommended minimum, and suboptimal dissociation equipment was therefore identified as a critical limitation, and the dissociation method was flagged as a key parameter requiring optimization once the recommended equipment became available.

2) Tissue ruptor: not sufficient for low-input samples

Once the tissue ruptor recommended by the manufacturer became available, the dissociation method was switched to align the protocol with the Bionano specifications. To assess whether the use of the recommended equipment would resolve the previous extraction failures, a low-input myxoid mesenchymal tumor sample (~11 mg) was processed using the tissue ruptor. Despite this protocol alignment, the extraction again yielded no detectable DNA (0 ng/µL). Although the input mass approached the manufacturer's recommended minimum of approximately 10 mg, the persistent extraction failure prompted us to test substantially higher tissue inputs in subsequent experiments (≥ 18 mg) to increase the likelihood of recovering sufficient UHMW DNA. The tissue ruptor was retained as the standard dissociation method for all further extractions, in line with the manufacturer's protocol.

3) Effect of cell strainer filtration on DNA yield

Building on the previous observations, the primary aim of this experiment was to test whether a substantially increased tissue input would improve UHMW DNA recovery. Two chondrosarcoma fragments from the same tumor sample were processed under otherwise identical conditions, with input masses of ~18 mg and ~25 mg, both well above the manufacturer's recommended minimum of 10 mg. During the protocol it was decided to additionally evaluate the influence of the post-dissociation cell strainer filtration step. The ~18 mg fragment was passed through a cell strainer following the standard manufacturer's protocol to remove undissociated tissue debris, while the ~25 mg fragment was processed without cell strainer filtration as a one-off comparison. Notably, both higher-input fragments yielded recoverable DNA, a marked improvement compared to the previous low-input attempts (Steps 1 and 2), confirming that increased tissue input mass enabled successful DNA recovery. The filtered sample yielded 7.3 ng/µL, which was insufficient to proceed to the subsequent labeling step, whereas the unfiltered sample yielded 101.6 ng/µL, a more than tenfold difference.

A possible explanation is that small clumps of dissociated cells and tissue debris are retained on the cell strainer mesh, reducing the cellular material available for downstream lysis and DNA extraction. However, as this comparison was performed only once, the result should be interpreted with caution and would require further replication before drawing firm conclusions. The cell strainer step was retained in subsequent extractions in accordance with the manufacturer's protocol, but the observation flagged this filtration step as a candidate parameter for future systematic optimization.

The unfiltered chondrosarcoma sample (~25 mg) was subsequently analyzed by OGM. While the molecule N50 of molecules ≥ 150 kbp (317.63 kbp) and the average label density (17.77 labels/100 kbp) met the recommended thresholds, additional quality metrics revealed substantial limitations. The N50 of molecules ≥ 20 kbp was only 90.75 kbp, indicating a large fraction of short DNA fragments alongside the longer UHMW molecules, and the molecule integrity number was 0.28, reflecting overall poor DNA integrity. The map rate reached only 17.8% and effective coverage was 47.05x, well below the 70% and 300x thresholds required for reliable downstream analysis. The negative label variance (NLV) was elevated at 22.72%, while the positive label variance (PLV) of 3.91% remained within acceptable range, indicating that a substantial proportion of expected reference labels were missing from the molecules and pointing to suboptimal labeling efficiency on this material. The presence of short DNA fragments may originate from pre-analytical factors prior to freezing, including extended ischemic time during sample transport, during which dying cells release shorter, degraded DNA while viable cells retain intact UHMW DNA. Additionally, chondrosarcoma is recognized as a particularly challenging tumor type for nucleic acid extraction due to its low cellularity and dense, glycosaminoglycan- and collagen-rich extracellular matrix, which may further impede efficient cell recovery and uniform labeling. Together, these factors indicate that further upstream optimization, potentially including chondrosarcoma-specific adaptations to the dissociation and pre-analytical workflow, would be needed before any modification to the filtration step could be reliably evaluated.

4) Tissue input format: cryosection versus bulk frozen tissue

A key requirement for routine diagnostic OGM analysis is reliable confirmation of tumor cell content in the input material, which is most commonly assessed on cryosections prior to or in parallel with DNA extraction. DNA extraction directly from cryosections is also widely described in the literature and would, in principle, allow the same physical material used for tumor cellularity assessment to be carried forward into the extraction workflow. To evaluate whether this approach was feasible with the current UHMW DNA isolation protocol, two aliquots from the same Ewing sarcoma sample were processed in parallel: one consisting of cryosections (20 sections of 20µg) and one consisting of bulk frozen tissue (20 mg). Pathological review confirmed an estimated tumor cell content of approximately 40% in the analyzed material. No detectable DNA was obtained from the cryosection sample (0 ng/µL), whereas the bulk frozen tissue yielded 72.8 ng/µL and was considered suitable for downstream OGM labeling. As tumor cellularity was confirmed to be adequate, the failed extraction from cryosections was unlikely to be explained solely by insufficient tumor content. However, because cryosections are the standard substrate for tumor cellularity assessment in routine diagnostic workflows, and because DNA extraction from cryosections is well established for other molecular assays, further optimization of UHMW DNA extraction from cryosections will be important to enable integration of OGM into routine diagnostic practice.

5) Impact of post-resection freezing delay on DNA quality

Following the observation that the chondrosarcoma sample contained a substantial fraction of short DNA fragments alongside the longer UHMW molecules (N50 ≥ 20 kbp of 90.75 kbp), a possible role of pre-analytical factors prior to snap-freezing was hypothesized: ischemic time between tumor resection and freezing may allow ongoing DNA degradation in dying cells, while shorter delays would be expected to better preserve intact UHMW DNA. To test this hypothesis, multiple tumor samples were collected directly from the operating theatre in a single session and processed under otherwise identical conditions, differing primarily in the time interval between resection and snap-freezing.

Two malignant peripheral nerve sheath tumor (MPNST) samples were included in this comparison. The first MPNST sample (~43.8 mg) was snap-frozen approximately 40 minutes after resection. The second MPNST sample (~39.5 mg) followed the routine clinical pathway, in which the tissue first passes through pathology before being transferred to the genetics laboratory, resulting in a freezing delay of approximately 2 hours.

The early-frozen MPNST sample yielded 241 ng/µL of UHMW DNA, while the routinely processed sample yielded 120.3 ng/µL, approximately half of the early-frozen sample. All OGM quality control metrics for the early-frozen sample met or exceeded the recommended thresholds (**Table 9**). For the routinely processed sample, all metrics were within the recommended ranges except for the molecule N50 (≥ 20 kbp), which was marginally below the threshold (145.68 kbp versus the recommended > 150 kbp). The reduced yield and the lower N50 (≥ 20 kbp) of the routinely processed sample compared to the early-frozen sample are consistent with the hypothesis that prolonged ischemic time contributes to DNA degradation, particularly affecting the proportion of short fragments in the overall DNA pool. Notably, both N50 (≥ 20 kbp) values remained substantially higher than that observed in the chondrosarcoma sample (90.75 kbp), supporting the interpretation that pre-analytical conditions influence the size distribution of recovered DNA. Despite the freezing delay, the routine 2-hour processing still produced material of sufficient quantity and quality for reliable OGM analysis. This is encouraging for the future application of OGM in a clinical-diagnostic workflow, where immediate freezing after resection is not always feasible and tissue typically follows the standard route through pathology before reaching molecular analysis. Importantly, this experiment also represented the first successful generation of high-quality OGM data from primary sarcoma tissue in this study, validating the workflow established up to this point (tissue ruptor dissociation in line with the manufacturer's protocol, bulk frozen tissue input, and sufficient input mass).

In contrast, two synovial chondromatosis samples were also retrieved from the operating theatre and processed in parallel using the same protocol. The first sample (~50 mg) was snap-frozen shortly after resection, while the second sample (~46 mg) followed the routine clinical pathway with a freezing delay of approximately 4 hours, providing an additional indication of the extent to which freezing delays can accumulate under standard diagnostic conditions. Despite the use of sufficient input masses, substantially exceeding those of all previous successful extractions, both samples failed to yield detectable DNA (0 ng/µL). Because both the early-frozen and the routinely processed synovial chondromatosis samples failed under otherwise validated conditions, the effect of freezing delay could not be isolated in this case. However, the consistent failure across both conditions suggested that the high extracellular matrix (ECM) content typical of cartilaginous tissue may have formed a physical barrier for efficient cell lysis and DNA release, regardless of input quantity or freezing delay. This observation indicated that input mass alone is not a reliable predictor of extraction success and that tissue composition, particularly ECM content, must be taken into account when planning sample workup. As the focus of this experiment was on the influence of freezing delay rather than on tissue composition, no specific pre-treatment for ECM-rich tissues had been incorporated; for such tumor types, additional pre-treatment steps (e.g., extended enzymatic digestion or matrix dissolution) would likely be required.

Of the seven primary sarcoma samples processed during this optimization, four produced UHMW DNA of sufficient quantity to proceed to OGM labeling and data collection: the unfiltered chondrosarcoma, the bulk frozen Ewing sarcoma, and the two MPNST samples (early frozen and routinely processed). Both MPNST samples met all recommended quality thresholds and were considered suitable for full downstream structural variant and copy number analysis. The chondrosarcoma sample, although meeting the molecule N50 and label density thresholds, failed both the map rate (17.8%) and effective coverage (47.05x) criteria; this dataset was nevertheless retained for downstream analysis, with results interpreted with appropriate caution given the reduced quality metrics. The Ewing sarcoma sample similarly failed the map rate (30.1%) and effective coverage (37.66x) thresholds and was excluded from further analysis.

i. OGM analysis of Chondrosarcoma

Quality control analysis of the chondrosarcoma OGM run showed that several metrics fell below the manufacturer's recommended thresholds (**Table 8**). The extracted DNA was extensively fragmented, resulting in short DNA molecules that contained too few fluorescent label patterns for reliable alignment to the reference genome. This was reflected in a markedly reduced map rate and an effective coverage far below the recommended ≥ 300x threshold. In contrast, the label density remained within the expected range, indicating that the DLE-1 labeling reaction itself had functioned properly. The reduced run quality was therefore mainly attributable to upstream DNA fragmentation rather than a failure of the labeling process.

	Molecule N50 (≥ 150kbp)	Molecule N50 (≥ 20kbp)	Label density (/100 kbp)	Map rate (%)	Effective coverage (x)	Positive label variance (PLV)(%)	Negative label variance (NLV)(%)
Chondrosarcoma	317.63	90.75	17.77	17.8	47.05	3.91	22.72
TRESHOLD	≥ 250	≥ 150	14-17	≥ 70	≥ 300	< 10	< 15

Table 8. Quality control metrics of the Optical Genome Mapping run for the primary chondrosarcoma sample. *Metric definitions and recommended thresholds are described in the Data analysis workflow section. Values below the recommended thresholds are highlighted in red.*

The impact of the low coverage differed between CNV and SV analysis. CNV detection is primarily based on read-depth across larger genomic regions and can still be performed at relatively low coverage. However, the broad and noisy CNV profile observed in this sample was difficult to interpret using OGM alone, as some apparent alterations may partly reflect baseline noise rather than true genomic events. To address this limitation, shallow whole-genome CNV sequencing (CNV-seq) was performed in parallel for orthogonal comparison. Structural variant detection was more strongly affected by the reduced coverage. At the obtained effective coverage of approximately 34x, high-clonality events and germline variants were still expected to be detectable, whereas low-frequency subclonal rearrangements likely fell below the minimum molecule support threshold applied in this study. As a result, the SV call set is likely biased toward larger clonal events, with smaller subclonal alterations potentially being missed.

Despite these technical limitations, OGM revealed a highly complex genomic landscape with widespread copy number gains and losses across nearly all chromosomes. Multiple gains involved regions containing oncogenes, including *RAF1*, *EGFR*, *CDK6*, *MET*, *NTRK2*, *KRAS*, *YAP1*, and *PRKCA*. Several losses involved regions containing the tumor suppressor genes CDH1, *SMAD4*, and *CIC*. Particularly notable was a deletion at 12q13-q14 involving *COL2A1*, the main extracellular matrix gene of cartilage, which is recurrently altered in chondrosarcoma. Several other copy number alterations involved genes whose direction of alteration is not consistent with their canonical role in tumorigenesis and were therefore considered likely passenger events within larger chromosomal segments; a complete overview is provided in **ADDENDUM I**. Both the OGM and CNV-seq profiles displayed substantial background noise and used different thresholds for gain/loss calling, so the two techniques cannot be directly compared call-by-call. On a global scale, however, the two profiles showed a broadly similar pattern of chromosomal imbalances, suggesting that the major clonal copy number events are captured by both techniques, although only the largest, clearly visible alterations can be considered reliable in this dataset (**Figure 24**).

Structural variant analysis identified 23 intrachromosomal rearrangements, including deletions, duplications, insertions, and inversions, with a notable clustering of events on chromosome 11p12. In addition, nine inter-chromosomal translocations were detected. Given the limited overall number of structural variants in this sample, all events were screened individually without restricting the analysis to the cancer-related gene panel applied for the other samples. None of the intrachromosomal rearrangements involved panel-relevant genes. Among the inter-chromosomal translocations, three generated putative fusion transcripts: *NAALADL2::PEX7, KANK1::DMRTA1*, and *LINC02594::PRKCA*. Visual inspection of the SV call set in Bionano Access showed that not all calls were equally well supported, with some events backed by adequate molecule coverage on both sides of the breakpoint and others poorly supported, likely reflecting artefacts caused by the compromised DNA integrity and reduced effective coverage. None of the three putative fusions has been previously described, and their clinical relevance remains unclear. The SV call set in this sample should therefore be regarded as preliminary.

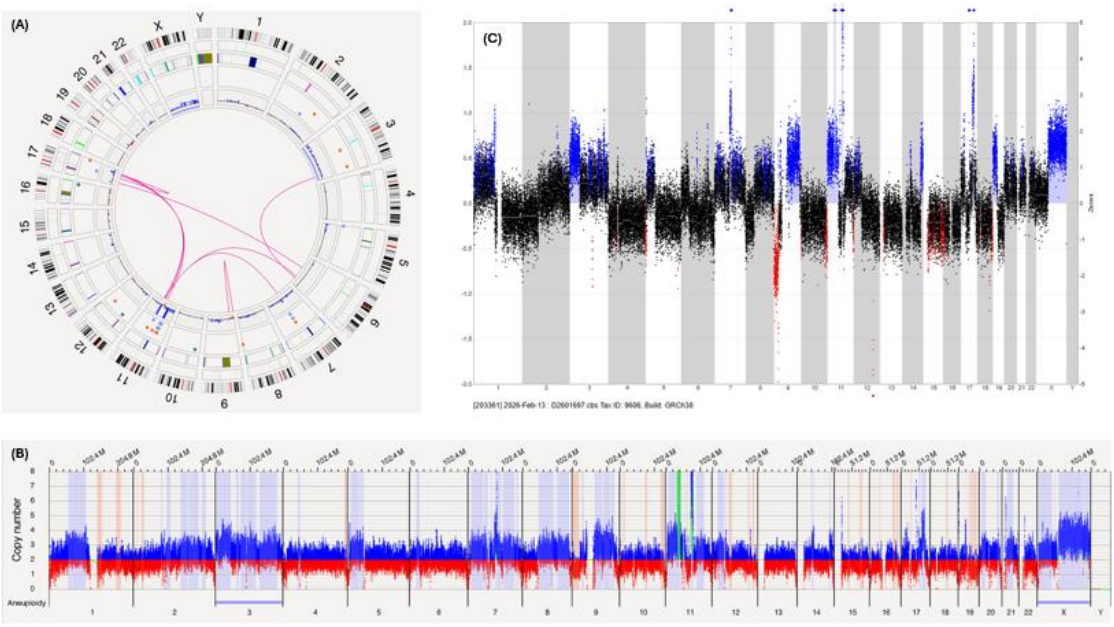

Figure 24. Genomic profiling of a chondrosarcoma sample using Optical Genome Mapping (OGM) and CNV sequencing*. (A) Circos plot derived from OGM showing genome-wide structural variants. (B) Copy number variation (CNV) profile obtained from OGM data, illustrating genome-wide gains (blue) and losses (red). (C) CNV plot obtained by sWGS.*

ii. OGM analysis of A Malignant Peripheral Nerve Sheath Tumor (MPNST)

The two paired MPNST samples: snap-frozen approximately 40 minutes versus 2 hours after surgical resection (see UHMW DNA extraction optimization), both yielded OGM data of sufficient quality for downstream analysis (**Table 9**). For the OT sample, all quality control metrics met or exceeded the manufacturer's recommended thresholds. For the routine sample, the N50 (≥ 20 kbp) was marginally below the recommended threshold (145.68 kbp versus the recommended > 150 kbp), consistent with a slightly higher proportion of short DNA fragments in the longer-stored sample. All other metrics, including the N50 (≥ 150 kbp), label density, map rate, effective coverage, and label variances, met the recommended thresholds in both samples. It is important to note that the OT and routine samples were obtained from two different fragments of the same tumor, so any differences observed between the two profiles may reflect not only technical detection differences between the two runs but also genuine intra-tumoral heterogeneity at the cellular level.

	Molecule N50 (≥ 150kbp)	Molecule N50 (≥ 20kbp)	Label density (/100 kbp)	Map rate (%)	Effective coverage (x)	Positive label variance (PLV)(%)	Negative label variance (NLV)(%)
MPNST (OT)	254.63	173.63	14.5	82.3	378.87	4.13	11.9
MPNST (Routine)	243.75	145.68	14.87	84.2	348.2	4.36	10.75
TRESHOLD	≥ 250	≥ 150	14-17	≥ 70	≥ 300	< 10	< 15

Table 9. Quality control metrics of the Optical Genome Mapping runs for the paired MPNST samples (OT and routine). *Metric definitions and recommended thresholds are described in the Data analysis workflow section. Values below the recommended thresholds are highlighted in red.*

The two samples showed a high degree of concordance in their genomic profiles, particularly at the copy number level. All 43 copy number alterations were similar between both samples in terms of chromosomal region, abnormality type, involved genes, and copy number state. Structural variant calls were also largely shared: three inter-chromosomal translocations (t(7;7), t(14;17), and t(17;17)) and four intrachromosomal events (*CDK6* deletion, *NRG1* duplication, *NF1* insertion, and *GNAS* duplication) were detected in both samples. Beyond these shared calls, the OT sample contained five additional sample-specific structural variants that were not detected in the routine sample, while the routine sample contained only one additional sample-specific event. Specifically, the OT sample additionally harboured a t(7;20) inter-chromosomal translocation, an inversion and a duplication involving *EGFR* (7p11.2), a *HRAS* duplication (11p15.5), and a deletion involving *RNF43* and *RAD51C* (17q22). The routine sample uniquely contained a *MYCN* deletion (2p24.3). Overall, the OT sample therefore yielded a higher total number of detected structural variants (12 versus 8 in the routine sample, considering panel-relevant events only). This higher SV yield in the OT sample is consistent with its better preserved DNA integrity, as reflected in the higher N50 (≥ 20 kbp), and likely indicates increased sensitivity for detection of smaller or lower-clonality structural events under optimal pre-analytical conditions. The presence of sample-specific events in both directions (five in OT, one in routine) further suggests that intra-tumoral heterogeneity between the two analyzed tumor fragments also contributed to the observed differences.

Both samples displayed a highly complex genomic landscape characterized by widespread copy number alterations affecting nearly all chromosomes (**Figure 25**). The profile was dominated by broad chromosomal gains involving numerous oncogenes, including regions containing *NRAS*, *ALK*, *RAF1*, *PDGFRB*, *CDK6*, *MET*, *SMO*, *BRAF*, *FGFR1*, *NTRK2*, *CCND1*, *YAP1*, *PRKCA*, *SS18*, and *GNAS*. Particularly notable were focal amplifications involving the oncogenes *CDK6*, *MET*, and *BRAF* on chromosome 7q.

Several biologically important losses were also identified. Most striking was a homozygous deletion at chromosome 9p21.3 involving the tumor suppressor genes *CDKN2A*, *CDKN2B*, and *MTAP*, a well-known recurrent alteration in MPNST. In addition, a deletion involving the tumor suppressor gene *NF1* on chromosome 17q11.2 was detected, consistent with the central role of *NF1* loss in MPNST pathogenesis. A concurrent loss of the tumor suppressor gene *TP53* at chromosome 17p13.1 was also observed. The combined loss of *NF1*, *CDKN2A/CDKN2B*, and *TP53* corresponds to the classical genomic profile of high-grade MPNST. Additional losses affected regions containing the tumor suppressor genes *BRCA2* and *RB1*. Several other copy number alterations involved genes whose direction of alteration is not consistent with their canonical role in tumorigenesis (e.g., gain of tumor suppressors or loss of oncogenes) and were therefore considered likely passenger events within larger chromosomal segments; a complete overview is provided in **ADDENDUM J and K**

Beyond copy number alterations, OGM revealed an extremely complex structural variant landscape in both samples. Unfiltered circos plots demonstrated dense networks of interconnected rearrangements involving multiple chromosomes simultaneously, particularly chromosomes 7, 11, 14, 17, and 20.

After filtering against the cancer-related gene panel, four inter-chromosomal translocations remained in the OT sample, involving *EGFR*, *GNAS*, *PRKCA*, and *RAD51C*. Three of these rearrangements: t(7;7), t(14;17), and t(17;17) were also identified in the routine sample, demonstrating a high degree of concordance between both conditions. The fourth translocation, a t(7;20) associated with *GNAS*, was detected only in the OT sample. Visual inspection of this call in Bionano Access showed adequate molecule and label support on both sides of the breakpoint, indicating that it represents a true structural event. A separate intrachromosomal duplication involving the *GNAS* region on 20q13.32 was independently detected in both samples, indicating that the *GNAS* locus is recurrently rearranged in this tumor; the t(7;20) translocation and the 20q duplication are however structurally distinct alterations and should not be considered the same underlying event.

Several intrachromosomal structural variants were also shared between both samples, including alterations involving *CDK6*, *NRG1*, *NF1*, and *GNAS*. The OT sample additionally showed alterations involving *EGFR*, *HRAS*, *RNF43*, and *RAD51C*, whereas the routine sample uniquely contained a deletion involving *MYCN*.

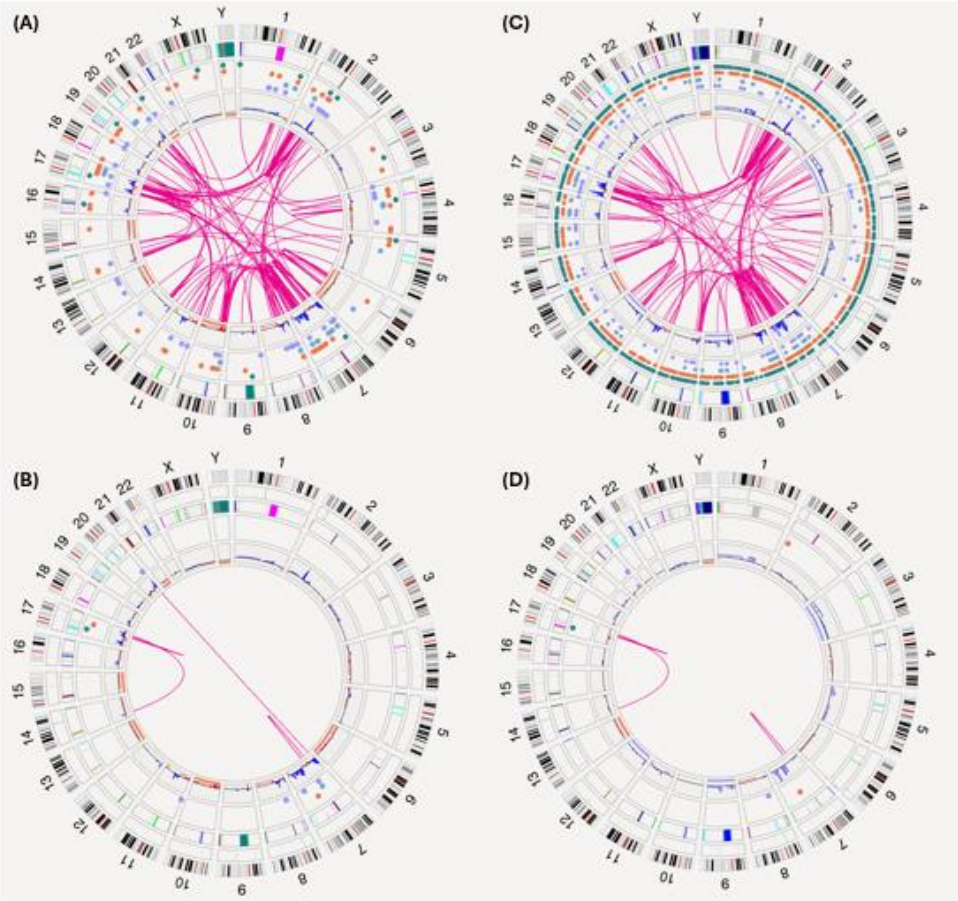

Figure 25. Optical Genome Mapping (OGM) circos plots of MPNST samples with different freezing conditions ((A,B) = OT vs (C,D) = routine condition). *(A) Circos plot of the MPNST sample that was snap-frozen 40 minutes after surgical resection (OT sample). (B) Corresponding circos plot filtered for sarcoma-associated gene panels. (C) Circos plot of the MPNST sample processed under routine conditions and frozen after 4 hours. (D) Filtered circos plot for the routine sample, focusing on cancer-related genes.*

The genome-wide copy number profile of the MPNST routine sample obtained by shallow whole-genome sequencing (CNV-seq) was compared to the profile derived from Optical Genome Mapping (OGM) (**Figure 26**). The two profiles were generated from two different aliquots of tumor tissue, both obtained under routine pathology handling but not from strictly identical fragments.

Visual inspection on a chromosome-by-chromosome basis revealed essentially matching patterns across the majority of chromosomes between both techniques. The major MPNST-defining copy number alterations were detected by both assays, including the homozygous deletion of *CDKN2A*, *CDKN2B*, and *MTAP* on 9p21.3, as well as gains involving *SPOP*, *RNF43*, *RAD51C*, *BRIP1*, and *PRKCA*. A loss within 4q was identified by both assays, although the exact boundaries differed slightly between methods. One notable region of discordance was observed on chromosome 12: OGM called a chromosome-wide gain, while the CNV-seq profile showed the same overall pattern but positioned closer to the baseline rather than as a clear gain. Additional smaller copy number changes called by OGM were not always supported by CNV-seq, and a small number of CNV-seq calls were not confirmed by OGM.

Beyond the copy number profile, OGM detected several structural variants that are by definition not visible to CNV-seq, including intragenic deletions of *MYCN* and *CDK6*, duplications of *NRG1* and *GNAS*, an insertion in *NF1*, and translocations with breakpoints in *EGFR*, *PRKCA*, and *RAD51C*.

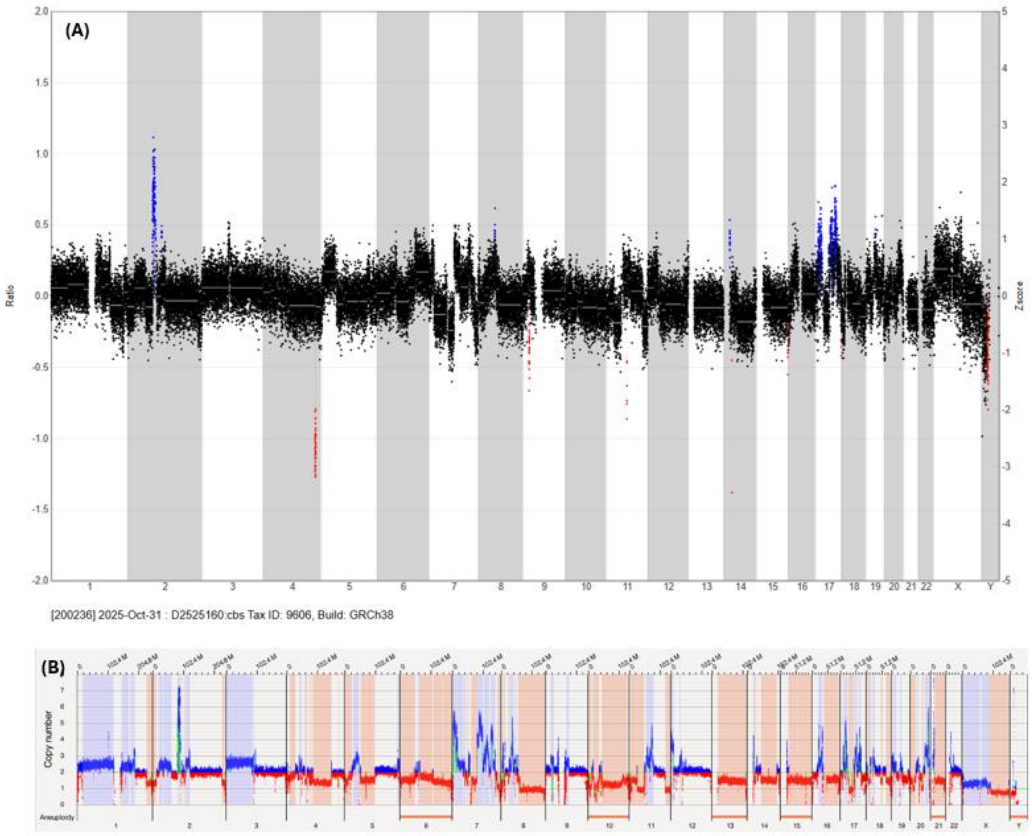

Figure 26. Genome-wide copy number profile of MPNST sample. *(A) CNV-seq plot. (B) OGM-derived CNV plot. Gains are shown in blue and losses in red.*

Overall, OGM analysis of the paired MPNST samples revealed a highly complex and genomically unstable tumor characterized by the three hallmark alterations of MPNST: *NF1* loss, *CDKN2A/CDKN2B/MTAP* deletion, and *TP53* loss. Importantly, the genomic profiles obtained from the OT and routine samples were highly concordant, including the major diagnostic alterations and the majority of structural rearrangements. A modest reduction in sensitivity for detecting smaller structural variants was observed in the routine sample, consistent with the slightly increased DNA fragmentation associated with the longer pre-analytical delay, and part of the sample-specific differences likely also reflects intra-tumoral heterogeneity between the two analyzed tumor fragments. Together, these findings demonstrate that routine clinical pre-analytical handling did not substantially compromise the diagnostic quality of the OGM data, which is encouraging for future implementation of OGM in routine sarcoma diagnostics where immediate snap-freezing may not always be feasible.

iii. OGM analysis of Ewing sarcoma

The Ewing sarcoma case provided two paired samples processed in parallel: one as cryosections (20 sections of 20µg) and one as bulk frozen tissue (20 mg). The cryosection material yielded no detectable DNA and could not be processed further (Step 4 in **Table 7**). The bulk frozen aliquot yielded 72.8 ng/µL of UHMW DNA and was loaded onto the Saphyr instrument.

As summarized in the table below, the run failed to meet several key OGM quality criteria. Although the molecule N50 (250.5 kbp) reached the recommended threshold, both the map rate and effective coverage were markedly below the required values, while the label density exceeded the optimal range. The combination of excessive label density with a low map rate suggests non-specific or over-labeling, resulting in DNA molecules that could not be reliably aligned to the reference genome. Because multiple QC parameters failed simultaneously, no downstream analysis was performed for this sample (**Table 10**).

This case nonetheless yielded two practical insights complementing the extraction-step optimizations: cryosection material was not viable as input format under the conditions tested, and adequate DNA yield does not guarantee adequate downstream OGM data quality (**Table 7**).

	Molecule N50 (≥ 150kbp)	**Molecule N50 (≥ 20kbp)**	**Label density (/100 kbp)**	**Map rate (%)**	**Effective coverage (x)**	**Positive label variance (PLV)(%)**	**Negative label variance (NLV)(%)**
Ewing sarcoma	250.5	66.75	19.99	30.1	37.66	3.44	19.45
TRESHOLD	≥ 250	≥ 150	14-17	≥ 70	≥ 300	< 10	< 15

Table 10. Quality control metrics of the Optical Genome Mapping runs for Ewing sarcoma. *Metric definitions and recommended thresholds are described in the Data analysis workflow section. Values below the recommended thresholds are highlighted in red.*

6. Discussion

The aim of this study was to evaluate whether Optical Genome Mapping (OGM) can serve as a clinically relevant method for detecting structural variants in sarcomas, and how it differs from diagnostic workflows that are currently used in clinical practice. To address this question, OGM was applied to three different types of sarcoma material: rhabdomyosarcoma (RMS) cell lines, patient-derived RMS tumoroids, and primary sarcoma tissue samples, including chondrosarcoma, malignant peripheral nerve sheath tumor (MPNST), and Ewing sarcoma.

The study first started with cell lines, as these represent a relatively homogeneous and well-characterized model system with established molecular profiles. In addition, the extraction of ultra-high molecular weight (UHMW) DNA from cell pellets using the Bionano Prep SP Frozen Cell Pellet DNA Isolation Kit is technically straightforward and had already been validated in our laboratory, consistently yielding DNA of sufficient quality for OGM analysis. Cell lines therefore provided an ideal starting point to gain familiarity with the OGM workflow without the need for additional protocol optimization.

After establishing confidence in the workflow, patient-derived RMS tumoroids were introduced as an intermediate model. Compared with conventional cell lines, tumoroids more closely preserve the biological heterogeneity and genomic complexity of the original patient tumor. The PEDSAR tumoroids analyzed in this study are recently developed models with only limited prior molecular characterization, and genome-wide profiling by OGM therefore contributed not only to evaluating the technique itself, but also to a better understanding of the genomic background of these novel preclinical models. This genomic characterization is particularly relevant in the context of ongoing preclinical drug screening work in our laboratory, in which the same tumoroids are being used to evaluate the response of patient-derived rhabdomyosarcoma models to targeted therapies. Practically, because these are still cultured cells, the same validated cell pellet-based extraction protocol could be applied. Tumoroids therefore formed a logical bridge between highly controlled cell line experiments and the more technically demanding analysis of primary tumor tissue. The final stage of this project focused on primary sarcoma tissue samples, which represented the most challenging and exploratory component of the study. Unlike the cell pellet workflow, the Bionano Prep SP Tissue and Tumor DNA Isolation Kit had not previously been implemented in our laboratory for sarcoma samples, and no optimized protocol for UHMW DNA extraction from these tissue types was available. As a result, this part of the study involved extensive optimization of tissue processing, dissociation conditions, and DNA isolation parameters to determine which conditions were most compatible with the specific characteristics of sarcoma tissue.

The findings of this study are discussed in the context of four themes: (1) pre-analytical feasibility and technical optimization, (2) diagnostic accuracy, (3) characterization of genomic complexity, and (4) the potential clinical and prognostic implications of implementing OGM in sarcoma diagnostics.

I. Pre-analytical Feasibility and Technical Optimization of UHMW DNA extraction

One of the main findings of this study was that the success of Optical Genome Mapping (OGM) is highly dependent on pre-analytical factors, particularly the ability to extract ultra-high molecular weight (UHMW) DNA from primary sarcoma tissue. In total, eleven primary tissue extractions were performed under varying experimental conditions during the optimization phase, of which two ultimately yielded DNA of sufficient quality and quantity for downstream OGM analysis. This outcome should not be interpreted as a representative success rate of the technique itself, since the samples were intentionally processed under a range of different conditions rather than according to a single validated protocol. Establishing a true success rate for our laboratory will require applying the optimized workflow to a larger series of consecutive samples. Nevertheless, the comparison with previously reported success rates in studies that already used optimized workflows (72%, 38/53 and 62.3%, 33/53, respectively) is informative.[3,33] Even under optimized conditions, success rates of around 60–70% indicate that OGM extraction from primary sarcoma tissue does not always succeed, underlining that this remains a technically demanding application. The experiments performed here therefore primarily provided insight into the parameters that most strongly determine extraction success, rather than a benchmark of overall feasibility.

In contrast to primary tissue, UHMW DNA extraction from RMS cell lines and patient-derived tumoroids using the Bionano Prep SP Frozen Cell Pellet DNA Isolation Kit was successful in nearly all samples. Of the cultured samples processed in this study, only one tumoroid (PEDSAR01) failed to meet the quality control thresholds and had to be excluded from further analysis, whereas all other cell lines and tumoroids yielded DNA of sufficient quality and quantity for OGM analysis. This single failure is consistent with the known sensitivity of OGM to even subtle reductions in DNA integrity: as soon as cells begin to undergo cell death, the resulting DNA fragmentation becomes detectable in the OGM quality metrics. The exclusion of PEDSAR01 therefore falls within the expected behavior of the technique rather than indicating a problem with the cell pellet workflow itself. This clear difference between cultured cell pellets and primary tissue demonstrates that the main technical bottleneck for clinical OGM implementation lies in the extraction of intact long DNA molecules from heterogeneous tumor tissue. This observation is in line with previous studies identifying tissue dissociation as one of the most challenging steps in applying OGM to solid tumors.[54]

The first parameter we evaluated in this study was the tissue dissociation method. According to the manufacturer's protocol, approximately 10 mg of tissue is recommended as starting input material, and tissue dissociation is ideally performed using a tissue ruptor to minimize excessive DNA shearing. Because a tissue ruptor was initially not available in our laboratory, the first extractions were performed on small leiomyosarcoma fragments (~8–9 mg) using a pestle followed by a tissue lyser as an alternative dissociation strategy. However, these attempts yielded no detectable DNA yield. The aggressive mechanical disruption generated by the tissue lyser likely caused excessive DNA fragmentation, compromising the integrity of the ultra-high molecular weight DNA molecules required for OGM. Once a tissue ruptor became available, the dissociation method was adapted to align with the manufacturer's recommendations. Nevertheless, applying the tissue ruptor to a low-input myxoid mesenchymal tumor sample (~11 mg) still did not immediately provide extraction success. This finding suggests that sufficient tissue input mass is a prerequisite for successful DNA recovery, regardless of the dissociation method used. Overall, these experiments highlighted the central technical challenge of OGM pre-analytical parameters: achieving enough mechanical disruption to release DNA from the tissue matrix while simultaneously preserving long DNA molecule integrity. Compared with homogeneous cell lines, maintaining this balance proved considerably more difficult in heterogeneous sarcoma tissue, consistent with previous reports.[54]

A second parameter examined was the use of the 40 µm cell strainer included in the manufacturer's protocol to remove undissociated tissue debris. A direct comparison of two chondrosarcoma fragments demonstrated that the unfiltered sample (~25 mg) yielded a markedly higher DNA concentration than the filtered sample (~18 mg), with concentrations of 101.6 ng/µL and 7.3 ng/µL, respectively. However, despite the higher DNA yield, the unfiltered sample produced poor-quality OGM data characterized by a reduced map rate and a markedly lower N50 (≥ 20 kbp) than the recommended threshold, indicating substantial DNA fragmentation. This finding is methodologically important because it demonstrates that DNA quantity alone is not predictive of successful OGM performance. High DNA concentration does not necessarily suggest preservation of long intact molecules. Once fragmentation occurs during upstream tissue dissociation, downstream workflow optimization cannot restore DNA integrity. Although this comparison was performed only once and involved samples with slightly different input masses, it identified the filtration step as a parameter requiring further systematic investigation. In subsequent experiments, the cell strainer step was retained according to the manufacturer's protocol, while tissue ruptor processing times were minimized to reduce shear-induced fragmentation.

The physical format of the starting tissue also proved to be important. A direct comparison was performed between cryosections and bulk frozen tissue from the same Ewing sarcoma specimen, with both fragments obtained from the same tumor sample and processed in parallel under otherwise identical conditions to minimize confounding variables. One fragment was used to prepare 20 cryosections, while the second fragment was retained as bulk frozen tissue (~20 mg). The cryosection sample yielded no detectable DNA despite an estimated tumor cell content of approximately 40%, while the bulk frozen fragment yielded 72.8 ng/µL of UHMW DNA. Several technical explanations may account for the cryosection failure, including interference from OCT embedding medium during lysis, loss of fragile tissue sections during handling, or reduced recovery of intact tissue from sectioned material. Although the bulk frozen sample ultimately failed several OGM quality metrics, the comparison established bulk frozen tissue as the more robust starting material in our hands. Importantly, this observation should be interpreted cautiously, as OGM has previously been performed successfully on cryosection-derived material, indicating that cryosections are not inherently incompatible with OGM.[3] The failure observed here may therefore reflect technical variability during the initial optimization phase rather than a fundamental limitation of cryosections themselves. Nevertheless, based on the present findings, a minimum tissue input of approximately 20–40 mg of bulk frozen tissue appears advisable, in agreement with previous recommendations.[33] This input requirement is notably higher than the ~10 mg minimum specified in the Bionano manufacturer's protocol, suggesting that in practice substantially more starting material may be required for reliable UHMW DNA extraction from sarcoma tissue than the manufacturer's recommendations indicate. From a practical perspective, these observations suggest that biobanks intending to support future OGM analysis should preferentially preserve sufficiently large bulk frozen tissue fragments. However, bulk frozen tissue alone is not an ideal long-term solution for routine diagnostic implementation: cryosections remain the standard substrate for assessing tumor cell content, are widely used for DNA extraction in other molecular assays, and offer the advantage of directly linking the analyzed material to a defined tumor area. Further optimization of UHMW DNA extraction from cryosections is therefore an important step toward integrating OGM into routine sarcoma diagnostics, and represents a clear priority for future technical development.

The influence of post-resection delay before snap-freezing was evaluated using two MPNST samples processed under otherwise identical conditions. The first sample, which was snap-frozen approximately 40 minutes after surgical resection using an operating-theater workflow, yielded 241 ng/µL of UHMW DNA and generated high-quality OGM data. The second sample, frozen approximately two hours after resection following routine pathology handling, yielded a lower DNA concentration (120.3 ng/µL) but still produced OGM data of comparable quality, with all recommended quality metrics achieved and a genomic profile highly concordant with the first sample, including the major MPNST-associated alterations. From a translational perspective, this is one of the most clinically relevant findings of the study. Although rapid snap-freezing improved DNA yield, even a routine two-hour delay still resulted in diagnostically usable material. This suggests that OGM can be integrated into existing biobanking and pathology workflows without requiring immediate processing directly after surgery. While this observation is based on only a single paired comparison, it nevertheless provides encouraging evidence that OGM may be compatible with routine clinical handling procedures. As a side note, the synovial chondromatosis samples in this study were also processed with two different delays (immediately after resection and after approximately four hours), but as both extractions failed for reasons attributable to the ECM-rich tissue composition rather than the freezing delay, it remains unknown whether a four-hour delay would still allow successful OGM analysis. Whether routine workflows with even longer pre-analytical delays remain compatible with OGM will therefore need to be addressed in future, dedicated experiments.

Another important determinant of extraction success was tissue composition. Two synovial chondromatosis samples (~50 and ~46 mg) failed to yield detectable DNA despite sufficient input quantities that exceeded all previously successful extractions. Because at least one of these samples was processed under otherwise optimized conditions, with immediate snap-freezing after resection, the failure cannot be attributed to pre-analytical delay and strongly suggests that the dense extracellular matrix (ECM) characteristic of cartilaginous tissue acts as a physical barrier that limits efficient lysis and DNA release. For the second sample, which was frozen approximately four hours after resection, an additional contribution of the freezing delay cannot be excluded. This observation closely matches tissue-dependent extraction patterns described in the literature. Substantially lower extraction success rates have previously been reported in adipocytic and bone-derived tumors compared with non-adipocytic sarcomas.[3,33] Biologically, this is likely explained by the high lipid content of liposarcomas, low cellularity of myxoid tumors, and dense ECM composition of cartilaginous and osseous tissue, all of which interfere with efficient recovery of intact DNA molecules. For ECM-rich tissues, additional pre-treatment strategies such as prolonged enzymatic digestion or matrix dissolution may be necessary, although these approaches were beyond the scope of the current study. Importantly, these findings demonstrate that tissue input mass alone is not a reliable predictor of extraction success and that tissue composition must be considered when selecting samples for OGM analysis.

Overall, the optimization experiments performed in this study identified tissue dissociation method, tissue input mass, sample format, tissue composition, and post-resection handling time as the major determinants of successful UHMW DNA extraction from primary sarcoma tissue. Based on these findings, the most reliable workflow consisted of using bulk frozen tissue with a minimum input of 20–40 mg, combined with carefully controlled tissue ruptor dissociation while minimizing excessive mechanical processing. Although this workflow provides a practical foundation for future studies and potential clinical implementation, ECM-rich tumor types remain particularly challenging, as demonstrated in the present study by the failed synovial chondromatosis extractions. Adipocytic tumor types were not tested in this study, but have previously been described in the literature as particularly difficult substrates for UHMW DNA extraction due to their high lipid content.[3,33] Further protocol development specific to these tissue types will therefore be required before OGM can be applied reliably across the entire spectrum of sarcoma subtypes.

II. Diagnostic accuracy: From Targeted Detection to Comprehensive Profiling

The second major theme of this study was the diagnostic accuracy of OGM compared with standard cytogenomic techniques. Across all RMS cell lines and tumoroids analyzed, OGM consistently detected the canonical *PAX3::FOXO1* fusion in fusion-positive samples (RH30, PEDSAR02, and PEDSAR03) and correctly confirmed its absence in fusion-negative samples (RMS-YM, MSKPED0023, and MSKPED0087). These findings were independently confirmed by *FOXO1* break-apart FISH, with complete concordance between both methods. This is consistent with previously published data, where OGM showed high detection rates for diagnostic structural variants in sarcoma cohorts, with reported concordance rates of 91% and 95.2%, respectively.[3,33] In both studies, the small fraction of discordant cases is informative. In the first cohort, the single missed alteration was a *COL6A3::CSF1* fusion in a tenosynovial giant cell tumor, which is characterized by an intrinsically low percentage of neoplastic cells and is therefore poorly suited to OGM analysis of bulk DNA.[33] In the second cohort, the three discordant cases each illustrated a different limitation of the technique: one *MDM2* amplification, one *STAT6::NAB2* small intrachromosomal inversion fell below the resolution determined by the average label density, and one *CIC::DUX4* fusion involved breakpoints in highly repetitive genomic regions that cannot be reliably mapped by OGM.[3] These observations highlight that even in optimized clinical settings, OGM is sensitive to a combination of pre-analytical factors (tumor cellularity, DNA quality), the size and type of the rearrangement, and the genomic context of the breakpoints.

The RH30 cell line illustrates one of the key conceptual advantages of OGM over break-apart FISH. Break-apart FISH can demonstrate that a genomic locus is rearranged, but it cannot identify the fusion partner involved. OGM, in contrast, directly visualizes the structural rearrangement at the DNA level and identifies both fusion partners within a single assay, without requiring prior assumptions about the expected fusion. In conventional diagnostic workflows, the absence of recurrent fusions is often established through sequential targeted testing using multiple FISH probes or RNA panels. OGM offers a genome-wide alternative that can simultaneously exclude canonical fusions while also providing information about the broader structural architecture of the tumor genome, as illustrated by MSKPED0023 and MSKPED0087.

The RH41 cell line, however, highlighted an important limitation of both OGM and FISH. Although RH41 has been described to harbor a *PAX3::FOXO1* fusion, neither OGM nor break-apart FISH detected the rearrangement in the cell line used in our laboratory. Because two independent techniques failed to identify the fusion, two possible explanations should be considered. First, this result may reflect the atypical breakpoint structure of RH41 described in the literature: previous breakpoint analysis demonstrated that RH41 contains a 4.9 kb insertion of chromosome 9 material between the *PAX3* and *FOXO1* breakpoints, creating a more complex three-way rearrangement rather than the classic reciprocal t(2;13) translocation.[57] While OGM is in principle capable of detecting three-way translocations, mapping accuracy can decrease when rearrangements become highly complex, and such a complex breakpoint architecture may fall outside the design of standard FISH break-apart probes, which are optimized for canonical reciprocal translocations. Second, given that classical break-apart FISH probes target flanking regions on either side of the *FOXO1* gene and would be expected to show a split signal even in the presence of a complex rearrangement, the concurrent negative FISH result cannot rule out the possibility that the specific RH41 subline used in our laboratory no longer carries the *PAX3::FOXO1* fusion, for example as a consequence of clonal drift during prolonged in vitro culture. Definitive discrimination between these two possibilities would require an orthogonal confirmation at the transcript level, such as RT-PCR or RNA sequencing, which can directly detect the functional fusion transcript independently of the underlying DNA architecture. This observation fits well with previous reports concluding that missed variants in OGM are usually related to biological complexity, such as atypical breakpoint architecture or tumor heterogeneity, rather than purely technical failure of the platform itself.[3] More generally, in cases where the underlying DNA rearrangement is difficult to resolve structurally, complementary RNA-based methods such as RT-PCR or RNA sequencing remain important, as they can still detect the functional fusion transcript.

Beyond detecting canonical fusions, OGM also provided additional diagnostic information in several samples. In both PEDSAR02 and PEDSAR03, secondary *FOXO1*-associated rearrangements were identified alongside the canonical t(2;13) translocation, suggesting a more complex structural rearrangement at the *FOXO1* locus. Although the biological significance of these additional events still requires RNA-level validation, they illustrate the ability of OGM to uncover structural complexity that would remain undetected by break-apart FISH or targeted fusion assays. Diagnostic refinement based on OGM findings has been described in 9.1% of cases, including the reclassification of a presumed high-grade myxofibrosarcoma after detection of an *OGA::TGFBR3* fusion and *VGLL3* amplification.[33] Likewise, unique fusion partners such as *POU2AF3::EWSR1* that were not resolved by conventional approaches have also been described.[3] Together, these findings emphasize that OGM not only confirms known abnormalities but can also reveal additional genomic features with potential diagnostic relevance.

III. Quantifying Genomic Complexity

A major strength of OGM, beyond the simple detection of gene fusions, is its ability to provide a broader overview of the structural complexity of the tumor genome. This is particularly relevant in sarcomas, where processes such as chromothripsis and chromoplexy are increasingly recognized as important biological drivers with potential clinical significance. Previous studies have already demonstrated that these large-scale rearrangement processes occur frequently in sarcomas, especially in genomically complex subtypes such as dedifferentiated liposarcoma, where chromothripsis involving chromosome 12 and the *MDM2/CDK4* locus has repeatedly been described.[3,33]

The samples analyzed in this study clearly illustrated this added value of OGM. Cell line RH30 showed widespread copy number alterations affecting nearly all chromosomes, including amplification of *CDK4* at 12q13.3-q14.1 and deletion of *CDKN2A/CDKN2B/MTAP* at 9p21.3, all detected within the same assay that simultaneously identified the *PAX3::FOXO1* fusion. Cell lines RH41 and RMS-YM both harbored a focal high-level FGFR1 amplification at the 8p11 region together with several additional alterations affecting known sarcoma-associated genes. Cell line RMS-YM additionally showed a focal *MDM2* amplification at 12q15 accompanied by four independent intragenic structural variants. A similar pattern was observed in tumoroid MSKPED0023, where a high-level *MDM2* amplification co-occurred with multiple intragenic insertions, deletions, and a duplication, together with a t(12;12) translocation located close to the *MDM2* locus. The coexistence of focal amplification and extensive local rearrangement strongly resembles a chromothripsis-like pattern and illustrates how OGM can capture not only the presence of genomic alterations, but also their structural organization within a single experiment.[33] The two MPNST samples further highlighted the value of OGM for resolving highly rearranged genomes. Both samples displayed dense networks of interconnected rearrangements involving chromosomes 7, 11, 14, 17, and 20, suggestive of large-scale events such as chromoplexy or chromothripsis, which have previously been associated with aggressive MPNST biology. At the same time, OGM identified the characteristic MPNST genomic profile within the same assay, including combined loss of *NF1*, *CDKN2A/CDKN2B/MTAP*, and *TP53*. Particularly interesting was the detection of *NF1* alterations through both copy number loss and structural rearrangements. Because *NF1* is a very large gene located within a repetitive genomic region, it is often difficult to fully characterize this locus using short-read sequencing technologies. The long-molecule approach used by OGM therefore offers a clear advantage for detecting these types of complex structural events.

At the same time, this study also confirmed several technical and practical limitations of OGM. Structural variants with breakpoints located in highly repetitive genomic regions, such as centromeric or telomeric sequences, may escape detection because OGM depends on a sufficient density of fluorescent labels across the genome; the *CIC::DUX4* fusion missed in a cohort is a clear example of this limitation.[3] Likewise, very small inversions and other sub-resolution events can remain undetected, as illustrated by the missed *STAT6::NAB2* fusion in the same study.[3] In addition, the chondrosarcoma sample analyzed in this study demonstrated how compromised DNA integrity can negatively influence OGM data quality. In this respect, OGM is notably more sensitive to DNA fragmentation than complementary techniques such as FISH or shallow whole-genome CNV sequencing, which can still generate interpretable results from partially degraded DNA. This sensitivity is an intrinsic consequence of the long-molecule approach on which OGM is based and reinforces the importance of optimized pre-analytical handling and high-quality UHMW DNA extraction for reliable OGM analysis. When DNA quality is suboptimal, orthogonal validation remains essential. However, comparison between OGM and CNV-seq cannot be performed by directly matching the called events from both techniques, as the underlying detection algorithms and cutoffs differ substantially between the two methods. Reliable cross-technique comparison therefore requires visual inspection of the alignment tracks rather than reliance on automated calls alone. In hematological samples and well-characterized cell lines, both processed in our laboratory and described in previous OGM validation studies, OGM-derived copy number profiles have shown high concordance with results obtained by conventional cytogenetic and CNV detection methods. Direct comparison with shallow CNV sequencing in solid tumors has been less extensively documented in the literature, but visual inspection of the alignment tracks generally yields a high degree of concordance when DNA integrity is preserved.[37] A further analytical limitation shared by both OGM and CNV-seq is the inability to reliably detect whole-genome aneuploidy, since both techniques estimate copy number from relative coverage rather than absolute ploidy. In a research or routine diagnostic setting, this limitation is typically addressed by complementary karyotyping or, when fresh tissue is unavailable, by targeted FISH analysis to establish the baseline ploidy of the tumor. Finally, OGM is a relatively expensive technique with a low sample throughput compared with FISH or sequencing-based assays, which currently limits its practical scalability. However, this cost should be evaluated in context: if OGM can replace the combination of FISH, CNV-seq, and karyotyping in a single comprehensive assay, the overall cost-effectiveness becomes considerably more favorable, particularly for genomically complex sarcoma subtypes that would otherwise require multiple targeted analyses.

IV. Clinical and Prognostic Implications

The fourth translational theme of this study relates to the potential clinical impact of OGM and its relevance for therapeutic decision-making. Several of the genomic alterations detected across the analyzed samples are known to have important prognostic or therapeutic implications in sarcomas. One of the most recurrent findings was the loss of *CDKN2A* and *CDKN2B*, observed in RH30, RH41, RMS-YM, MSKPED0023, MSKPED0087, and both MPNST samples. *CDKN2A/B* loss has previously been identified as a biomarker of poor prognosis across multiple soft tissue sarcoma subtypes.[58,59] The frequency of this alteration varies considerably between subtypes: in embryonal rhabdomyosarcoma, *CDKN2A* deletions have been reported in approximately 13% of cases.[59] Although comparable cohort-level frequencies for alveolar rhabdomyosarcoma are less well documented in the literature, *CDKN2A*/*B* loss is consistently described as a recurrent secondary event in fusion-positive RMS cell line models and tumor samples. In MPNST, *CDKN2A/B* loss is substantially more frequent: a meta-analysis combining multiple next-generation sequencing studies reported homozygous *CDKN2A* loss in 54 of 72 cases (75%), positioning *CDKN2A/B* inactivation as one of the hallmark events in MPNST pathogenesis, occurring as an early step in malignant transformation following biallelic *NF1* loss.[60] The consistent detection of homozygous *CDKN2A/CDKN2B/MTAP* deletion in both MPNST samples in the present study is therefore in line with the expected hallmark profile of high-grade MPNST.

In addition, PEDSAR02, MSKPED0023, MSKPED0087, and both MPNST samples all showed combined disruption of *TP53* and *RB1*, indicating simultaneous inactivation of the two major cell cycle checkpoint pathways, a genomic pattern that is strongly linked to tumor progression and aggressive biology.[22] This combined disruption is particularly informative when interpreted against the background frequencies in the literature. In pediatric rhabdomyosarcoma, *TP53* mutations have been reported in only 1.3% of cases in the largest series analyzed to date (1 of 75 tumors), with no *MDM2* amplifications detected.[61] The detection of combined *TP53* and *RB1* disruption in three of the pediatric RMS-derived samples in our cohort is therefore relatively uncommon for typical pediatric RMS and suggests a molecular profile that may be more aggressive than expected from histology alone, in line with the proposed role of TP53/RB1 co-disruption as a marker of disease progression.[22] In MPNST, *TP53* inactivation has been reported in approximately 40% of cases (29 of 72 across multiple cohorts) and frequently co-occurs with *CDKN2A/B* loss and *NF1* inactivation as part of the classical multi-step model of malignant transformation.[60] The combined *NF1/CDKN2A/B/TP53* profile detected in both MPNST samples in the present study therefore closely matches the canonical high-grade MPNST signature described in the literature.

In PEDSAR02, OGM additionally detected loss of both *PTEN* and PIK3R1, suggesting dysregulation of the *PI3K/AKT/mTOR* signaling pathway. This pathway has previously been implicated in therapy resistance in fusion-positive rhabdomyosarcoma and may therefore represent an additional biologically relevant alteration beyond the canonical fusion event itself.[62] Several findings in this study also pointed toward possible therapeutic vulnerabilities. Cell line RH30 showed the combination of *CDK4* amplification together with *CDKN2A* loss, while RMS-YM, *MSKPED0023*, and MSKPED0087 all harbored focal *MDM2* amplifications at 12q15. This molecular pattern resembles the genomic profile currently being explored in clinical trials involving *CDK4/6* inhibitors such as palbociclib and *MDM2*-targeted therapies. Previous studies have specifically highlighted how comprehensive structural profiling may help identify patients who could benefit from these targeted approaches, including ongoing trials with *MDM2* inhibitors such as milademetan.[33]

Similarly, *FGFR1* amplifications identified in RH41 and RMS-YM, together with *FGFR4* amplification detected in MSKPED0087, suggest potential involvement of the *FGFR* signaling pathway. *FGFR*-targeted therapies are currently being investigated in several sarcoma subtypes, making these findings potentially clinically relevant.[63] Another interesting observation was the recurrent gain of chromosome arm 17q in PEDSAR02, which contains multiple sarcoma-associated genes and has previously been linked to more aggressive clinical behavior in fusion-positive alveolar rhabdomyosarcoma. This suggests that secondary genomic alterations may provide additional prognostic information beyond fusion status alone.[64]

Taken together, these findings support the broader idea that OGM may contribute to more refined molecular stratification of sarcoma patients. Rather than only confirming the presence or absence of a diagnostic fusion, OGM simultaneously captures secondary copy number changes and complex structural alterations within the same assay. This is particularly relevant in sarcoma subtypes where current prognostic classification still relies heavily on fusion status alone, despite growing evidence that additional genomic events may further influence prognosis, treatment response, and disease behavior.

V. From Targeted to Genome-Wide Diagnostics: A Paradigm Shift

Taken together, these findings highlight how OGM could fundamentally change the way sarcomas are diagnosed. Current diagnostic workflows are often fragmented and rely heavily on hypothesis-driven testing. In practice, this means that pathologists first need to decide which FISH probe to use, which targeted RNA panel to request, or which copy number assay might be most informative based on the suspected diagnosis. As a result, multiple separate techniques are often needed to piece together the genomic profile of a single tumor. OGM offers a more integrated approach by detecting translocations, deletions, amplifications, and complex rearrangements within one genome-wide assay, without requiring prior assumptions about which alterations are present. This is especially valuable for complex events such as chromoplexy, which can arise early during tumor development and are often missed by conventional cytogenomic methods, but can be resolved much more effectively using OGM.

Despite these advantages, OGM also has several important limitations that should be considered. The technique requires fresh or frozen tissue because extraction of ultra-high molecular weight DNA is not compatible with formalin-fixed paraffin-embedded (FFPE) material, which remains the standard tissue format in routine pathology laboratories. This represents a significant practical challenge for broader clinical implementation. In addition, OGM cannot detect single-nucleotide variants or small insertions and deletions, despite the fact that these alterations can also carry important diagnostic and therapeutic information in sarcomas. A third important limitation concerns the functional interpretation of novel translocations. When OGM identifies a previously undescribed putative fusion gene, the DNA-level breakpoint resolution is not always precise enough to determine whether the rearrangement results in a productive, in-frame fusion transcript, nor whether this transcript is actually expressed in the tumor cells. This limitation was directly relevant in this study, where several of the newly detected putative fusions in RH30, PEDSAR02 and the chondrosarcoma sample could not be assigned a clear functional or clinical relevance based on the OGM data alone. In such cases, complementary RNA-based methods such as RT-PCR or RNA sequencing remain essential, as they can directly detect the expressed fusion transcript and confirm whether the rearrangement is functional at the transcriptional level. Previous studies have emphasized this limitation as well, underscoring that OGM cannot function as a completely stand-alone diagnostic platform.[33]

Instead, the findings of this study support a more integrated diagnostic strategy in which OGM is combined with targeted next-generation sequencing approaches. In such a workflow, OGM would provide comprehensive detection of structural variants and large-scale genomic rearrangements, while targeted NGS panels would complement this with high-resolution analysis of sequence-level mutations, and RNA sequencing would confirm the functional consequences of novel structural rearrangements. Together, these approaches could offer a much more complete genomic characterization of sarcomas than is currently achievable with conventional multimodal workflows alone.

VI. Future Perspectives

The findings of this study should also be placed in the broader context of rapidly evolving genomic technologies. In particular, long-read sequencing platforms such as Oxford Nanopore Technologies and Pacific Biosciences have been increasingly applied to comprehensive analysis of complex tumor genomes.[65,66] Long-read sequencing shares the key advantage of OGM by generating reads of tens to hundreds of kilobases, allowing reliable detection of large structural variants, including translocations, complex rearrangements, and breakpoints in repetitive genomic regions that remain challenging for short-read sequencing.[65] Unlike OGM, long-read sequencing additionally provides nucleotide-level resolution, allowing detection of single-nucleotide variants, small insertions and deletions, and structural variants from the same dataset.[66] In a recent advanced cancer cohort, a study demonstrated that single PromethION flow cells at an average coverage of 26x were sufficient to recover all clinically relevant fusions and to phase the majority of somatic small mutations affecting tumor suppressor genes.[66] However, reliable detection of low-frequency somatic single-nucleotide variants in tumors generally requires substantially higher sequencing depth, which translates into longer turnaround times and higher costs than current OGM workflows. For context, OGM can typically be completed within 5–7 days, whereas whole-genome or whole-exome sequencing generally requires 7–14 days, particularly when deep coverage is needed for somatic variant calling.[33]

A second feature of long-read sequencing that is particularly relevant for sarcoma diagnostics is the simultaneous detection of DNA methylation. Both Oxford Nanopore and PacBio platforms can directly identify 5-methylcytosine modifications during native DNA sequencing, without requiring bisulfite conversion or a separate methylation assay.[65,67] This capability is becoming increasingly relevant in sarcoma diagnostics, where DNA methylation profiling has rapidly gained importance as a complementary classification tool. The DKFZ Sarcoma Classifier, based on array-generated DNA methylation profiles, has been shown to provide diagnostic predictions in 55–75% of samples, with 83–88% concordance with the histological diagnosis.[68,69] In addition, long-read sequencing allows haplotype phasing, which has been used to identify allelically differentially methylated regions in cancer genes such as *RET* and *CDKN2A*.[66]

Taken together, OGM currently provides a powerful and clinically applicable approach for the detection of structural variants and complex genomic rearrangements in sarcomas, with the additional practical advantage of a shorter turnaround time compared with deep sequencing approaches.[33] Whether long-read sequencing will eventually consolidate the information currently obtained from OGM, targeted DNA sequencing, RNA sequencing, and methylation arrays into a single assay is a question that will need to be addressed in dedicated comparative studies, particularly in the context of sarcoma diagnostics where such direct comparisons remain limited.

7. Conclusion

This study demonstrates that Optical Genome Mapping can reliably detect canonical fusions and complex structural variants in rhabdomyosarcoma cell lines and patient-derived tumoroids, with full concordance to *FOXO1* break-apart FISH for fusion status. In samples meeting quality thresholds, OGM delivered a comprehensive structural and copy-number profile in a single assay, including clinically relevant alterations such as *PAX3::FOXO1*, MDM2/CDK4 amplification, CDKN2A/B loss and NF1 disruption.

Extraction of ultra-high molecular weight DNA from primary sarcoma tissue was identified as the pre-analytical bottleneck. Through systematic variation of experimental conditions, tissue dissociation method, input mass, sample format, tissue composition and post-resection handling time were established as the major determinants of extraction success. Bulk frozen tissue (≥20–40 mg) combined with controlled tissue-ruptor dissociation provided the most reliable workflow in our hands, while ECM-rich and adipocytic tissues require further dedicated optimization. Encouragingly, paired MPNST samples showed that even a routine two-hour post-resection delay before snap-freezing remained compatible with high-quality OGM data, supporting feasibility within standard pathology workflows.

Together, these findings position OGM as a valuable complement to current sarcoma diagnostics rather than a stand-alone replacement. Optimal clinical implementation will likely combine OGM with targeted next-generation sequencing for sequence-level variants and RNA sequencing for functional validation of novel structural rearrangements, while further protocol development will be needed to extend the workflow reliably across the full spectrum of sarcoma subtypes.

8. References

1. Sbaraglia, M., Bellan, E. & Dei Tos, A. P. The 2020 WHO Classification of Soft Tissue Tumours: News and perspectives. *Pathologica* vol. 113 70–84 Preprint at https://doi.org/10.32074/1591-951X-213 (2021).

2. Damerell, V., Pepper, M. S. & Prince, S. Molecular mechanisms underpinning sarcomas and implications for current and future therapy. *Signal Transduction and Targeted Therapy* vol. 6 Preprint at https://doi.org/10.1038/s41392-021-00647-8 (2021).

3. Baelen, J. *et al.* Optical Genome Mapping for Comprehensive Cytogenetic Analysis of Soft-Tissue and Bone Tumors for Diagnostic Purposes. *Journal of Molecular Diagnostics* **26**, 374–386 (2024).

4. Ferrari, A. *et al.* Soft tissue sarcoma across the age spectrum: A population-based study from the surveillance epidemiology and end results database. *Pediatr. Blood Cancer* **57**, 943–949 (2011).

5. Gronchi, A. *et al.* Soft tissue and visceral sarcomas: ESMO–EURACAN–GENTURIS Clinical Practice Guidelines for diagnosis, treatment and follow-up☆. *Annals of Oncology* **32**, 1348–1365 (2021).

6. EURACAN. European Reference Network for Rare Adult Solid Cancers (EURACAN).

7. Liu, H. *et al.* Pan-Soft Tissue Sarcoma Analysis of the Incidence, Survival, and Metastasis: A Population-Based Study Focusing on Distant Metastasis and Lymph Node Metastasis. *Front. Oncol.* **12**, (2022).

8. Hesla, A. C., Papakonstantinou, A. & Tsagkozis, P. Current status of management and outcome for patients with ewing sarcoma. *Cancers* vol. 13 1–22 Preprint at https://doi.org/10.3390/cancers13061202 (2021).

9. Fukushima, T., Ogura, K., Akiyama, T., Takeshita, K. & Kawai, A. Descriptive epidemiology and outcomes of bone sarcomas in adolescent and young adult patients in Japan. *BMC Musculoskelet. Disord.* **19**, (2018).

10. de Bree, E. *et al.* Retroperitoneal Soft Tissue Sarcoma: Emerging Therapeutic Strategies. *Cancers* vol. 15 Preprint at https://doi.org/10.3390/cancers15225469 (2023).

11. Sambri, A. *et al.* Margin assessment in soft tissue sarcomas: Review of the literature. *Cancers* vol. 13 Preprint at https://doi.org/10.3390/cancers13071687 (2021).

12. Lesluyes, T., Delespaul, L., Coindre, J. M. & Chibon, F. The CINSARC signature as a prognostic marker for clinical outcome in multiple neoplasms. *Sci. Rep.* **7**, (2017).

13. Merry, E., Thway, K., Jones, R. L. & Huang, P. H. Predictive and prognostic transcriptomic biomarkers in soft tissue sarcomas. *npj Precision Oncology* vol. 5 Preprint at https://doi.org/10.1038/s41698-021-00157-4 (2021).

14. Levy, B. *et al.* Optical genome mapping in acute myeloid leukemia: a multicenter evaluation. *Blood Adv.* **7**, 1297–1307 (2023).

15. van Oost, S., Meijer, D. M., Kuijjer, M. L., Bovée, J. V. M. G. & de Miranda, N. F. C. C. Linking immunity with genomics in sarcomas: Is genomic complexity an immunogenic trigger? *Biomedicines* vol. 9 Preprint at https://doi.org/10.3390/biomedicines9081048 (2021).

16. Taylor, B. S. *et al.* Advances in sarcoma genomics and new therapeutic targets. *Nature Reviews Cancer* vol. 11 541–557 Preprint at https://doi.org/10.1038/nrc3087 (2011).

17. Olanich, M. E. & Barr, F. G. A call to ARMS: Targeting the PAX3-FOXO1 gene in alveolar rhabdomyosarcoma. *Expert Opinion on Therapeutic Targets* vol. 17 607–623 Preprint at https://doi.org/10.1517/14728222.2013.772136 (2013).

18. Pavlidis, E. T. & Pavlidis, T. E. New trends in the surgical management of soft tissue sarcoma: The role of preoperative biopsy. *World J. Clin. Oncol.* **14**, 89–98 (2023).

19. Galili1, N. *et al. Fusion of a Fork Head Domain Gene to PAX3 in the Solid Tumour Alveolar Rhabdomyosarcoma*. http://www.nature.com/naturegenetics (1993).

20. Linardic, C. M. PAX3-FOXO1 fusion gene in rhabdomyosarcoma. *Cancer Letters* vol. 270 10–18 Preprint at https://doi.org/10.1016/j.canlet.2008.03.035 (2008).

21. Abeshouse, A. *et al.* Comprehensive and Integrated Genomic Characterization of Adult Soft Tissue Sarcomas. *Cell* **171**, 950-965.e28 (2017).

22. Gounder, M. M. *et al.* Clinical genomic profiling in the management of patients with soft tissue and bone sarcoma. *Nat. Commun.* **13**, (2022).

23. Espejo Valle-Inclan, J. *et al.* Ongoing chromothripsis underpins osteosarcoma genome complexity and clonal evolution. *Cell* **188**, 352-370.e22 (2025).

24. Cortés-Ciriano, I. *et al.* Comprehensive analysis of chromothripsis in 2,658 human cancers using whole-genome sequencing. *Nat. Genet.* **52**, 331–341 (2020).

25. de Juan Ferré, A. *et al.* SEOM Clinical Guideline of management of soft-tissue sarcoma (2020). *Clinical and Translational Oncology* **23**, 922–930 (2021).

26. Gerrand, C. *et al.* UK guidelines for the management of bone sarcomas. *Clin. Sarcoma Res.* **6**, 7 (2016).

27. Gonzalez, M. R., Mendez-Guerra, C., Goh, M. H. & Pretell-Mazzini, J. Principles of Surgical Treatment of Soft Tissue Sarcomas. *Cancers* vol. 17 Preprint at https://doi.org/10.3390/cancers17030401 (2025).

28. Cammelli, S. *et al.* The role of radiotherapy in adult soft tissues sarcoma of the extremities. *European Journal of Orthopaedic Surgery and Traumatology* vol. 31 1583–1596 Preprint at https://doi.org/10.1007/s00590-021-02990-6 (2021).

29. Lebas, A. *et al.* Factors Influencing Long-Term Local Recurrence, Distant Metastasis, and Survival in Patients with Soft Tissue Sarcoma of the Extremities Treated with Radiotherapy. *Cancers (Basel).* **16**, (2024).

30. Salerno, K. E. *et al.* Radiation Therapy for Treatment of Soft Tissue Sarcoma in Adults: Executive Summary of an ASTRO Clinical Practice Guideline. *Pract. Radiat. Oncol.* **11**, 339–351 (2021).

31. Judson, I. *et al.* Doxorubicin alone versus intensified doxorubicin plus ifosfamide for first-line treatment of advanced or metastatic soft-tissue sarcoma: A randomised controlled phase 3 trial. *Lancet Oncol.* **15**, 415–423 (2014).

32. Drilon, A. *et al.* Efficacy of Larotrectinib in TRK Fusion–Positive Cancers in Adults and Children . *New England Journal of Medicine* **378**, 731–739 (2018).

33. Berenguer-Rubio, A. *et al.* Exploring the Potential of Optical Genome Mapping in the Diagnosis and Prognosis of Soft Tissue and Bone Tumors. *Int. J. Mol. Sci.* **26**, (2025).

34. Jung, J. *et al.* TP53 mutations emerge with HDM2 inhibitor SAR405838 treatment in de-differentiated liposarcoma. *Nat. Commun.* **7**, (2016).

35. Wander, S. A. *et al.* The genomic landscape of intrinsic and acquired resistance to cyclin-dependent kinase 4/6 inhibitors in patients with hormone receptor–positive metastatic breast cancer. *Cancer Discov.* **10**, 1174–1193 (2020).

36. Crombé, A. *et al.* Soft-tissue sarcoma in adults: Imaging appearances, pitfalls and diagnostic algorithms. *Diagnostic and Interventional Imaging* vol. 104 207–220 Preprint at https://doi.org/10.1016/j.diii.2022.12.001 (2023).

37. Mantere, T. *et al.* Optical genome mapping enables constitutional chromosomal aberration detection. *Am. J. Hum. Genet.* **108**, 1409–1422 (2021).

38. Zago Baltazar, R. *et al.* Recurrent and novel fusions detected by targeted RNA sequencing as part of the diagnostic workflow of soft tissue and bone tumours. *Journal of Pathology: Clinical Research* **10**, (2024).

39. Xu, L. *et al.* Potential application of genomic profiling for the diagnosis and treatment of patients with sarcoma. *Oncol. Lett.* **21**, (2021).

40. Viafet. Karyotype testing vs chromosomal microarray.

41. Tien, J. D. Y., Lau, L. C., Tien, S. L. & Tan, M. H. The clinical utility of conventional karyotyping in the detection of cytogenetic abnormalities in soft tissue tumours: An asian institutional experience. *Hong Kong Medical Journal* **20**, 393–400 (2014).

42. Vauhkonen, H., Savola, S., Kaur, S., Larramendy, M. L. & Knuutila, S. *MOLECULAR KARYOTYPING IN SARCOMA DIAGNOSTICS AND RESEARCH*. (2006).

43. Invitra. What is the price of the FISH technique? .

44. Zhong, L. ling *et al.* Novel characteristics for immunophenotype, FISH pattern and molecular cytogenetics in synovial sarcoma. *Sci. Rep.* **13**, (2023).

45. Rottmann, D., Abdulfatah, E. & Pantanowitz, L. Molecular testing of soft tissue tumors. *Diagnostic Cytopathology* vol. 51 12–25 Preprint at https://doi.org/10.1002/dc.25013 (2023).

46. UHN Laboratory Medicine Program. New Reflex Fish Procedure For Large Cell Lymphoma and Change To BCL2 Break Apart Probe. (2021).

47. Cheng, L. *et al.* Integration of genomic copy number variations and chemotherapy-response biomarkers in pediatric sarcoma. *BMC Med. Genomics* **12**, (2019).

48. Curion, F. *et al.* Targeted RNA sequencing enhances gene expression profiling of ultra-low input samples. *RNA Biol.* **17**, 1741–1753 (2020).

49. *Accurate RNA Sequencing From Formalin-Fixed Cancer Tissue to Represent High-Quality Transcriptome From Frozen Tissue*. (2018).

50. Brancato, D. *et al.* NGS Approaches in Clinical Diagnostics: From Workflow to Disease-Specific Applications. *International Journal of Molecular Sciences* vol. 26 Preprint at https://doi.org/10.3390/ijms26199597 (2025).

51. College of American Pathologists. Molecular diagnostics in sarcoma pathology. .

52. Alioto, T. S. *et al.* A comprehensive assessment of somatic mutation detection in cancer using whole-genome sequencing. *Nat. Commun.* **6**, (2015).

53. *Transition to NGS. Here We Review the Current Sequencing Technology, Applications and Bioinformatics with Special Consideration given to the Development of Clinical DNA Sequencing*.

54. Goldrich, D. Y. *et al.* Identification of somatic structural variants in solid tumors by optical genome mapping. *J. Pers. Med.* **11**, 1–21 (2021).

55. Bionano. Bionano Genomics. How Optical Genome Mapping (OGM) works.

56. Tom Sante. ViVar: A Comprehensive Platform for the Analysis and Visualization of Structural Genomic Variation. *PLoS One* 1–12 (2014).

57. Vicente-García, C. *et al.* Regulatory landscape fusion in rhabdomyosarcoma through interactions between the PAX3 promoter and FOXO1 regulatory elements. *Genome Biol.* **18**, (2017).

58. Bui, N. Q. *et al.* A clinico-genomic analysis of soft tissue sarcoma patients reveals CDKN2A deletion as a biomarker for poor prognosis. *Clin. Sarcoma Res.* **9**, (2019).

59. Saoud, C. *et al.* Genomic profiling of pleomorphic rhabdomyosarcoma reveals a genomic signature distinct from that of embryonal rhabdomyosarcoma. *Genes Chromosomes Cancer* **63**, (2024).

60. Brohl, A. S., Kahen, E., Yoder, S. J., Teer, J. K. & Reed, D. R. The genomic landscape of malignant peripheral nerve sheath tumors: Diverse drivers of Ras pathway activation. *Sci. Rep.* **7**, (2017).

61. Ognjanovic, S. *et al.* Low prevalence of TP53 mutations and MDM2 amplifications in pediatric rhabdomyosarcoma. *Sarcoma* **2012**, (2012).

62. Versari, I. *et al.* The Emerging Role and Clinical Significance of PI3K-Akt-mTOR in Rhabdomyosarcoma. *Biomolecules* vol. 15 Preprint at https://doi.org/10.3390/biom15030334 (2025).

63. Zhou, W. Y., Zheng, H., Du, X. L. & Yang, J. L. Characterization of FGFR signaling pathway as therapeutic targets for sarcoma patients. *Cancer Biology and Medicine* vol. 13 260–268 Preprint at https://doi.org/10.20892/j.issn.2095-3941.2015.0102 (2016).

64. Skapek, S. X. *et al.* PAX-FOXO1 fusion status drives unfavorable outcome for children with rhabdomyosarcoma: A children's oncology group report. *Pediatr. Blood Cancer* **60**, 1411–1417 (2013).

65. Sakamoto, Y., Zaha, S., Suzuki, Y., Seki, M. & Suzuki, A. Application of long-read sequencing to the detection of structural variants in human cancer genomes. *Computational and Structural Biotechnology Journal* vol. 19 4207–4216 Preprint at https://doi.org/10.1016/j.csbj.2021.07.030 (2021).

66. O'Neill, K. *et al.* Long-read sequencing of an advanced cancer cohort resolves rearrangements, unravels haplotypes, and reveals methylation landscapes. *Cell Genomics* **4**, (2024).

67. Simpson, J. T. *et al.* Detecting DNA cytosine methylation using nanopore sequencing. *Nat. Methods* **14**, 407–410 (2017).

68. Koelsche, C. *et al.* Sarcoma classification by DNA methylation profiling. *Nat. Commun.* **12**, (2021).

69. Lyskjær, I. *et al.* DNA methylation-based profiling of bone and soft tissue tumours: a validation study of the 'DKFZ Sarcoma Classifier'. *Journal of Pathology: Clinical Research* **7**, 350–360 (2021).

9. Use of Artificial Intelligence

During the preparation of this thesis, Artificial Intelligence (AI) tools, including ChatGPT, were used as supportive instruments throughout different stages of the writing and research process. AI was not used to generate original scientific results, perform data analysis, or draw conclusions independently, but rather to assist in organizing, refining, and improving the presentation of the work.

At the start of the project, AI tools were primarily used to help structure the thesis outline by suggesting possible chapter divisions, subtitles, and key topics that could be addressed within each section. These suggestions served only as an initial framework and were further adapted, expanded, and critically evaluated based on scientific literature and personal interpretation.

During the literature review phase, AI-assisted notebook and search functionalities were occasionally used to identify potentially relevant publications, keywords, and concepts related to Optical Genome Mapping, structural variants, and sarcoma diagnostics. All retrieved literature was subsequently reviewed independently, and only sources considered scientifically reliable and relevant were included in the thesis. Throughout the writing process, AI tools were also used as a language-support and editing aid. This included checking grammar, improving sentence structure, enhancing readability, rephrasing certain passages into more natural academic English, and helping maintain consistent scientific terminology across chapters. In situations where the wording of a sentence or paragraph was uncertain, AI-generated alternatives were sometimes consulted and then manually revised where necessary.

All scientific interpretation, critical analysis, data processing, figure selection, and final conclusions were performed independently by the author. The author remained fully responsible for the content, accuracy, interpretation, and final form of this thesis.

10. The mid-term Poster

FACULTY OF MEDICINE AND HEALTH SCIENCES

APPLICATION OF OPTICAL GENOME MAPPING FOR THE DETECTION OF STRUCTURAL VARIANTS IN SARCOMAS

STUDENT: Jason Legein
PROMOTORS: Kaat Durinck, Nadine Van Roy **MENTOR**: Siebe Loontiens

INTRODUCTION

Sarcomas are rare, heterogeneous malignancies characterized by recurrent gene fusions or complex structural genomic alterations.[2] Accurate molecular classification is essential for diagnosis, prognosis, and treatment selection. However, current diagnostic workflows rely on multiple complementary techniques, including karyotyping, fluorescence in situ hybridization (FISH), copy number analysis, and RNA sequencing, each providing only partial insight into the tumor genome. As a result, clinically relevant structural variants, particularly complex or balanced rearrangements may remain undetected.[3]

Optical Genome Mapping (OGM) is a genome-wide technique that enables direct visualization of ultra-high molecular weight DNA molecules, allowing comprehensive detection of structural variants in a single assay. This approach has the potential to overcome limitations of current diagnostic methods and to improve the molecular characterization of sarcomas. [1]

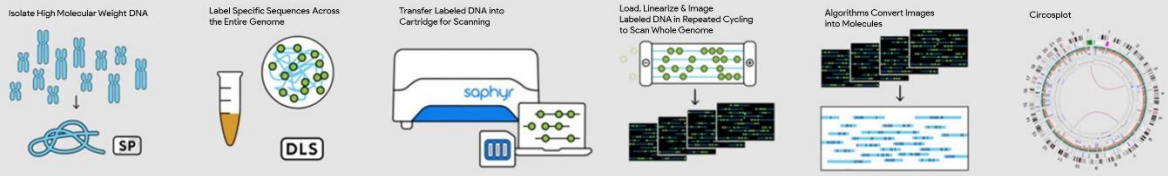

AIMS OF THE STUDY

To evaluate whether Optical Genome Mapping (OGM) can be implemented as a **robust** and **complementary** technique for detecting structural variants in sarcomas, and to compare its performance with current diagnostic techniques.

Objectives:

- Implementation and optimization of OGM for Sarcomas
- Validation of OGM detection capabilities
- Assessment of OGM's Added Clinical Value
- Evaluation of Clinical Feasibility and Implementation

METHODS

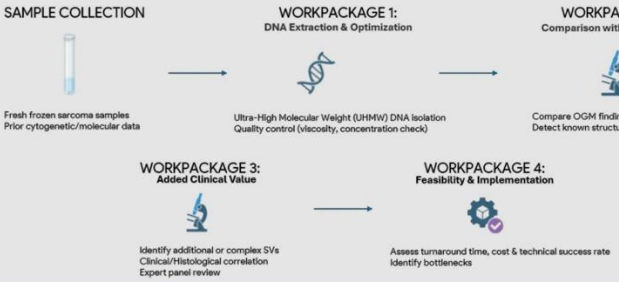

RESULTS

ULTRA-HIGH MOLECULAR WEIGHT DNA ISOLATION

ANALYSIS OF RH30 CELL LINE – ALVEOLAR RHABDOMYOSARCOMA (ARMS)

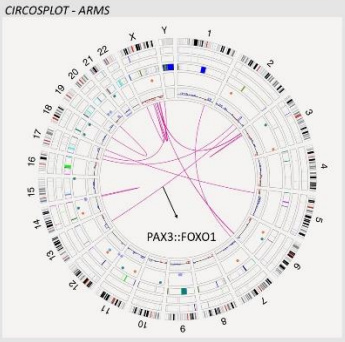

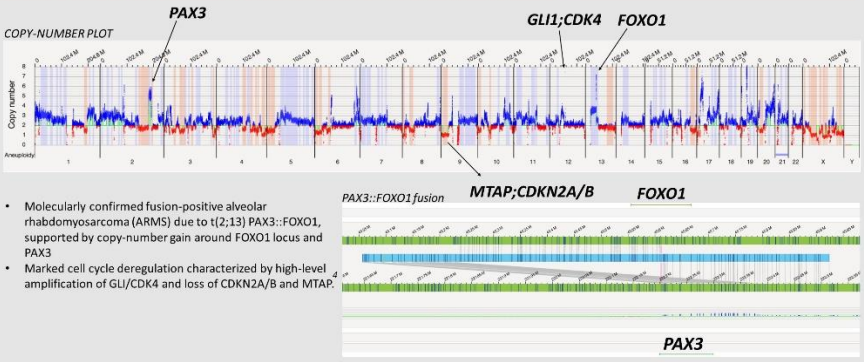

- Molecularly confirmed fusion-positive alveolar rhabdomyosarcoma (ARMS) due to t(2;13) PAX3::FOXO1, supported by copy-number gain around FOXO1 locus and PAX3
- Marked cell cycle deregulation characterized by high-level amplification of GLI/CDK4 and loss of CDKN2A/B and MTAP.

Reference List

1. Bionano Genomics. How OGM works. https://bionano.com/how-ogm-works/
2. Sbaraglia, M., Bellan, E. & Dei Tos, A. P. The 2020 WHO Classification of Soft Tissue Tumours: news and perspectives. Pathologica **113**, 70–84, doi:10.32074/1591-951x-213 (2021)
3. Baelen, J. et al. Optical Genome Mapping for Comprehensive Cytogenetic Analysis of Soft-Tissue and Bone Tumors for Diagnostic Purposes. J Mol Diagn **26**, 374–386, doi:10.1016/j.jmoldx.2024.02.003 (2024)..
4. Ziemba, B. & Łuków, K. Molecular targets in alveolar rhabdomyosarcoma: A narrative review of progress and pitfalls. Int J Mol Sci 26, 5204, doi:10.3390/ijms26115204 (2025).

GHENT UNIVERSITY

CRIG CANCER RESEARCH INSTITUTE GHENT

UZ GENT

11. Addendum

Overview

Addendum A	Solid Tumor Gene Panels
Addendum B	Results OGM analysis cell line RH30
Addendum C	Results OGM analysis cell line RH41
Addendum D	Results OGM analysis cell line RMS-YM
Addendum E	Results OGM analysis PEDSAR02 (tumoroid)
Addendum F	Results OGM analysis PEDSAR03 (tumoroid)
Addendum G	Results OGM analysis MSKPED0023 (tumoroid)
Addendum H	Results OGM analysis MSKPED0087 (tumoroid)
Addendum I	Results OGM analysis chondrosarcoma
Addendum J	Results OGM MPNST (routine)
Addendum K	Results OGM MPNST (OT)
Addendum L	Bionano Prep SP Frozen Cell Pellet DNA Isolation Protocol
Addendum M	Bionano Prep SP Tissue and Tumor DNA Isolation Protocol
Addendum N	Bionano Prep Direct Label and Stain (DLS) Protocol

Addendum A – Solid Tumor Gene Panels

DNA NGS SOLIDE TUMOR panel (112 genes)									
AKT1	ALK	APC	AR	ARID1A	ATM	BAP1	BARD1	BCOR	BRAF
BRCA1	BRCA2	BRIP1	CCND1	CCNE1	CDH1	CDK4	CDK6	CDK12	CDKN2A
CDKN2B	CHEK1	CHEK2	CTNNB1	DDX3X	DGCR8	DICER1	DPYD	DROSHA	EGFR
EIF1AX	ELP1	ERBB2	ERBB3	ESR1	FBXW7	FGFR1	FGFR2	FGFR3	FGFR4
FOXL2	FRK	GATA3	GNA11	GNAQ	GNAS	GPR161	H3-3A	H3-3B	H3C2
H3C3	HNF1A	HRAS	IDH1	IDH2	IL6ST	JAK1	JAK2	KBTBD4	KEAP1
KIT	KRAS	MAP2K1	MDM2	MET	MRE11	MTAP	MYC	MYCN	MYOD1
NBN	NF1	NF2	NOTCH1	NRAS	NTRK1	NTRK2	NTRK3	PALB2	PDGFRA
PDGFRB	PIK3CA	PIK3R1	POLE	PRKCA	PTCH1	PTEN	PTPN11	RAD50	RAD51B
RAD51C	RAD51D	RB1	RET	RNF43	ROS1	SDHA	SDHB	SDHC	SDHD
SF3B1	SMAD4	SMARCA4	SMARCB1	SMO	SPOP	STAT3	STK11	SUFU	TERT
TP53	VHL								

RNA NGS PANCANCER panel (175 genes)									
ABL1	ABL2	AFF2	ALK	BCL11B	BCOR	BCR	BRAF	CAMTA1	CBFA2T3
CBFB	CD28	CHMP2A	CIC	COL6A3	CREBBP	CRLF2	CSF1	CSF1R	CTNNB1
DEK	DUX4	EBF1	EGFR	EPC1	EPOR	ERBB2	ERG	ESR1	ETV5
ETV6	EWSR1	FGFR1	FGFR2	FGFR3	FIPL1	FLT3	FN1	FOS	FOSB
FOXO1	FOXR2	FRK	FUS	GLI1	GLIS2	GPI	GREB1	GRM1	HLF
HMGA2	HOXA10	HOXA11	HOXA9	IKZF1	IL2RB	JAK2	JAZF1	KDM2B	KMT2A
KRAS	LYL1	LYN	MAML2	MAML3	MAP3K3	MAP3K8	MDM2	MEAF6	MECOM
MEF2D	MET	MITF	MLLT10	MLLT4	MN1	MRTF	MRTFA	MSANTD3	MYB
MYBL1	MYC	MYH11	MYOD1	NCOA1	NCOA2	NOTCH1	NOTCH2	NOTCH3	NPM1
NR1D1	NR4A2	NR4A3	NRG1	NTRK1	NTRK2	NTRK3	NUP214	NUP98	NUTM1
OGA	P2RY8	PATZ1	PAX3	PAX5	PAX7	PBX1	PCM1	PDGFB	PDGFRA
PDGFRB	PHF1	PICALM	PLAG1	PML	PPARG	PRDM10	PRDM16	PRKACA	PRKCA
PRKCB	PRKCD	PRKD1	PRKD2	PRKD3	PTEN	PTK2B	RAB7A	RAD51B	RAF1
RARA	RARB	RARG	RASGRF1	RMB15	RELA	RET	ROS1	RSPO2	RSPO3
RUNX1	RUNX1T1	SET	SRF	SS18	STAT6	STIL	SUZ12	TAF15	TAL1
TCF3	TCF12	TCFP2	TFE3	TFEB	TFG	THADA	TLX1	TLX3	TMPRSS2
TRIM11	TSLP	TYK2	UBTF	USP6	VCP	VGLL2	VGLL3	WT1	YAP1
YWHAE	ZCCHC7	ZFTA	ZNF362	ZNF384					

Addendum B – Results OGM analysis cell line RH30

Table B.1 – Copy number variants (CNV)

Table 1. Overview of the detected copy number variants in sample RH30, indicating the type of abnormality, the reported genes from the sarcoma gene list and the copy number (CN).

Chromosome region	Abnormality type	Reported genes (sarcoma gene list)	Copy number (CN)
1p36.32p11.2	Gain	*CAMTA1, SDHB, ARID1A, MEAF6, JAK1, DPYD, CSF1, NRAS*	3
1q31.1q31.3	Loss	/	1
1q32.1q42.2	Gain	*H3-3A*	3/4
2p25.3p11.2	Gain	*NCOA1, ALK*	3
2q21.2q22.3	Gain	/	3
2q23.1q32.1	Loss	/	1
2q32.1q32.3	Gain	/	5
2q33.1	Loss	*SF3B1*	1
2q36.1q37.3	Gain	*PAX3*	3
3p26.1p25.2	Gain	*VHL, PPARG, RAF1*	3/4
3p24.3	Gain	/	4
3p22.3p22.1	Loss	*CTNNB1*	1
3p14.2p12.3	Loss	/	1

Chromosome region	Abnormality type	Reported genes (sarcoma gene list)	Copy number (CN)
3p12.3	Gain	/	2/3
3q11.2q12.3	Gain	*TFG*	3
3q13.11q13.13	Loss	/	1
3q21.1q24	Gain	/	2/3
3q26.2q26.33	Gain	*PIK3CA*	2/3
3q28	Loss	/	1
4p16.3q23	Gain	*FGFR3, PDGFRA, KIT*	2/3
4q23q25	Loss	/	1
4q26q28.1	Gain	/	3
4q28.2q28.3	Loss	/	
4q31.23q32.1	Loss	*FBXW7*	1
4q34.1q35.1	Loss	/	1
5p15.33p14.1	Loss	/	1
5p11q35.3	Gain	*IL6ST, PIK3R1, APC, RAD50, PDGFR, FGFR4*	2/3
6p25.3p22.3	Loss	/	1
6p12.3p12.1	Loss	/	1

Chromosome region	Abnormality type	Reported genes (sarcoma gene list)	Copy number (CN)
6q25.1q27	Gain	*ESR1*	3
7p22.3	Loss	/	1
7p22.2p11.2	Gain	*JAZF1, EGFR*	2/3
7q11.21q21.3	Gain	*CDK6*	3
8p23.3p23.2	Loss	/	1
8p21.2p11.23	Loss	*NRG1, FGFR1*	1
8q24.22q24.23	Gain	/	2/3
9p24.3p21.3	Loss	*JAK2, MTAP, CDKN2A, CDKN2B*	1
9q21.12q34.11	Gain	*GNAQ, NTRK2, PTCH1, NR4A3, ELP1*	2/3
10p15.3p14	Loss	*GATA3*	1
10p14p11.2	Gain	*EPC*	3
10q11.22q11.22	Loss	*RET*	1
10q22.2q22.3	Gain	/	3
10q24.2q26.2	Gain	*SUFU, FGFR2*	3/4
11p15.4p11.2	Gain	/	2/3
11q12.1q14.2	Gain	/	2/3

Chromosome region	Abnormality type	Reported genes (sarcoma gene list)	Copy number (CN)
11q24.1q24.3	Gain	*CHEK1*	2/3
12p12.1p11.21	Gain	*KRAS*	3
12q12q13.12	Gain	/	3/4
12q13.3q14.1	Gain	*STAT6, GLI1, CDK4*	> 8
13q12.11q13.3	Gain	*BRCA2*	3/4
13q14.11q14.2	Gain	*FOXO1*	8
14q12q21.2	Gain	/	2/3
15q13.1q15.3	Gain	/	2/3
15q21.3q25.1	Gain	*TCF12, MAP2K1*	
15q25.3q26.3	Gain	*IDH2*	3
16q12.1q21	Gain	/	2/3
16q22.1q23.3	Loss	*CDH1*	1
17p13.3p13.2	Loss	*YWHAE, USP6*	1
17p13.1	Gain	*TP53*	3
17p12p11.2	Gain	/	5/6
17q12q21.33	Gain	*CDK12, ERBB2, STAT3, BRCA1, SPOP*	3/4

Chromosome region	Abnormality type	Reported genes (sarcoma gene list)	Copy number (CN)
17q22q25.3	Gain	*RNF43, RAD51C, BRIP1, PRKCA, H3-3B*	3
18q12.1q21.33	Gain	*SMAD4*	2/3
19p13.11p12	Gain	/	7/8
19q12q13.33	Gain	*CIC, FOSB*	2/3
20p13	Gain	/	4
20p12.3p11.23	Loss	/	1
20q11.1q13.33	Gain	*GNAS*	4
21q11.2q22.3	Gain	*ERG, TMPRSS2*	2/3
Xp22.33p22.31	Loss	/	1
Xp22.11p11.22	Loss	*BCOR, DDX3X, TFE3*	1
Xq11.1q13.1	Loss	*AR*	1
Xq13.3q21.1	Loss	/	1
Xq21.31q21.32	Loss	/	1

Table B.2 – Translocations and fusion genes

Table 2. Overview of the detected translocations and the corresponding fusion genes in sample RH30.

Chromosome region	SV type	Reported fusion genes
t(1;7)(q32.1;p22.3)	Translocation	*MROH3P::MAD1L1*
t(2;17)(q32.1;p12)	Translocation	/
t(2;13)(q36.1;q14.11)	Translocation	PAX3::FOXO1
t(X;3)(p26.1;q22.1)	Translocation	*GRM7::PCDH19*
t(3;3)(p24.3;p24.1)	Translocation	/
t(5;17)(q25.3;p13.3)	Translocation	/
t(X;6)(q22.1;q25.3)	Translocation	/
t(14;14)(q32.33;q32.2)	Translocation	/
t(X;17)(q28;q12)	Translocation	/
t(18;20)(q23;p13)	Translocation	/
t(X;X)(p22.11;q13.3)	Translocation	/
t(X;X)(q13.3;q23)	Translocation	/
t(X;X)(q13.3;q25)	Translocation	/

Table B.3 – Other structural variants

Table 3. Overview of the other detected structural variants (deletions, insertions, duplications) in sample RH30.

Chromosome	SV type	Genes involved
2p16.3	Deletion	/
3p21.2	Insertion	/
3q28	Deletion	/
6p21.1	Deletion	/
6q13	Insertion	/
7q11.21	Deletion	/
9q21.11	Duplication	/
9q21.13	Duplication	/
10p12.2	Insertion	/
11p14.3	Deletion	/
11q14.3	Insertion	/
11q25	Duplication	/
12p13.33	Duplication	/
12q13.3	Deletion	/
14q12	Deletion	/
14q23.3	Insertion	/

Chromosome	SV type	Genes involved
14q32.2q32.33	Duplication	/
15q26.3	Insertion	/
18p11.21	Insertion	/
18q22.3	Insertion	/
20p12.3	Duplication	/
20q11.1	Duplication	/
21q21.1	Insertion	/

Addendum C – Results OGM analysis cell line RH41

Table C.1 – Copy number variants (CNV)

Table 1. Overview of the detected copy number variants in sample RH41, indicating the type of abnormality, the reported genes from the sarcoma gene list and the copy number (CN).

Chromosome region	Abnormality type	Reported genes (sarcoma gene list)	Copy number (CN)
1p36.23p36.11	*Gain*	*SDHB, ARID1A*	*3*
1p36.11p35.2	*Loss*	*/*	*1*
1p35.1p31.3	*Gain*	*MEAF6*	
1p13.1p11.2	*Gain*	*/*	*3*
1q21.1q32.1	*Gain*	*NTRK1, SDHC, GPR161*	*3*
2p22.1p11.2	*Gain*	*/*	*3*
2q11.2q37.3	*Gain*	*SF3B1, IDH1, BARD1, PAX3*	*3*
3q21.3	*Gain*	*/*	*3*
3q22.3q24	*Gain*	*/*	*3/4*
3q26.33	*Gain*	*/*	*3*
4q25q35.2	*Gain*	*FBXW7*	*3*
6p25.3p11.1	*Gain*	*PHF1*	*3*
7p22.2p14.1	*Gain*	*JAZF1*	*3/4*
7q11.21q36.3		*CDK6, MET, SMO, BRAF*	

Chromosome region	Abnormality type	Reported genes (sarcoma gene list)	Copy number (CN)
8p11.23p11.21	*Gain*	*FGFR1*	*> 8*
8q11.1q24.23	*Gain*	*PLAG1, MYBL1, NCOA2, NBN, RSPO2, MYC*	*3/4*
9q22.1q22.33	*Gain*	*PTCH1, NR4A3*	*3*
10p15.3p11.1	*Loss*	*GATA3, EPC1*	*1*
11p14.1p11.12	*Gain*	*/*	*3*
11q12.1q13.2	*Gain*	*RELA*	*3*
11q23.2q25	*Gain*	*CHEK1*	*3/4*
12p13.33p11.1	*Gain*	*KRAS*	*3*
12q12q21.1	*Gain*	*ERBB3, STAT6, GLI1, CDK4, HMGA2, MDM2*	*3*
12q24.31q24.33	*Gain*	*/*	*3*
15q26.2q26.3	*Gain*	*/*	*3/4*
16q21	*Loss*	*/*	*1*
17q21.32q25.3	*Gain*	*SPOP, RNF43, RAD51C, BRIP1, PRKCA, H3-3B*	*4*
18q11.2q21.1	*Gain*	*SS18*	*4*
18q21.1q23	*Loss*	*SMAD4*	*1*

Chromosome region	Abnormality type	Reported genes (sarcoma gene list)	Copy number (CN)
19p13.2p12	*Gain*	*/*	*3*
19q12q13.43	*Gain*	*CIC, FOSB*	*3*

Table C.2 – Translocations and fusion genes

Table 2. Overview of the detected translocations and the corresponding fusion genes in sample RH41.

Chromosome region	SV type	Reported fusion genes
t(1;1)(p36.13;p35.2)	Translocation	/
t(9;16)(q21.32;q22.1)	Translocation	/
t(11;22)(q13.2;q13.31)	Translocation	/
t(11;20)(q11.23;q13.2)	Translocation	*DHX35::PPP6R3*
t(12;16)(q22.1;p11.21)	Translocation	/
t(11;17)(q25;q21.32)	Translocation	/
t(20;22)(q13.31;q12)	Translocation	/

Table C.3 – Other structural variants

Table 3. Overview of the other detected structural variants (deletions, insertions, duplications, inversions) in sample RH41.

Chromosome region	SV type	Reported fusion genes
5q35.3	Deletion	*FGFR4*

Chromosome region	SV type	Reported fusion genes
9p21.3	Deletion	*MTAP, CDKN2A, CDKN2B*
12q15	Inversion	*MDM2*

Addendum D – Results OGM analysis cell line RMS-YM

Table D.1 – Copy number variants (CNV)

Table 1. Overview of the detected copy number variants in sample RMS-YM, indicating the type of abnormality, the reported genes from the sarcoma gene list and the copy number (CN).

Chromosome region	Abnormality type	Reported genes (sarcoma gene list)	Copy number (CN)
1p36.23p36.11	Gain	*SDHB*	3
1p36.11p35.2	Loss	/	1
1p35.1p31.3	Gain	*MEAF6*	3
1p13.1p12	Gain	/	3
1q21.1q32.1	Gain	*NTRK1, SDHC, GPR161*	3
2p22.1p11.2	Gain	/	3
2q11.1q22.1	Gain	/	3
2q22.1q22.2	Loss	/	1
2q22.2q37.3	Gain	*SF3B1, IDH1, BARD1, PAX3*	3
3q21.3	Gain	/	3
3q22.3q24	Gain	/	4
3q26.33	Gain	/	3
3q29	Gain	/	4
4q25q35.2	Gain	*FBXW7*	3

Chromosome region	Abnormality type	Reported genes (sarcoma gene list)	Copy number (CN)
5q13.2	Gain	/	3
6p	Gain	*PHF1*	3
7p22.2p14.1	Gain	*JAZF1*	3/4
7q	Gain	*CDK6, MET, SMO, BRAF*	4/5
8p12p11.21	Gain	*FGFR1*	6
8q	Gain	*PLAG1, MYBL1, NCOA2, NBN, RSPO2*	4
9q21.31	Gain	/	3
9q21.33q22.33	Gain	*PTCH1, NR4A3*	3
10p	Loss	*GATA3, EPC1*	1
10q21.1	Loss	/	1
10q21.2	Gain	/	3
11p14.1p11.12	Gain	*KBTBD4*	3
11q12.1q13.2	Gain	*RELA*	4
11q23.2q25	Gain	*CHEK1*	3/4
12p13.33p11.1	Gain	*KRAS*	1
12q12q13.13	Gain	/	3

Chromosome region	Abnormality type	Reported genes (sarcoma gene list)	Copy number (CN)
12q15	Gain	*MDM2*	8
12q24.31q24.33	Gain	/	3
13q11q13.3	Gain	*BRCA2*	3
15q26.2q26.3	Gain	/	3
16q21	Loss	/	1
17q21.33q25.3	Gain	*RNF43, SPOP, RAD51C, BRIP1, PRKCA, H3-3B*	4
18q11.2q21.1	Gain	*SS18*	3/4
18q21.1q23	Loss	*SMAD4*	1
19p/q	Gain	*STK11, GNA11, KEAP1, SMARCA4, CCNE1, CIC, FOSB*	3
20q12	Loss	/	1
Xq21.2q28	Gain	/	2

Table D.2 – Structural variants

Table 2. Overview of the detected structural variants (insertions, deletions, duplications, inversions) in sample RMS-YM, with the genes involved.

Chromosome region	SV type	Genes involved
3p25.2	Insertion	*RAF1*
7p11.2	Deletion	*EGFR*
7q21.2	Duplication	*CDK6*
8p12	Deletion	*NRG1*
9p21.3	Deletion	*MTAP, CDKN2A, CDKN2B*
9q34.3	Insertion	*NOTCH1*
12q15	Insertion	*MDM2*
12q15	Deletion	*MDM2*
12q15	Inversion	*MDM2*
12q15	Deletion	*MDM2*
14q24.1	Duplication	*RAD51B*
14q32.33	Insertion	*AKT1*
15q14	Insertion	*NUTM1*
17q24.2	Insertion	*PRKCA*
18p13.3	Insertion	*STK11*
18p13.2	Deletion	*KEAP1*

Addendum E – Results OGM analysis PEDSAR02 (tumoroid)

Table E.1 – Copy number variants (CNV)

Table 1. Overview of the detected copy number variants in tumoroid sample PEDSAR02, indicating the type of abnormality, the reported genes from the sarcoma gene list and the copy number (CN).

Chromosome region	Abnormality type	Reported genes (sarcoma gene list)	Copy number (CN)
1q21.1q43	Gain	*NTRK1, SDHC, GPR161*	3
5q12.1q23.1	Loss	*PIK3R1, APC*	1
10q22.3q26.3	Loss	*PTEN, SUFU, FGFR2*	1
13q14.11q14.3	Loss	*RB1*	1
17p13.3p11.2	Loss	*YWHAE, USP6, TP53*	1
17q	Gain	*NF1, RAD51D, TAF15, CDK12, ERBB2, STAT3, BRCA1, SPOP, RNF43, RAD51C, BRIP1, PRKCA, H3-3B*	
21q	Gain	*ERG, TMPRSS2*	3

Table E.2 – Translocations and fusion genes

Table 2. Overview of the detected translocations and the corresponding fusion genes in tumoroid sample PEDSAR02.

Chromosome region	SV type	Reported fusion genes
t(1;X)(p21.2;p11.3)	Translocation	/
t(1;2)(p36.31;q34)	Translocation	/
t(1;7)(p21.2;q21.12)	Translocation	/
t(2;10)(p25.3;q22.3)	Translocation	/
t(2;3)(p22.3;p21.1)	Translocation	*ST3GAL5::CACNA2D3*
t(2;13)(q36.1;q14.11)	Translocation	*PAX3::FOXO1*
t(4;13)(q34.3;q31.1)	Translocation	/
t(4;6)(q34.3;q22.31)	Translocation	/
t(4;8)(q34.3;q13.2)	Translocation	*LINC02509::CSPP1*
t(5;5)(q12.1;q23.1)	Translocation	/
t(X;7)(p11.3;q21.12)	Translocation	*ABCB1:: RBM10*
t(13;13)(q14.11;q14.3)	Translocation	*FOXO1::WDFY2*

Table E.3 – Other structural variants

Table 3. Overview of the other detected structural variants (insertions) in tumoroid sample PEDSAR02, with the genes involved.

Chromosome region	SV type	Genes involved
2q36.1	Insertion	/
14q24.1	Insertion	*RAD51B*
14q32.13	Insertion	*DICER1*
15q21.3	Insertion	*TCF12*
17	Insertion	*TP53*

Addendum F – Results OGM analysis PEDSAR03 (tumoroid)

Table F.1 – Copy number variants (CNV)

Table 1. Overview of the detected copy number variants in sample PEDSAR03, indicating the type of abnormality, the reported genes from the sarcoma gene list and the copy number (CN).

Chromosome region	Abnormality type	Reported genes (sarcoma gene list)	Copy number (CN)
1p	Gain	*SDHB, ARID1A, MEAF6, JAK1, DPYD, CSF1, NRAS*	3
1q	Gain	*NTRK1, SDHC, GPR161, H3-3A*	3
2p/q	Gain	*NCOA1, ALK, SF3B1, IDH1, BARD1, PAX3*	3/4
4p	Gain	/	3
4q12	Gain	*KIT, PDGFRA*	3
5p/q	Gain	*DROSHA, IL6ST, PIK3R1, APC, RAD50*	3
7p/q	Gain	*JAZF1, EGFR, CDK6, MET, BRAF*	3
9p24.1	Gain	*JAK2*	4
9q21.33	Gain	*NTRK2*	3
9q22.32	Gain	*PTCH1*	6
9q31.1	Gain	*NR4A3*	4
9q31.3	Gain	*ELP1*	5
9q34.13	Gain	/	4/5

Chromosome region	Abnormality type	Reported genes (sarcoma gene list)	Copy number (CN)
11p/q	Gain	*MRE11, YAP1, ATM, SDHD, CHEK1*	3
13q12.11q13.3	Gain	*BRCA2, FOXO1*	3
14q23.1	Gain	/	3
16p/q	Gain	*PALB2, PRKCB*	3
16q12.1q24.1	Gain	*CDH1*	3
17p13.2p11.2	Gain	*YWHAE, USP6, TP53*	3
18p/q	Gain	*SS18, SMAD4*	3
20p/q	Gain	*GNAS*	3/4
21q	Gain	*ERG, TMPRSS2*	3
22q	Gain	*DGCR8, SMARCB1, CHEK2, EWSR1, NF2, PDGFB*	3
Xq24q28	Gain	/	3

Table F.2 – Translocations and fusion genes

Table 2. Overview of the detected translocations and the corresponding fusion genes in sample PEDSAR03.

Chromosome region	SV type	Reported fusion genes
t(2;13)(q36.1;q14.11)	Translocation	*PAX3::FOXO1*
t(2;13)(q36.1;q31.1)	Translocation	/

Table F.3 – Other structural variants

Table 3. Overview of the other detected structural variants (insertions, deletions, duplications) in sample PEDSAR03, with the genes involved.

Chromosome region	SV type	Genes involved
3p25.2	Insertion	*RAF1*
5p15.33	Deletion	/
6q25.2	Deletion	*ESR1*
8p12	Deletion	*NRG1*
9q31.1	Duplication	/
14q32.33	Insertion	*AKT1*
15q14	Insertion	*NUTM1*
17q11.2	Insertion	*NF1*
17q24.2	Deletion	*PRKCA*
19p13.3	Insertion	*STK11*
22q12.2	Deletion	/

Addendum G – Results OGM analysis MSKPED0023 (tumoroid)

Table G.1 – Copy number variants (CNV)

Table 1. Overview of the detected copy number variants in sample MSKPED0023, indicating the type of abnormality, the reported genes from the sarcoma gene list and the copy number (CN).

Chromosome region	Abnormality type	Reported genes (sarcoma gene list)	Copy number (CN)
1q23.2	Gain	/	4
2p/q	Gain	*MYCN, NCOA1, ALK, SF3B1, IDH1, BARD1, PAX3*	3
5p	Gain	*TERT, DROSHA*	3
5q11.2q34	Gain	*APC, RAD50, PDGFRB, FGFR4*	3
5q34	Loss	/	1
6p22.1	Loss	/	1
6q15q16.1	Gain	/	2/3
7q31.1	Loss	/	1
8q24.12	Loss	/	1
9p	Loss	*JAK2, MTAP, CDKN2A, CDKN2B*	1
9q21.11q22.31	Loss	*GNAQ, NTRK2*	1
9q22.32q32	Gain	*PTCH1, NR4A3, ELP1*	3
10q21.1	Loss	/	1
10q22.3	Gain	/	3

Chromosome region	Abnormality type	Reported genes (sarcoma gene list)	Copy number (CN)
11p	Gain	*KBTBD4*	3
11q12.1q22.3	Gain	*RELA, CCND1, MRE11, YAP1, ATM, SDHD*	3
11q24.1q25	Gain	*CHEK1*	3
12p13.33p13.1	Loss	/	1
12q15	Gain	*MDM2*	7/8
15q11.2q23	Loss	*NUTM1, TCF12, MAP2K1*	1
17p	Loss	*TP53*	1
17q11.2q21.32	Loss	*NF1, RAD51D, TAF15, CDK12, ERBB2, STAT3, BRCA1*	1
17q21.33q25.3	Gain	*SPOP, RNF43, RAD51C, BRIP1, PRKCA*	2/3
18q12.2q23	Loss	*SMAD4*	1
20p/q	Gain	*GNAS*	3
21q11.2q21.2	Gain	/	2/3
21q22.11q22.3	Loss	*ERG, TMPRSS2*	1

Table G.2 – Other structural variants

Table 2. Overview of the other detected structural variants (insertions, deletions, duplications) in sample MSKPED0023, with the genes involved.

Chromosome region	SV type	Genes involved
3p25.2	Insertion	*RAF1*
3p22.2	Insertion	/
8p12	Deletion	*NRG1*
9q34.3	Deletion	*NOTCH1*
12q15	Insertion	*MDM2*
12q15	Deletion	*MDM2*
12q15	Duplication	*MDM2*
14q32.33	Insertion	*AKT1*
15q14	Insertion	*NUTM1*
18q21.2	Deletion	*SMAD4*
19p13.3	Insertion	*STK11*

Addendum H – Results OGM analysis MSKPED0087 (tumoroid)

Table H.1 – Copy number variants (CNV)

Table 1. Overview of the detected copy number variants in sample MSKPED0087, indicating the type of abnormality, the reported genes from the sarcoma gene list and the copy number (CN).

Chromosome region	Abnormality type	Reported genes (sarcoma gene list)	Copy number (CN)
1q21.1q44	Gain	*NTRK1, SDHC, GPR161, H3-3A*	3
2p23.3p11.2	Gain	*ALK*	3
2q14.1q22.3	Gain	/	3
2q23.3q24.2	Gain	/	3
2q31.1q32.2	Gain	/	3
2q32.3q33.3	Gain	*SF3B1*	3
2q34q37.3	Gain	*PAX3, BARD1*	3
5p15.33p12	Gain	*DROSHA*	3
5q11.2q13.3	Gain	*IL6ST, PIK3R1*	3
5q14.3q35.3	Gain	*APC, RAD50, PDGFRB, FGFR4*	3
7p22.3p11.2	Gain	*JAZF1, EGFR*	
7q11.21q31.2	Gain	*CDK6*	3
8p23.3p11.21	Gain	*NRG1, FGFR1*	3
8q11.1q24.21	Gain	*NBN, RSPO2*	3

Chromosome region	Abnormality type	Reported genes (sarcoma gene list)	Copy number (CN)
9p24.3p21.1	Loss	*JAK2, CDKN2A*	1
9p13.3	Gain	/	3
9q21.11q21.32	Gain	*GNAQ*	3
9q22.32q31.1	Loss	*PTCH1, NR4A3*	1
11p15.4p11.12	Gain	/	3
11q12.1q14.1	Gain	*RELA, CCND1*	3
12p13.33p11.21	Gain	*KRAS*	3
12q12q21.31	Gain	*ERBB3, STAT6, GLI1, CDK4, HMGA2, MDM2*	3
13q11q31.2	Loss	*BRCA2, FOXO1, RB1*	1
17p13.1p11.2	Loss	*TP53*	1
17q11.1q21.2	Loss	*NF1, RAD51D, TAF15, CDK12, ERBB2*	1
17q21.2q25.3	Gain	*STAT3, BRCA1, SPOP, RNF43, RAD51C, BRIP1, PRKCA, H3-3B*	3
18p11.32p11.21	Gain	/	3
18q11.2q21.2	Gain	*SS18, SMAD4*	3
18q21.2q23	Loss	/	1

Chromosome region	Abnormality type	Reported genes (sarcoma gene list)	Copy number (CN)
20p13p11.21	Gain	/	3
20q11.21q13.33	Gain	*GNAS*	3
Xq26.3q28	Gain	/	3

Table H.2 – Other structural variants

Table 2. Overview of the other detected structural variants (deletions) in sample MSKPED0087, with the genes involved.

Chromosome region	SV type	Genes involved
5q35.3	Deletion	*FGFR4*
9p21.3	Deletion	*MTAP, CDKN2A, CDKN2B*

Addendum I – Results OGM analysis chondrosarcoma

Table I.1 – Copy number variants (CNV)

Table 1. Overview of the detected copy number variants in the chondrosarcoma sample, indicating the type of abnormality, the reported genes from the sarcoma gene list and the copy number (CN).

Chromosome region	Abnormality type	Reported genes (sarcoma gene list)	Copy number (CN)
1p33	Duplication	/	4
1p32.2p31.3	Duplication	*JAK1*	3
1p31.2p13.3	Duplication	*DPYD*	3
1q21.1q22	Deletion	*NTRK1*	1
1q23.3	Deletion	*SDHC*	1
1q32.1q32.3	Deletion	/	1
2p25.1	Deletion	/	1
2p23.3p23.2	Deletion	*NCOA1, ALK*	1
2p12p11.2	Duplication	/	3/4
2q11.2q13	Duplication	/	3/4
2q22.1q32.3	Duplication	/	3
2q33.3q34	Duplication	*IDH1, BARD1*	3
3p26.3p22.1	Duplication	*VHL, PPARG, RAF1, CTNNB1*	3/4
3p14.2p14.1	Duplication	/	3

Chromosome region	Abnormality type	Reported genes (sarcoma gene list)	Copy number (CN)
3p12.3p11.1	Duplication	/	3
3q11.1q13.31	Duplication	*TFG*	3
3q22.1q26.33	Duplication	*PIK3CA*	3
4p13p12	Duplication	/	3
4q35.1q35.2	Deletion	/	1
5p15.33	Duplication	/	4
5p15.31p13.3	Duplication	*DROSHA*	3
5p13.3p13.2	Duplication	/	3
5p13.1p12	Duplication	/	3
6p22.3p22.1	Duplication	/	3
7p21.3p14.1	Duplication	*JAZF1, EGFR*	3
7q11.21q11.22	Duplication	/	3
7q21.11q21.3	Duplication	*CDK6*	3
7q22.1q33	Duplication	*MET, SMO*	3
7q35	Duplication	/	3
8q11.1q21.3	Duplication	*PLAG1, MYBL1, NCOA2, NBN*	3

Chromosome region	Abnormality type	Reported genes (sarcoma gene list)	Copy number (CN)
8q22.3q24.23	Duplication	*RSPO2*	3
9p24.3p22.1	Deletion	*JAK2*	1
9p21.2p21.1	Duplication	/	3
9q21.11q21.13	Duplication	/	3/4
9q21.2q21.33	Duplication	*GNAQ, NTRK2*	3/4
9q22.2q22.31	Duplication	/	3/4
9q22.31q31.3	Duplication	*PTCH1, NR4A3, ELP1*	3/4
9q33.1q33.2	Duplication	/	3/4
10p14	Deletion	/	1
10q22.2q22.3	Deletion	/	1
10q26.12q26.3	Deletion	*FGFR2*	1
11p15.4p13	Duplication	/	4
11q14.3q23.2	Duplication	*MRE11, YAP1, ATM, SDHD*	3
12p12.3p11.21	Duplication	*KRAS*	3
12q12	Duplication	/	3
12q13.12q14.1	Deletion	*COL2A1, ERBB3, STAT6, GLI1, CDK4*	1

Chromosome region	Abnormality type	Reported genes (sarcoma gene list)	Copy number (CN)
12q23.3q24.11	Deletion	/	0
12q24.23q24.31	Deletion	*HNF1A*	
14q21.1q21.3	Duplication	/	3
14q32.13q32.2	Duplication	*DICER1*	3
15q14q15.3	Deletion	/	1
15q24.1q25.1	Deletion	/	1
16p13.12p13.11	Deletion	/	1
16p12.1p11.2	Deletion	/	1
16q22.1q23.1	Deletion	*CDH1*	1
17q21.33q22	Duplication	/	3
17q21.33q22	Duplication	/	3
17q23.2q24.2	Duplication	*BRIP1, PRKCA*	4/5
17q24.2q24.3	Duplication	/	3
18q21.1	Deletion	*SMAD4*	1
19p12	Duplication	/	4
19q12	Deletion	*CCNE1*	1

Chromosome region	Abnormality type	Reported genes (sarcoma gene list)	Copy number (CN)
19q13.11q13.41	Deletion	*CIC, FOSB*	1
20p12.3p12.1	Duplication	/	3
20q13.2q13.32	Duplication	/	3
21q11.2q22.11	Duplication	/	3
Xp22.33p11.4	Duplication	*EIF1AX, BCOR, DDX3X*	3
Xq11.1q28	Duplication	*AR*	4/5

Table I.2 – Translocations and fusion genes

Table 2. Overview of the detected translocations and the corresponding fusion genes in the chondrosarcoma sample.

Chromosome region	SV type	Reported fusion genes
t(3;6)(q26.31;q23.3)	Translocation	*NAALADL2::PEX7*
t(6;17)(q12;p11.2)	Translocation	*ADGRB3:: DRC3*
t(6;11)(q22.32;q14.1)	Translocation	/
t(9;9)(p24.3;p21.3)	Translocation	*KANK1::DMRTA1*
t(17;11)(q23.2;q13.2)	Translocation	*LINC01999::RBM4B*
t(17;11)(q24.1;q14.1)	Translocation	*CEP112::AAMDC*
t(17;11)(q24.2;q14.1)	Translocation	/

Chromosome region	SV type	Reported fusion genes
t(17;17)(q24.2;q21.31)	Translocation	*LINC02594::PRKCA*

Table I.3 – other structural variants

Table 3. Overview of the other detected structural variants (deletions, insertions, duplications, inversions) in the chondrosarcoma sample.

Chromosome region	SV type	Genes involved
2q21.1	Duplication	/
2q31.2	Deletion	/
3q12.3	Deletion	/
3q26.31	Deletion	/
5p15.33	Duplication	/
7q21.11	Deletion	/
7q21.11	Inversion	/
7q21.11	Duplication	/
10p12.31	Insertion	/
11p13	Deletion	/
11p12	Deletion	/
11q12.1	Deletion	/
11q14.1	Deletion	/

Chromosome region	SV type	Genes involved
11p12	Inversion	/
11p12	Inversion	/
11p12	Inversion	/
11p12	Deletion	/
11q13.3	Duplication	/
11p12	Duplication	/
11p12	Duplication	/
12q12	Insertion	/
12q23.1	Deletion	/
17q21.31	Duplication	/

Addendum J – Results OGM analysis MPNST (routine)

Table J.1 – Copy number variants (CNV)

Table 1. Overview of the detected copy number variants in sample MPNST (routine), indicating the type of abnormality, the reported genes from the sarcoma gene list and the copy number (CN).

Chromosome region	Abnormality type	Reported genes (sarcoma gene list)	Copy number (CN)
1p	Duplication	*CAMTA1*, *SDHB*, *ARID1A*, *MEAF6*, *JAK1*, *DPYD*, *CSF1*, *NRAS*	3
1q21.3q25.3	Duplication	*NTRK1*, *SDHC*, *GPR161*	4
1q42.3q44	Deletion	/	1
2p24.1p16.1	Duplication	*NCOA1*, *ALK*	3
2p15p12	Deletion	/	1
2q11.2	Deletion	/	1
2q13q14.2	Duplication	/	3
2q37.1q37.3	Deletion	/	1
3p	Duplication	*VHL*, *PPARG*, *RAF1*, *CTNNB1*, *BAP1*, *PRKCD*	3/4
3q	Duplication	*PIK3CA*	2/3
4p16.1p14	Deletion	/	1
4q22.1q31.23	Deletion	/	1

Chromosome region	Abnormality type	Reported genes (sarcoma gene list)	Copy number (CN)
5p15.2p12	Duplication	*DROSHA*	3/4
5q21.1q35.2	Duplication	*APC*, *RAD50*, *PDGFRB*	3
6q	Deletion	*FRK*, *ROS1*, *RSPO3*, *MYB*, *ESR1*	1
7p22.2p14.3	Duplication	*JAZF1*	2/3
7q21.11q21.3	Duplication	*CDK6*	6
7q22.1q31.31	Duplication	*MET*	4
7q31.32q34	Duplication	*SMO*, *BRAF*	5
8p23.2	Duplication	/	4
8p22p21.3	Duplication	/	2/3
8p21.2p11.21	Duplication	*NRG1*, *FGFR1*	4
8q12.3q24.3	Deletion	*MYBL1*, *NCOA2*, *NBN*, *RSPO2*	1
9p24.3p22.1	Duplication	*JAK2*	3
9p21.3	Deletion	*MTAP*, *CDKN2A*, *CDKN2B*	1
9p21.3p13.1	Duplication	/	3

Chromosome region	Abnormality type	Reported genes (sarcoma gene list)	Copy number (CN)
9q21.11q34.2	Duplication	*GNAQ*, *NTRK2*, *PTCH1*, *NR4A3*, *ELP1*, *NOTCH1*	3
10p15.2p14	Deletion	*GATA3*	1
11p14.3p11.2	Deletion	/	1
11q12.1q13.5	Duplication	*RELA*, *CCND1*	4
11q14.1q22.3	Duplication	*MRE11*, *YAP1*, *ATM*	2/3
11q23.3q25	Deletion	*CHEK1*	1
12p13.33p13.31	Duplication	/	4
13q	Deletion	*BRCA2*, *FOXO1*, *RB1*	1
17p13.1	Deletion	*TP53*	1
17p13.1p11.2	Duplication	/	4
17q11.2q21.31	Deletion	*NF1*, *RAD51D*, *TAF15*, *CDK12*, *ERBB2*, *STAT3*, *BRCA1*	1
17q21.32q24.2	Duplication	*SPOP*, *RNF43*, *RAD51C*, *BRIP1*, *PRKCA*	3/4
18p11.31p11.22	Duplication	/	1
18q11.2q12.3	Duplication	*SS18*	3

Chromosome region	Abnormality type	Reported genes (sarcoma gene list)	Copy number (CN)
19q12q13.12	Duplication	*CCNE1*	3
20p13p12.2	Deletion	/	1
20q13.32	Duplication	*GNAS*	4

Table J.2 – Translocations and fusion genes

Table 2. Overview of the detected translocations and the corresponding fusion genes in sample MPNST (routine).

Chromosome region	SV type	Reported fusion genes
t(7;7)(p11.2;p14.1)	Translocation	-
t(14;17)(q11.2;q24.2)	Translocation	-
t(17;17)(q22;q22)	Translocation	-

Table J.3 – Other structural variants

Table 3. Overview of the other detected structural variants (insertions, deletions, duplications) in sample MPNST (routine), with the genes involved.

Chromosome region	SV type	Genes involved
2p24.3	Deletion	*MYCN*
7q21.2	Deletion	*CDK6*
8p12	Duplication	*NRG1*
17q11.2	Insertion	*NF1*

Chromosome region	SV type	Genes involved
20q13.32	Duplication	*GNAS*

Addendum K – Results OGM analysis MPNST (OT)

Table K.1 – Copy number variants (CNV)

Table 1. Overview of the detected copy number variants in sample MPNST (OT), indicating the type of abnormality, the reported genes from the sarcoma gene list and the copy number (CN).

Chromosome region	Abnormality type	Reported genes (sarcoma gene list)	Copy number (CN)
1p	Duplication	*CAMTA1*, *SDHB*, *ARID1A*, *MEAF6*, *JAK1*, *DPYD*, *CSF1*, *NRAS*	3
1q21.3q25.3	Duplication	*NTRK1*, *SDHC*, *GPR161*	4
1q42.3q44	Deletion	/	1
2p24.1p16.1	Duplication	*NCOA1*, *ALK*	3
2p15p12	Deletion	/	1
2q11.2	Deletion	/	1
2q13q14.2	Duplication	/	3
2q37.1q37.3	Deletion	/	1
3p	Duplication	*VHL*, *PPARG*, *RAF1*, *CTNNB1*, *BAP1*, *PRKCD*	3/4
3q	Duplication	*PIK3CA*	2/3

Chromosome region	Abnormality type	Reported genes (sarcoma gene list)	Copy number (CN)
4p16.1p14	Deletion	/	1
4q22.1q31.23	Deletion	/	1
5p15.2p12	Duplication	*DROSHA*	3/4
5q21.1q35.2	Duplication	*APC*, *RAD50*, *PDGFRB*	3
6q	Deletion	*FRK*, *ROS1*, *RSPO3*, *MYB*, *ESR1*	1
7p22.2p14.3	Duplication	*JAZF1*	2/3
7q21.11q21.3	Duplication	*CDK6*	6
7q22.1q31.31	Duplication	*MET*	4
7q31.32q34	Duplication	*SMO*, *BRAF*	5
8p23.2	Duplication	/	4
8p22p21.3	Duplication	/	2/3
8p21.2p11.21	Duplication	*NRG1*, *FGFR1*	4
8q12.3q24.3	Deletion	*MYBL1*, *NCOA2*, *NBN*, *RSPO2*	1
9p24.3p22.1	Duplication	*JAK2*	3
9p21.3	Deletion	*MTAP*, *CDKN2A*, *CDKN2B*	1
9p21.3p13.1	Duplication	/	3

Chromosome region	Abnormality type	Reported genes (sarcoma gene list)	Copy number (CN)
9q21.11q34.2	Duplication	*GNAQ*, *NTRK2*, *PTCH1*, *NR4A3*, *ELP1*, *NOTCH1*	3
10p15.2p14	Deletion	*GATA3*	1
11p14.3p11.2	Deletion	/	1
11q12.1q13.5	Duplication	*RELA*, *CCND1*	4
11q14.1q22.3	Duplication	*MRE11*, *YAP1*, *ATM*	2/3
11q23.3q25	Deletion	*CHEK1*	1
12p13.33p13.31	Duplication	/	4
13q	Deletion	*BRCA2*, *FOXO1*, *RB1*	1
17p13.1	Deletion	*TP53*	1
17p13.1p11.2	Duplication	/	4
17q11.2q21.31	Deletion	*NF1*, *RAD51D*, *TAF15*, *CDK12*, *ERBB2*, *STAT3*, *BRCA1*	1
17q21.32q24.2	Duplication	*SPOP*, *RNF43*, *RAD51C*, *BRIP1*, *PRKCA*	3/4
18p11.31p11.22	Duplication	/	1
18q11.2q12.3	Duplication	*SS18*	3
19q12q13.12	Duplication	*CCNE1*	3

Chromosome region	Abnormality type	Reported genes (sarcoma gene list)	Copy number (CN)
20p13p12.2	Deletion	/	1
20q13.32	Duplication	*GNAS*	4

Table K.2 – Translocations and fusion genes

Table 2. Overview of the detected translocations and the corresponding fusion genes in sample MPNST (OT).

Chromosome region	SV type	Reported fusion genes
t(7;7)(p11.2;p14.1)	Translocation	-
t(7;20)(p22.1;q13.32)	Translocation	-
t(14;17)(q11.2;q24.2)	Translocation	-
t(17;17)(q22;q22)	Translocation	-

Table K.3 – Other structural variants

Table 3. Overview of the other detected structural variants (insertions, deletions, duplications) in sample MPNST (OT), with the genes involved.

Chromosome region	SV type	Genes involved
7p11.2	Inversion	*EGFR*
7p11.2	Duplication	*EGFR*
7q21.2	Deletion	*CDK6*
8p12	Duplication	*NRG1*

Chromosome region	SV type	Genes involved
11p15.5	Duplication	*HRAS*
17q11.2	Insertion	*NF1*
17q22	Deletion	*RNF43*, *RAD51C*
20q13.32	Duplication	*GNAS*

ADDENDUM L

Bionano Prep SP Frozen Cell Pellet DNA Isolation Protocol

Document Number: 30268

Document Revision: D

Table of Contents

Legal Notice

For Research Use Only. Not for use in diagnostic procedures.

Revision History

Revision	Notes
A	Initial Release
B	Updated name for Bionano Prep SP Magnetic Retriever
C	Included additional indications, pointing the user towards the Appendix for preparing frozen cell pellets.
D	Corrected Part Number of Standard Microfuge Tubes, 2.0 ml

Workflow Overview

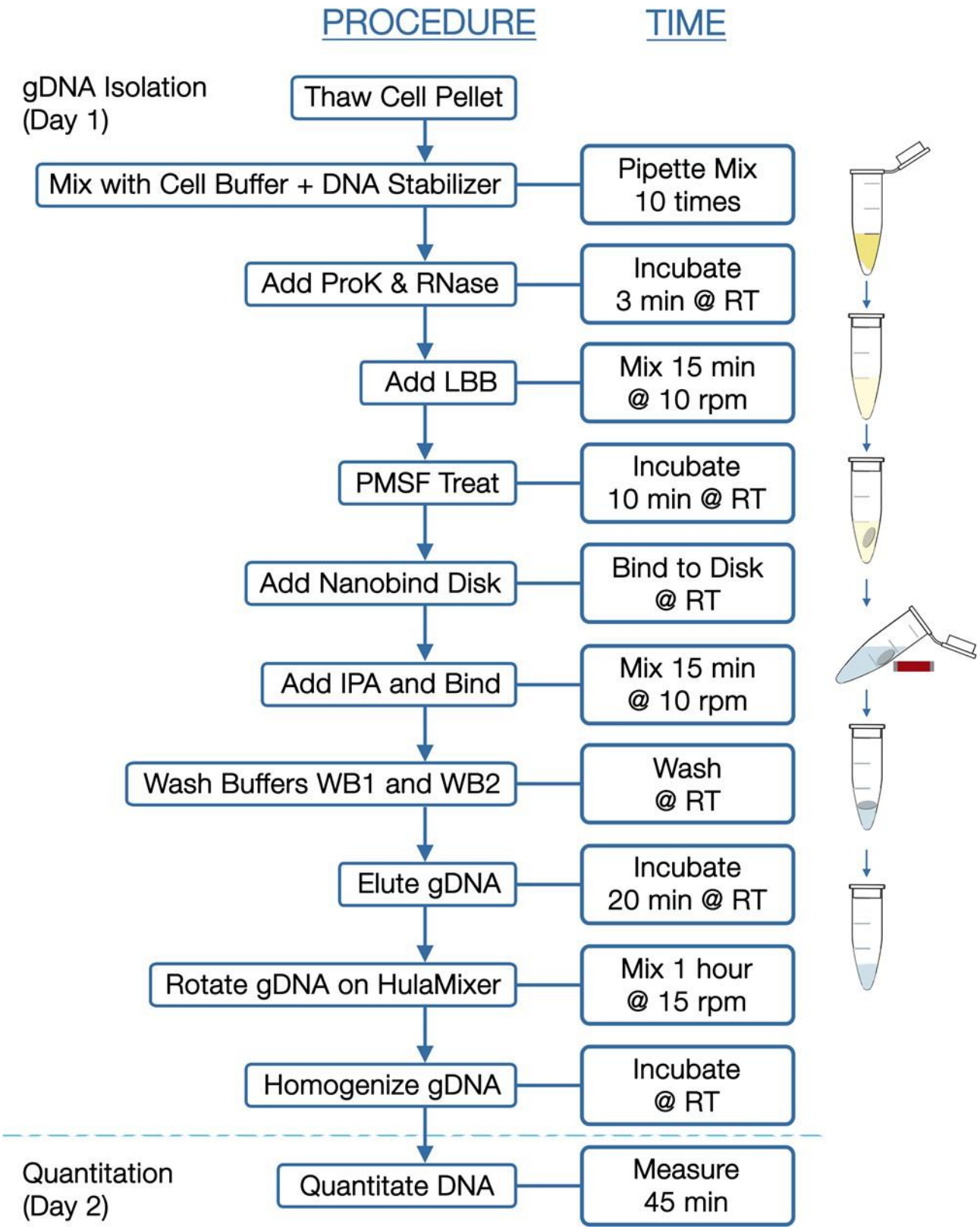

Bionano Prep SP DNA Isolation Kit and User-Supplied Materials

Table 1: Bionano Prep SP Blood & Cell Culture DNA Isolation Kit Contents (Part # 800030, 10 preps)

Item	Amount	Part Number	Storage
Nanobind Disks	10 disks	20379	Room Temp (18-25°C)
Protein LoBind Microcentrifuge Tubes, 1.5 ml	20 tubes	20380	Room Temp (18-25°C)
RNase A Enzyme	200 µl	20373	Refrigerate (4°C)
DNA Stabilizer	20 µl	20397	Room Temp (18-25°C)
Standard Microfuge Tubes, 2.0 ml	10 tubes	20396	Room Temp (18-25°C)
Cell Buffer	50 ml	20374	Room Temp (18-25°C)
Proteinase K Enzyme	0.5 ml	20372	Room Temp (18-25°C)
Lysis and Binding Buffer (LBB)*	2.5 ml	20375	Room Temp (18-25°C)
Wash Buffer 1 Concentrate (2.5X) (WB1)*	3.25 ml	20376	Room Temp (18-25°C)
Wash Buffer 2 Concentrate (2.5X) (WB2)	5 ml	20377	Room Temp (18-25°C)
Elution Buffer (EB)	1.1 ml	20378	Room Temp (18-25°C)
Magnetic Disk Retriever Plastic Sheath	10	20381	Room Temp (18-25°C)

* See Important Notes Section for hazardous waste information

Table 2: User-Supplied Materials

Item	Supplier	Catalog #
Day 1 – Counting, Pelleting, gDNA Isolation and Homogenization		
Bionano Prep SP Magnetic Retriever (2 pack)	Bionano Genomics	80031
Hemocytometer & Phase Contrast Microscope or Automated Cell Counter	General Lab Supplier	
DynaMag-2 Magnetic Tube Rack	Thermo Fisher	12321D
HulaMixer Sample Mixer	Thermo Fisher	15920D
Microcentrifuge Tubes, 1.5 ml, Nuclease Free	VWR	87003-294
Phenylmethylsulfonyl Fluoride Solution (PMSF),100 mM	Sigma-Aldrich	93482
Ethanol, 200 Proof, Molecular Biology Grade	Sigma-Aldrich	E7023
Isopropanol (IPA), ≥ 99.5%, Molecular Biology Grade	Fisher Scientific	A461-212
Disinfectant Concentrate, TexQ TX651	Texwipe	TX651
Bleach for Cell Media Disposal	General Lab Supplier	
Conical Centrifuge Tubes, 50 ml, PP	Thermo Fisher or Equivalent	14-432-22
Conical Centrifuge Tubes, 15 ml, PP	Fisher Scientific	05-539-12
Centrifuge with 1.5 ml Tube Rotor (2,200 x g spin)	General Lab Supplier	
Centrifuge with a Swinging Bucket Rotor for 15 ml Conical Tubes to Concentrate Cells From Media (2,200 x g spin)	General Lab Supplier	
Ice Bucket and Ice	General Lab Supplier	
Sterile 5 and 10 ml Disposable Pipettes (TD+)	General Lab Supplier	
Mini Benchtop Microcentrifuge (2,200 x g spin)	Labnet	C1301B
Pointed Forceps	Electron Microscopy Sciences, or Equivalent	78141-01
Wide-Bore Pipette Tips, Filtered, Aerosol, 200 µl	VWR or Rainin Equivalent	46620-642
Extra Long 1000 µl Tips, Sterile	VWR or Rainin Equivalent	16466-008
Pipettes (10, 20, 200, and 1,000 µl) and Nuclease Free, Filtered Pipette Tips	General Lab Supplier	
Day 2 - Quantitation		
Benchtop Vortexer	General Lab Supplier	
Bath Sonicator (recommended)	Branson or Equivalent	CPX 952-119R
15 ml Conical Tube	Fisher Scientific	05-539-12
Fluorometer, Qubit	Thermo Fisher or Equivalent	Q33216
Qubit® BR (Broad Range) dsDNA Assay Kit	Thermo Fisher or Equivalent	Q32853
Qubit Assay Tubes	Thermo Fisher	Q32856
Positive-Displacement Pipette MR-10 (optional)	Rainin or Equivalent	17008575
Pipette Tips, 10 µl, C-10 for Pos. Displ. Pipette (optional)	Rainin or Equivalent	17008604

Introduction and Important Notes

Introduction

This Bionano Prep Frozen Cells DNA Isolation Protocol can provide ultra-high molecular weight (UHMW) gDNA in less than 4 hours from 1.5 million mammalian cells. It utilizes a lyse, bind, wash, and elute procedure that is common for silica-based gDNA extraction technologies in combination with a novel paramagnetic disk. Unlike magnetic beads and silica spin columns, which shear large gDNA, the Nanobind Disk binds and releases gDNA with significantly less fragmentation, resulting in UHMW gDNA. High gDNA binding capacity is the result of a novel nano structured silica on the outside of the thermoplastic paramagnetic disk. This protocol was tested using an EBV immortalized human lymphoblastoid cell line (GM12878) that grows in suspension culture. gDNA prepared using this protocol has been validated only with DLS labeling. See Training Video for technically critical steps and troubleshooting; the steps mentioned in the video correspond to the Frozen Blood Protocol, but are the same processes as here.

Overview

Cell lysis and Proteinase K digestion occurs in a chaotropic buffer and the released gDNA binds to the Nanobind Disk upon the addition of isopropanol. After three wash steps, the disk is transferred to a fresh tube and the gDNA is eluted from the disk. The recovered UHMW gDNA is subjected to limited shearing to make the UHMW gDNA more homogeneous. The gDNA is then mixed and equilibrated overnight at room temperature to facilitate DNA homogeneity and the concentration is determined. Typical gDNA size range is from 50 Kbp to ≥ 1 Mbp.

Important Notes

DNA Homogeneity

Recovered gDNA is subjected to pipette mixing with a 200 µl standard pipet tip to increase homogeneity, ensuring consistent DNA sampling for labeling.

gDNA Quantitation

gDNA quantitation is used to measure concentration and serves as a gauge of UHMW gDNA homogeneity. Qubit quantitation is preferred over other quantitation methods since it can also be used for measuring gDNA concentration of the labeling reaction. The Qubit Broad Range (BR) dsDNA Assay measures gDNA concentration after isolation, while the High Sensitivity (HS) dsDNA Assay measures gDNA concentration after labeling.

To gauge gDNA homogeneity, it is essential to measure the concentration of gDNA at multiple positions in the solution. Since viscous gDNA is difficult to pipet, follow guidelines in the Important Notes and gDNA Quantitation sections below for accurate pipetting. Standard assays for quantification of gDNA concentration will not provide accurate measurements of long gDNA due to its viscous nature.

- Effective fragmentation of sampled gDNA via sonication or extensive vortexing is necessary for accurate quantitation.
- The coefficient of variation (CV) from three unique samplings should be less than 0.30.

- Typical gDNA concentration is 50-120 ng/µl.

Pipetting Viscous Genomic DNA (gDNA)

To draw viscous gDNA, hold the stock tube for close-up visualization, depress the pipette plunger until the first stop, submerge the pipette tip and carefully and slowly release the plunger to start drawing the viscous gDNA into the tip while carefully monitoring uptake. Keep the tip submerged even after the viscous solution stops moving upward and levels off. Be patient. Viscous gDNA can take a few seconds to fill up to 2 µl. Releasing the plunger too fast can produce a bubble in the tip leading to under-sampling (start over if this occurs). After the solution in the tip has leveled off and while the tip is still submerged in the gDNA solution, scrape the tip against the bottom of the tube 3-5 times using a circular motion. Remove the tip from the gDNA solution and visually inspect to confirm that it is filled to 2 µl. Removing the pipette tip from the gDNA solution too early, or ineffectively scraping the tip to break gDNA strands from the tip, can produce a bubble at the tip of the pipette tip indicating under-sampling (start over if this happens).

gDNA Handling

- Mixing of recovered gDNA is always carried out with a wide bore pipette tip to prevent shearing.
- Recovered gDNA should never be frozen or vortexed.
- Pipetting of recovered gDNA for accurate sampling is always carried out with a standard tip or positive displacement pipette.

Characteristics of High Quality gDNA for Bionano Mapping

- A clear gDNA solution is ideal, but an unclear solution does not always correlate with poor sample quality.
- Recovered gDNA in solution is viscous.
- Presence of mega base size gDNA is measured by pulsed field gel electrophoresis (PFGE).
- Recovered gDNA is homogenous as measured with Qubit gDNA quantitation assay with CV < 0.30.

Using the Bionano Prep SP Magnetic Retriever

a. Hold a plastic sheath on the sides near the top and insert the Bionano Prep SP Magnetic Retriever into the sheath, positioning it such that it is sitting at the bottom of the sheath.
b. Insert the sheathed retriever into the Protein LoBind microfuge tube to attract the Nanobind Disk to the retriever in the sheath.
c. Carefully lift the sheathed retriever with the bound disk out of tube and insert the sheathed retriever into a new Protein LoBind microfuge tube.
d. Holding the sheath on the side near the top, with one hand pull the retriever up until the Nanobind Disk disassociates from the sheath and drops into the new tube.
e. Change sheath for each new sample.

Batch Size

- We recommend processing up to 6 samples at a time.

Hazardous Waste Disposal

Buffers LBB and WB1 contain guanidine hydrochloride (GuHCl). GuHCl is harmful if swallowed or inhaled and causes skin and eye irritation. DO NOT mix with bleach or acidic reagents. Liquid waste containing GuHCl should be safely decontaminated with a quaternary ammonium disinfectant before disposal in a hazardous waste stream. We recommend bleach for decontamination of pellet supernatant and TexQ for decontamination of all solutions mixed with GuHCl. This conforms to disposal requirements in the state of California, US, but may be different for your location. Please consult local requirement for decontamination and disposal.

Bionano Prep SP Frozen Cells DNA Isolation Protocol

Preparation for gDNA Isolation from Frozen Cell Pellets

Note: For best results, we encourage preparing frozen cell pellets as described in the Appendix.

Before First Use

- Verify access to tabletop centrifuge with swinging bucket rotor that can accommodate 15 ml polypropylene conicals to concentrate cells from media.
- Verify mini benchtop microcentrifuge spin speed is 2,200 x g.
- PMSF decomposes rapidly in aqueous solutions. Create aliquots of 120 µl in 1.5 ml screw cap tubes and store stock and aliquots at 4°C. Each aliquot will be sufficient for ten gDNA isolations.
- Add 100% Ethanol to Wash Buffers (WB1 and WB2) and mix thoroughly:
    - Add 5 ml of 100% Ethanol to Wash Buffer 1 (WB1) for a final volume of 8.25 ml.
    - Add 7.5 ml of 100% Ethanol to Wash Buffer 2 (WB2) for a final volume of 12.5 ml.

Set Up

- Gather materials (see “User Supplied Material” section above).
- Prepare 37°C water bath or heat block to thaw frozen cell pellets. Verify temperature with thermometer.
- For each sample, prepare Stabilizing Buffer by mixing Cell Buffer (Bionano) with DNA Stabilizer (Bionano):
    - 50 µl Stabilizing Buffer = 49 µl Cell Buffer + 1 µl DNA Stabilizer, vortex to mix and pulse spin.
- For waste disposal, prepare:
    - One 50 ml conical with 5 ml bleach + 20 ml water; invert several times to mix.
    - One 50 ml conical with 100 µl TexQ decontaminant per sample (to be disposed as hazardous waste).
- For each sample, label two Protein LoBind Tubes (Bionano) and one 2.0 ml microfuge tube (Bionano).
- Invert tubes of PMSF, RNase A (Bionano) and Proteinase K (Bionano) three times to mix, pulse spin briefly. Place PMSF and RNase A on ice.

gDNA Isolation (3 hours)

Thaw frozen Cell Pellets, add Stabilizing Buffer, Resuspend Cells and Transfer to Protein LoBind Tubes

Note: For important instructions on preparing Frozen Cell Pellets, please refer to Appendix.

1. Thaw the cell pellets containing 1.5 million cells in a 37°C water bath or heat block for 30 seconds.
2. Add 40 µl of Stabilizing Buffer on the top of each pellet.
3. Disrupt the pellet with a 200 µl wide bore tip, then continue to resuspend the pellet by pipetting up and down 10 times. Transfer the entire volume of suspension (>40 µl) into previously labeled Protein LoBind tube with a standard 200 µl tip.

Lyse and Digest Cells

4. Add 50 µl of Proteinase K and 20 µl of RNase A to each of the Protein LoBind tubes containing resuspended cells. **DO NOT PIPET MIX.**
5. Incubate at room temperature for 3 minutes.
6. Add 225 µl Buffer LBB to sample with a standard 1,000 µl tip. Cap and invert tube 15 times to mix.

   Note: Buffer LBB is a viscous and foamy solution which will adhere to pipette tip. Dispense slowly and change tips between dispensing to ensure accuracy of dispense volume.
7. Rotate sample on HulaMixer for 15 minutes at room temperature at 10 rpm. No shaking/vibration.
8. Pulse spin tube for 2 seconds to collect liquid at the bottom of the tube.
9. Add 10 µl of 100 mM PMSF into the liquid portion of tube. Cap and invert tube 5 times to mix, pulse spin tube for 2 seconds to collect liquid at the bottom of the tube.
10. Incubate at room temperature for 10 minutes.

gDNA Bind, Wash and Elute

11. Using forceps, carefully transfer a single Nanobind Disk to the lysate.

    Note: Disks can sometimes stick together.
12. Add 340 µl 100% isopropanol to all tubes. Cap and invert tubes 5 times to mix.
13. Rotate sample on HulaMixer for 15 minutes at room temperature at 10 rpm. No shaking/vibration.

    Note: Ensure that the Nanobind Disk does not remain in the lid of the tube during initial rotations. If it does, turn off rotator and invert microfuge tube until the Nanobind Disk goes back into the solution. Replace the tube on the HulaMixer and resume mixing.
14. Examine gDNA association with Nanobind Disk and invert to increase binding (See Training Video, 0:25):
    a. Place sample tubes into clear Dynamag tube rack and visually inspect all tubes in rack to ensure that gDNA is tethered to the Nanobind Disk.
    b. If gDNA strands are visibly hanging low, quickly invert 180° to bring the gDNA into closer association with the Nanobind Disk.
    c. 180° inversions can be done many times until the gDNA association with the Nanobind Disk appears unchanged.

15. Combine clear rack with the magnetic base as outlined below, making sure Nanobind Disk is secured by the magnet near the top of the liquid level. If not, re-rack (See Training Video, 0:50).

    Note: The color of liquid in the pictures below was modified for illustrative purposes.

    a. Invert clear Dynamag tube rack and place upside down with sample lids touching the work surface. The tubes will be on the same row of the rack, and in the row furthest from you.

    b. Invert Dynamag magnetic base and lower onto clear rack.

    c. Tilt combined apparatus slowly 90° towards you while it continues to rest on surface. The tubes will now be horizontal and visible to you.

    d. Tilt combined apparatus slowly 90° towards you while it continues to rest on surface, so that it stands fully upright and tubes are facing you.

    e. Make sure Nanobind Disk is held to the magnet near the top of the liquid level.

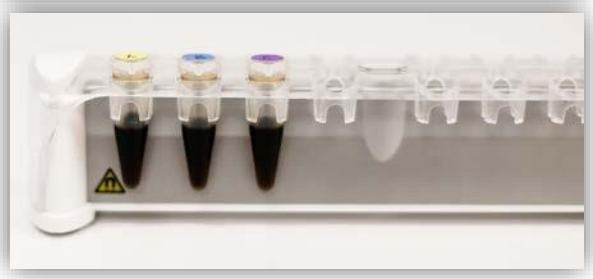

16. Set one 1,000 µl pipette to 1,000 µl and a second to 700 µl.
17. Remove supernatant as outlined below, careful not to aspirate the gDNA (See Training Video, 1:15):
    a. Angle entire rack at a 45° angle by holding in one hand (grasping the entire apparatus from below with tubes visible to you and lids towards your other hand).
    b. Wait 2 seconds for gDNA to lay on the Nanobind Disk.
    c. Slowly remove all liquid with a 1,000 µl extra-long tip angled away from the Nanobind Disk and/or gDNA to avoid disruption.
    d. Dispense supernatant into conical containing TexQ.

⚠ Ensure that the gDNA is not removed by visually inspecting the tip containing buffer before discarding. If gDNA is accidentally aspirated or becomes unbound from the disk, refer to Troubleshooting section below.

18. Perform Wash WB1 (See Training Video, 2:21):
    a. Dispense 700 µl of Buffer WB1 directly onto the disks in the tubes and cap tubes.
    b. Lift clear tube rack to separate from magnetic base.
    c. Invert clear rack with tubes 180° 4 times to wash.
    d. Re-rack clear tube rack and tubes with magnetic base as described in Step 15.
    e. Remove supernatant as described in Step 17.

⚠ Ensure that the gDNA is not removed by visually inspecting the tip containing buffer before discarding. If gDNA is accidentally aspirated or becomes unbound from the disk refer to Troubleshooting section below.

19. Set the second pipette to 500 µl (previously at 700 µl).
20. Perform Wash WB2 (See Training Video, 4:10):
    a. Dispense 500 µl of Buffer WB2 directly onto the disks in the tubes and cap.
    b. Lift clear rack to separate from magnetic base.
    c. Invert clear rack 180° 10 times to wash.
    d. Re-rack clear tube rack and tubes with magnetic base as described in Step 15.
    e. Remove supernatant as described in Step 17.

⚠ Ensure that the gDNA is not removed by visually inspecting the tip containing buffer before discarding. If gDNA is accidentally aspirated or becomes unbound from the disk refer to Troubleshooting section below.

21. Repeat Wash WB2, Step 20 (See Training Video, 5:50).

    Note: Remove buffer from 2 or 3 tubes at a time and process through Buffer EB incubation step in small batches to prevent the disk/gDNA from drying out.

22. Open tube lid fully (parallel to lab bench) and lift each tube apart from base.

23. In close proximity to a new Protein LoBind tube, transfer Nanobind Disk to a new Protein LoBind tube using Bionano Prep SP Magnetic Retriever (see Important Notes section for proper usage). Cap tube to prevent disk drying (See Training Video, 7:30).
24. Spin the Protein LoBind tube in benchtop microcentrifuge for 5 seconds.
25. Remove all residual liquid at the bottom of the tube using a 10 µl standard tip.

    Note: It is necessary to displace the Nanobind Disk using the tip to reach the liquid at the bottom of the tube. Move tip around with small circular motion to remove all residual liquid.
26. Add 110 µl of Buffer EB to Protein LoBind tube.
27. Spin the tube on benchtop microcentrifuge for 5 seconds.
28. Using a 10 µl standard tip, gently nudge Nanobind Disk towards the bottom of the tube, making sure that it is fully submerged in liquid. The disk should remain parallel to the bench surface (See Training Video, 8:20).
29. Incubate submerged Nanobind Disk in Buffer EB at room temperature for 20 minutes.
30. Collect extracted gDNA by transferring eluate to previously labeled 2.0 ml microfuge tube with a 200 µl standard tip.
31. Spin the tube with the Nanobind Disk on benchtop microcentrifuge for 5 seconds and transfer all of the remaining eluate containing viscous gDNA to the same standard 2.0 ml microfuge tube as in previous step with a standard 200 µl tip. You may remove the disk before aspirating remaining elution buffer.

    Note: Almost all of the viscous gDNA comes off the Nanobind Disk during the spin.

Homogenization of gDNA Solution (70 minutes)

Homogenization of gDNA Solution

32. Slowly pipette the entire gDNA volume into a standard bore 200 µl tip, then slowly dispense the gDNA. Avoid creating bubbles.
    - Repeat this process 3 times for a total of 4 strokes: (1 stroke = 1 aspiration and 1 dispense).

    Note: If gDNA uptake stalls due to high viscosity, it may be necessary to stir gently while slowly releasing the plunger to withdraw the gDNA.
33. Place standard 2.0 ml microfuge tube containing gDNA in rack of Hula Mixer Sample Mixer and rotate at room temperature for 1 hour at 15 rpm.

    Note: During initial rotations, ensure that the gDNA gets drawn from the bottom of the microfuge tube to reside in the lid of the tube during rotations. If the DNA solution remains in the bottom of the tube during initial rotations, turn off Hula Mixer and position rack so the microfuge tube is oriented upside down. Gently flick the bottom of the microfuge tube until the gDNA is drawn to into the lid and resume mixing.

34. Remove microfuge tube from rack of Hula Mixer and spin tube on benchtop microcentrifuge for 2 seconds to bring the gDNA to the bottom of the tube. Allow the gDNA to equilibrate overnight at room temperature (25°C) to homogenize.

    Note: Most samples will become homogenous by the third day (from the start of the protocol), but samples may be labeled as soon as they become homogenous.

gDNA Quantitation (45 minutes)

Qubit Quantitation - BR dsDNA Assay

Refer to the Qubit dsDNA BR Assay Kit user manual for kit details and follow the methods described in the "Pipetting Viscous Genomic DNA" section, to ensure accurate pipetting of viscous gDNA.

1. Equilibrate Qubit BR Assay Kit Standards to room temperature.

   Note: If the gDNA has been stored at 4ºC, equilibrate at room temperature before moving to the next step.

2. Add Qubit BR Buffer to 0.5 ml Qubit Assay Tubes:
   a. For each sample, add 18 µl of Qubit BR Buffer to three separate Qubit Assay Tubes.
   b. For the Qubit Standards, add 10 µl Qubit BR Buffer to two separate Qubit Assay Tubes.
3. Using a 200 µl pipette with a wide bore tip, gently mix the entire gDNA sample volume by pipetting up and down 5 times, being careful not to generate bubbles.
4. Using a fresh standard bore pipette tip or positive displacement pipette tip for each draw:

   Remove 2 µl aliquots from the left side, middle, and right side of each sample and dispense into BR Buffer of corresponding Qubit Assay Tube, rinsing tip when dispensing. Place Assay Tubes in a floating rack and sonicate for 10 minutes. Perform Steps 5 and 6 during sonication.

   Note: If a bath sonicator is not available, vortex for at least 30 seconds at maximum speed, then spin down briefly for 2 seconds.

5. Prepare Working Solution by diluting the Dye Assay Reagent into BR Dilution Buffer (1:200):
   a. 200 µl Working Solution for each of the two standards (400 µl total).
   b. 200 µl Working Solution for each sample aliquot (600 µl for each sample).
6. For the Qubit DNA standards, add 10 µl of Standards 1 and 2 to the Assay Tubes containing BR Buffer from Step 2b.
7. Once sonication is complete, retrieve assay tubes and pulse spin briefly. Vortex tubes for 5 seconds at maximum speed, then pulse spin again.
8. Add 180 µl of Working Solution to each sonicated DNA aliquot and Qubit DNA Standard aliquot. Vortex for 5 seconds, and pulse spin tubes.
9. Incubate samples for at least 2 minutes, then read on the Qubit Fluorometer.

10. Coefficient of Variation (CV = standard deviation/mean) from three readings should be < 0.30.

    Note: If CV > 0.30, gently pipette-mix the entire volume of gDNA with five strokes (1 stroke = 1 up stroke + 1 down stroke) using a wide bore tip. Let the gDNA rest at least overnight at room temperature before repeating quantitation.

    Note: Typical DNA concentrations range from 50-120 ng/µl.

Sample ID	Left (ng/µl)	Middle (ng/µl)	Right (ng/µl)	CV (stdev/mean)

Labeling

DNA is ready for Direct Label and Stain (DLS) labeling. See “Kits and Consumables” section at https://bionanogenomics.com/support/ for applicable kits and protocols.

Troubleshooting

See Training Video starting at 8:40 for video explanations of troubleshooting.

The gDNA comes unbound from the Nanobind Disk.

Evidence: gDNA is aspirated or becomes detached from disk during binding or during washes.

Steps to follow if sample is aspirated:

1. Leaving the sample tube racked on the magnet, dispense gDNA-containing liquid back into tube containing disk.
2. Remove racked tube from magnet and invert rack multiple times by hand to re-establish binding.

Alternatively:

1. Leaving the sample tube racked on the magnet, dispense gDNA-containing liquid back into tube containing disk.
2. Aspirate liquid from tube such that a minimal volume (~50 µl) remains above unbound gDNA and discard supernatant leaving the DNA in a minimal volume at bottom of the tube.
3. Carefully aspirate unbound gDNA containing the minimal liquid into pipet tip and pipet directly onto racked disk on magnet to re-establish binding.

The gDNA is not homogeneous before labeling

Evidence: The gDNA quantitation CV of three measurements (top, middle and bottom) is > 0.30.

Steps to Follow:

1. Aspirate and dispense sample using a wide bore tip for a total of 5 times.
2. Incubate the gDNA at room temperature for 1 to 3 days.
3. After incubation, again aspirate and dispense the sample using a wide bore tip 5 times.
4. Quantitate with Qubit BR Assay.

The gDNA is not viscous

Evidence: Sample consistency is very thin and easily pipetted, but concentration is > 35 ng/µL.

The sample is likely not to have high molecular weight gDNA.

Check sample using pulse field gel electrophoresis before labeling to confirm presence of high molecular weight gDNA.

Evaluate sample prep method and input material quality/age and repeat DNA isolation from biological sample.

Appendix: Preparing Frozen Cell Pellets for Storage

Count Cells, Pellet, Remove Supernatant, Resuspend Cells and Transfer to Labeled Microfuge Tubes

Recommended input: 1.5 million viable mammalian cells.

Note: Cells less than this amount may not produce sufficient gDNA, and excessive amounts of cells may produce gDNA that is less pure and more difficult to become homogeneous.

1. Prepare Stabilizer Buffer by combining 49 µl of Cell Buffer + 1 µl DNA Stabilizer for each of the pellets you plan to prepare.
2. For each sample, pipet isolated cells in growth media repeatedly to ensure a uniform suspension.

   Note: If possible, make sure the cells are actively growing with high viability as this maximizes quality and size of isolated gDNA.
3. Quickly remove an aliquot, and with or without dilution, count cells with cell counting device.
4. Calculate the volume of original cell stock required for 1.5 million cells.
5. After pipet mixing to ensure a uniform suspension, transfer volume for 1.5 x 10^6 cells to a labeled 15 ml polypropylene conical.

   Note: You can make multiple pellets of the sample cell line or a few pellets of multiple cell lines.
6. After all the samples are in labeled conicals, pellet the cells by centrifugation using a swinging bucket rotor at 2,200 x g for 2 minutes at room temperature.
7. Remove the supernatants by decanting into the waste conical with bleach and use a Kimwipe® to absorb residual liquid from inverted cell pellet conical.
8. Add 40 µl of Stabilizer Buffer on top of each pellet.
9. Disrupt the pellet with a 200 µl wide bore tip, then continue to resuspend the pellet by pipetting up and down 10 times.
10. Transfer the entire volume of suspension (>40 µl) into a labeled 1.5 ml microcentrifuge tube with a standard 200 µl tip.
11. Pellet the cells in a microcentrifuge by spinning at 2,200 x g for 2 minutes at room temperature.
12. Using a standard 200 µl tip, carefully remove as much of the supernatant as possible without disturbing the pellet.
13. Freeze and store the cell pellets at -80°C.

Technical Assistance

For technical assistance, contact Bionano Genomics Technical Support.

You can retrieve documentation on Bionano products, SDS's, certificates of analysis, frequently asked questions, and other related documents from the Support website or by request through e-mail and telephone.

Type	Contact
Email	support@bionanogenomics.com
Phone	Hours of Operation: Monday through Friday, 9:00 a.m. to 5:00 p.m., PST US: +1 (858) 888-7663
Website	www.bionanogenomics.com/support

Bionano Genomics, Inc.
9540 Towne Centre Drive, Suite 100
San Diego, CA 92121

ADDENDUM M

Bionano Prep SP Tissue and Tumor DNA Isolation Protocol

Document Number: 30339

Document Revision: A

Table of Contents

Legal Notice

For Research Use Only. Not for use in diagnostic procedures.

Revision History

Revision	**Release Date**	Notes
1		Beta Release
2		Early Access Release
A	7/13/2020	Commercial Release

Workflow Overview

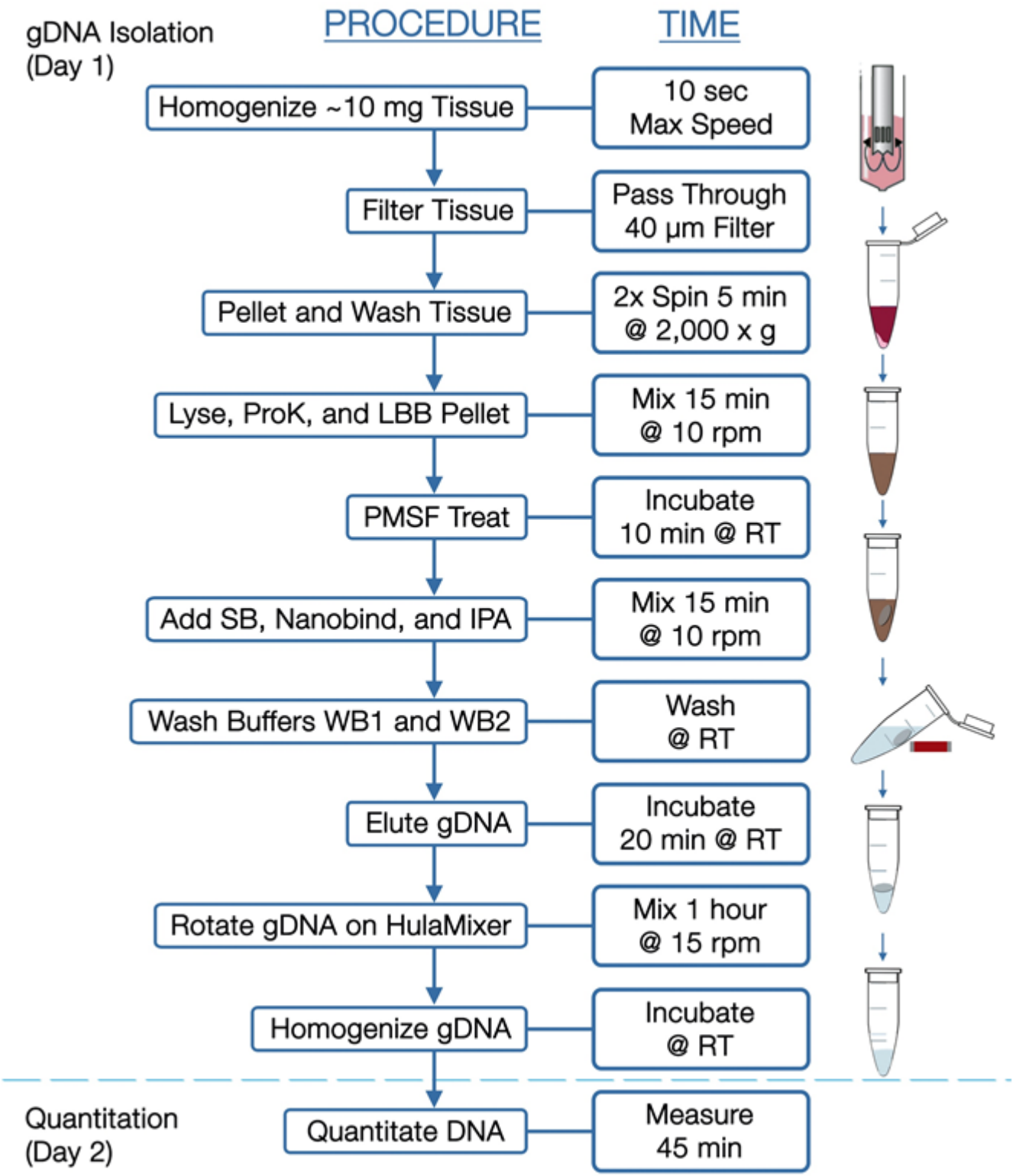

SP Tissue and Tumor DNA Isolation Kit and User-Supplied Materials

Table 1: Bionano Prep SP Tissue and Tumor DNA Isolation Kit Contents (Part # 80038, 10 preps)

Item	Amount	Part Number	Storage
4 mm Nanobind Disks	10 disks	20402	Room Temp (18-25°C)
Protein LoBind Microcentrifuge Tubes, 1.5 ml	10 tubes	20380	Room Temp (18-25°C)
Microcentrifuge Tubes, 2 ml	10 tubes	20396	Room Temp (18-25°C)
40 µm Cell Strainer	10 each	20403	Room Temp (18-25°C)
Detergent	150 µl	20405	Room Temp (18-25°C)
Salting Buffer	1.1 ml	20404	Room Temp (18-25°C)
Homogenization Buffer	96 ml	20406	Room Temp (18-25°C)
Wash Buffer A	12 ml	20407	Room Temp (18-25°C)
Proteinase K	0.5 ml	20372	Room Temp (18-25°C)
Lysis and Binding Buffer (LBB)*	2.5 ml	20375	Room Temp (18-25°C)
Wash Buffer 1 Concentrate (2.5X) (WB1)*	2 x 3.25 ml	20376	Room Temp (18-25°C)
Wash Buffer 2 Concentrate (2.5X) (WB2)	5 ml	20377	Room Temp (18-25°C)
Elution Buffer (EB)	1.1 ml	20378	Room Temp (18-25°C)
SP Sheaths	10 each	20381	Room Temp (18-25°C)

* See Important Notes Section for hazardous waste information

Table 2: User-Supplied Materials

Item	Supplier	Catalog #
Day 1 – Tissue disruption, Pelleting, gDNA Isolation and Homogenization		
Bionano Prep SP Magnetic Retriever (2 pack)	Bionano Genomics	80031
Rotor-stator: TissueRuptor (version I or II)	QIAGEN or Equivalent	9002755
Power Strip (recommended)	General Lab Supplier	
Disposable Probes for TissueRuptor	QIAGEN or Equivalent	990890
Ring Stand & Three Prong Clamp (e.g. VWR 76293-368)	General Lab Supplier	
DynaMag-2 Magnetic Tube Rack	Thermo Fisher	12321D
HulaMixer Sample Mixer	Thermo Fisher	15920D
Weigh Boats	General Lab Supplier	
Precision Scale	General Lab Supplier	
Microcentrifuge Tubes, 1.5 ml, Nuclease Free	VWR	87003-294
Screw Cap Tubes with O-Ring, 1.5 ml	General Lab Supplier	
Razor Blade	General Lab Supplier	
Biosafety Cabinet (optional)	General Lab Supplier	
Dry Ice (optional)	General Lab Supplier	
Aluminum Block	General Lab Supplier	
Metal Spatula	VWR	82027-530
Phenylmethylsulfonyl Fluoride Solution (PMSF),100 mM	Sigma-Aldrich	93482
Ethanol, 200 Proof, Molecular Biology Grade	Sigma-Aldrich	E7023
Isopropanol (IPA), ≥ 99.5%, Molecular Biology Grade	Fisher Scientific	A461-212
Disinfectant Concentrate, TexQ TX651	Texwipe	TX651
Conical Centrifuge Tubes, 50 ml, PP	Thermo Fisher or Equivalent	14-432-22
Conical Centrifuge Tubes, 15 ml, PP	Thermo Fisher or Equivalent	05-539-12
Refrigerated Centrifuge with 1.5/2.0 ml Tube Rotor (2,000 x g spin)	General Lab Supplier	
Refrigerated Centrifuge, Swinging Bucket Rotor for 15 ml Conical Tubes	General Lab Supplier	
Ice Bucket and Ice	General Lab Supplier	
Sterile 5 and 10 ml Disposable Pipettes (TD+)	General Lab Supplier	
Mini Benchtop Microcentrifuge (2,000 x g spin)	Labnet	C1301B
Pointed Forceps	Electron Microscopy Sciences, or Equivalent	78141-01
Wide-Bore Pipette Tips, Filtered, Aerosol, 200 µl	VWR or Rainin Equivalent	46620-642
Extra Long 1000 µl Tips, Sterile	VWR or Rainin Equivalent	16466-008

Pipettes (10, 20, 200, and 1,000 µl) and Nuclease Free, Filtered Pipette Tips	General Lab Supplier	
Day 2 - Quantitation		
Benchtop Vortexer	General Lab Supplier	
Bath Sonicator (optional)	Branson or Equivalent	CPX 952-119R
Fluorometer, Qubit	Thermo Fisher or Equivalent	Q33216
Qubit® BR (Broad Range) dsDNA Assay Kit	Thermo Fisher or Equivalent	Q32853
Qubit Assay Tubes	Thermo Fisher	Q32856
Positive-Displacement Pipette MR-10 (optional)	Rainin or Equivalent	17008575
Pipette Tips, 10 µl, C-10 for Pos. Displ. Pipette (optional)	Rainin or Equivalent	17008604

Introduction and Important Notes

Introduction

This Bionano Prep SP Tissue and Tumor DNA Isolation Protocol can provide ultra-high molecular weight (UHMW) gDNA in less than 6 hours from a batch of up to 8 samples (up to 4 recommended for novice users) with approximately 10 mg fresh or fresh frozen tissue or tumor. It utilizes a homogenization, lyse, bind, wash, and elute procedure that is common for silica-based gDNA extraction technologies in combination with a novel paramagnetic disk. Unlike magnetic beads and silica spin columns, which shear large gDNA, the Nanobind Disk binds and releases gDNA with significantly less fragmentation, resulting in UHMW gDNA. High gDNA binding capacity is the result of a novel nano structured silica on the outside of the thermoplastic paramagnetic disk. This protocol has been used to process liver, lung, kidney, colon, ovary, prostate, testes and uterus tissues from Brown Norway rats, and human bladder, lung, liver, kidney, colon, breast, prostate, brain, thyroid and ovary tumors. This protocol was fully validated in replicate by multiple users by testing human tumors from liver, lung, and breast, and normal rat kidney. gDNA prepared using this protocol has been tested with DLS labeling. See videos for tissue Homogenization and Filtration and SP gDNA Isolation Training Video for critical steps and troubleshooting; the steps mentioned in the video correspond to the Bionano Prep SP Frozen Human Blood DNA Isolation Protocol (30246), but are the same processes as here.

Overview

After homogenization in a buffer containing ethanol, tissue lysis and Proteinase K digestion occurs in a chaotropic buffer and the released gDNA binds to the Nanobind Disk upon the addition of salting buffer and isopropanol. After four wash steps, the disk is transferred to a fresh tube and the gDNA is eluted from the disk. The recovered UHMW gDNA is subjected to limited shearing to make the UHMW gDNA more homogeneous. The gDNA is then mixed and equilibrated overnight at room temperature to facilitate DNA homogeneity and the concentration is determined. Typical gDNA size range is from 50 Kbp to ≥ 1 Mbp.

Important Notes

DNA Homogeneity

Recovered gDNA is subjected to pipette mixing with a 200 µl standard pipet tip to increase homogeneity, ensuring consistent DNA sampling for labeling.

gDNA Quantitation

gDNA quantitation is used to measure concentration and serves as a gauge of UHMW gDNA homogeneity. Invitrogen™ Qubit™ quantitation is used instead of other quantitation methods since it can also be used for measuring gDNA concentration of the labeling reaction and is more accurate than spectrophotometer readings for our samples. The Qubit Broad Range (BR) dsDNA Assay measures gDNA concentration after isolation, while the High Sensitivity (HS) dsDNA Assay measures gDNA concentration after labeling.

To gauge gDNA homogeneity, it is essential to measure the concentration of gDNA at multiple positions in the solution. Since viscous gDNA is difficult to pipet, follow guidelines in the Important Notes and gDNA Quantitation sections below for accurate pipetting. Standard assays for quantification of gDNA concentration will not provide accurate measurements of long gDNA due to its viscous nature.

- Effective fragmentation of sampled gDNA via sonication or extensive vortexing is necessary for accurate quantitation.
- The coefficient of variation (CV) from three unique samplings should be less than 0.30.
- Typical gDNA concentration is 50-300 ng/µl.

Pipetting Viscous Genomic DNA (gDNA)

To draw viscous gDNA, hold the stock tube for close-up visualization, depress the pipette plunger until the first stop, submerge the pipette tip and carefully and slowly release the plunger to start drawing the viscous gDNA into the tip while carefully monitoring uptake. Keep the tip submerged even after the viscous solution stops moving upward and levels off. Be patient. Viscous gDNA can take a few seconds to fill up to 2 µl. Releasing the plunger too fast can produce a bubble in the tip leading to under-sampling (start over if this occurs). After the solution in the tip has leveled off and while the tip is still submerged in the gDNA solution, scrape the tip against the bottom of the tube 3-5 times using a circular motion. Remove the tip from the gDNA solution and visually inspect to confirm that it is filled to 2 µl. Removing the pipette tip from the gDNA solution too early, or ineffectively scraping the tip to break gDNA strands from the tip, can produce a bubble at the tip of the pipette tip indicating under-sampling (start over if this happens).

gDNA Handling

- Mixing of recovered gDNA is always carried out with a wide bore pipette tip to prevent shearing.
- Recovered gDNA should never be frozen or vortexed.
- Pipetting of recovered gDNA for accurate sampling is always carried out with a standard tip or positive displacement pipette.

Characteristics of High Quality gDNA for Bionano Mapping

- A clear gDNA solution is ideal, but an unclear solution does not always correlate with poor sample quality.
- Recovered gDNA in solution is viscous.
- Presence of mega base size gDNA is measured by pulsed field gel electrophoresis (PFGE).

- Recovered gDNA is homogenous as measured with Qubit gDNA quantitation assay with CV < 0.30.

Using the Bionano Prep SP Magnetic Retriever

a. Hold a plastic sheath on the sides near the top and insert the Bionano Prep SP Magnetic Retriever into the sheath, positioning it such that it is sitting at the bottom of the sheath.
b. Insert the sheathed retriever into the Protein LoBind microfuge tube to attract the Nanobind Disk to the retriever in the sheath.
c. Carefully lift the sheathed retriever with the bound disk out of tube and insert the sheathed retriever into a new Protein LoBind microfuge tube.
d. Holding the sheath on the side near the top, with one hand pull the retriever up until the Nanobind Disk disassociates from the sheath and drops into the new tube.
e. Change sheath for each new sample.

Suggested Input (mg Tissue) and Tissue Quality

- We recommend starting with 10 mg, where as low as 5 mg and 20 mg or more may be used depending upon the nuclei content of the tissue relative to the tissue mass.
- If possible, we strongly recommend preparing ~ 10 mg tissue pieces before the tissue is frozen. Ideally pre-weigh the fresh tissue before snap freeze and storage at -80˚C.
- We recommend using fresh or snap frozen tissues that are free of bone debris, blood clots and extensive necrosis.
- Surgical specimens should be stored on wet ice or in ice-cold PBS as soon as possible to minimize DNA degradation before cutting and/or snap freezing.
- Compromised tissues (not properly handled or stored) or tissues that have gone through freeze-thaw cycles should be avoided for UHMW DNA isolation.
- The internal success rate of UHMW DNA isolated from tumor samples with high RIN (RNA Integrity Number) ≥ 9.0 was > 90%, whereas the success rate of UHMW DNA isolated from a limited number of tumor samples with significantly lower RIN (5-6) was lower (< 50%).

Batch Size

- We recommend processing up to 8 samples at a time (up to 4 at a time for novice users).

Hazardous Waste Disposal

All biohazardous waste, including plasticware, should be disposed of in accordance with local regulations.

Buffers LBB and WB1 contain guanidine hydrochloride (GuHCl). GuHCl is harmful if swallowed or inhaled and causes skin and eye irritation. DO NOT mix with bleach or acidic reagents. Liquid waste containing GuHCl should be safely decontaminated with a quaternary ammonium disinfectant before disposal in a hazardous waste stream. We recommend bleach for decontamination of pellet supernatant and TexQ for decontamination of all solutions

mixed with GuHCl. This conforms to disposal requirements in the state of California, US, but may be different for your location. Please consult local requirement for decontamination and disposal.

Bionano Prep SP Tissue and Tumor DNA Isolation Protocol

Preparation for gDNA Isolation from Fresh or Fresh Frozen Tissue and Tumor

Note: For best results, we encourage preparing tissue as described in the Appendix.

Before First Use

- Verify access to refrigerated centrifuge with swinging bucket rotor that can accommodate 15 ml polypropylene conical tubes to pellet the homogenate.
- Verify mini benchtop refrigerated microcentrifuge spin speed is 2,000 x g.
- PMSF decomposes rapidly in aqueous solutions. Create aliquots of 120 µl in 1.5 ml screw cap tubes and store stock and aliquots protected from light at 4°C. Each aliquot will be sufficient for ten gDNA isolations.
- Add 125 µl Bionano Prep Detergent to Lysis and Binding Buffer (LBB) tube and invert 10 times to mix. Mark LBB tube that detergent was added.
- Add 100% Ethanol to Homogenization Buffer and Wash Buffers (WB1 and WB2), invert 10 times to mix, and check “Ethanol Added” boxes:
    - Add 96 ml of 100% Ethanol to Homogenization Buffer for a final volume of 192 ml.
    - Add 5 ml of 100% Ethanol to Wash Buffer 1 (WB1) for a final volume of 8.25 ml.
    - Add 7.5 ml of 100% Ethanol to Wash Buffer 2 (WB2) for a final volume of 12.5 ml.

Set Up

- Set refrigerated swinging bucket centrifuge and refrigerated microcentrifuge to 4°C.
- Immobilize the TissueRuptor (Qiagen) on a vertical stand. Connect TissueRuptor to a power strip switch.
- Gather materials (see “User Supplied Material” section above). Pre-chill Homogenization Buffer, Wash Buffer A, and TissueRuptor probe(s).
- For waste disposal, prepare 50 ml conical tubes (1 tube for every 2 samples) with 100 µl TexQ decontaminant per sample (to be disposed as hazardous waste).
- For each sample, label two 15 ml conical tubes and one 50 ml conical tube, and set on ice. Set a 40 µm Cell Strainer (Bionano) into the 50 ml conical tube.
- For each sample, label two 1.5 ml Protein LoBind Tubes (Bionano) and one 2.0 ml microfuge tube (Bionano). Set one of the labeled 1.5 ml Protein LoBind Tubes on ice.
- Invert tubes of PMSF and Proteinase K (Bionano) three times to mix, pulse spin briefly. Place PMSF on ice.
- For convenience, all buffers used at 4°C in this protocol can be stored long term at 4°C.

gDNA Isolation (4.5 hours)

Note: For important instructions on preparing Frozen Tissue, please refer to Appendix.

1. For each tissue sample, add 2 ml of chilled Bionano Prep SP Tissue and Tumor Homogenization Buffer to one 15 ml conical tube and keep on ice.
2. Retrieve tissue and prepare ~10 mg (refer to Suggested Input section above) portions:

   Note: Minimize exposure of tissue to room temperature while cutting ~10 mg portions. If a portion is weighed outside the range of 9 - 13 mg, it is recommended to discard that portion and cut a new piece (if more tissue is available).

   a. For **Fresh** Tissue - using a sterilized, ice-chilled aluminum block as your cutting surface, cut tissue with a sterilized razor blade and forceps and weigh ~10 mg in a weigh boat on a precision scale (if weight is not already known).

   b. For **Frozen** Tissue:

      1) If the piece of tissue is no more than 2 x 2 x 4 mm, cut in a weigh boat with a sterilized razor blade and forceps on an ice-chilled aluminum block. Weigh ~10 mg in a different weigh boat and either discard the remainder or refreeze and store at -80°C for isolating DNA that does not have to be UHMW.
      2) If the piece of tissue is larger, and you do not need to sample a specific region of the tissue, place the frozen tissue in a plastic bag that has been cooled on a dry-ice chilled aluminum block, seal the bag and break the tissue into smaller fragments with the aid of a large pestle or hammer. Remove a small piece and treat as above (Step 2.b.1). The remaining fragments can be put back at -80°C for storage.
      3) If the piece of tissue is larger, and you need to sample a specific region of the tissue, place the frozen tissue in a weigh boat on a pre-chilled aluminum block (-20°C) and cut a small piece with a scalpel or razor blade and forceps. Weigh ~10 mg in a different weigh boat and place the remaining large tissue piece back at -80°C for storage.

   Note: For fibrous tissues, it is recommended to cut tissue into small pieces in the weigh boat (1 - 2 mm)

3. Using a sterilized pre-chilled metal spatula, immediately transfer the cut tissue to the labeled 15 ml conical tube containing Homogenization Buffer. Make sure tissue pieces are submerged in the Homogenization Buffer, and the conical tube is set on ice. Transfer pre-chilled probe to conical tube.
4. Repeat steps 2-3 to prepare each additional sample, up to 8 samples total.

   Note: Before continuing to the next step, make sure to place each of tissue or tumor sample in a 15ml conical containing homogenization buffer, and a TissueRuptor probe on ice. See Tissue and Tumor Homogenization and Filtration video for steps 5-11.

5. Remove one conical tube from ice at a time and firmly attach the probe to the TissueRuptor device while holding the conical. Hold the tube in such a way that the tip of the TissueRuptor probe is immersed in the buffer and very close to the bottom of the tube.

6. Pulse the TissueRuptor using the power strip switch by turning it on and off. Check to see if the tissue pellet has been broken apart. If the tissue is particularly dense, pulse an additional 2-3 times in order to break it apart and achieve thorough homogenization.

   Note: Make sure the tissue is not sticking on the tube wall or probe tip. Submerge the tissue in Homogenization Buffer using spatula if needed. For fibrous tissue, we recommend cutting tissue into small pieces before TissueRuptor homogenization.

7. Blend continuously for 10 seconds at maximum speed with the probe tip submerged at all times. Move the tube in an up-down and circular motion during blending to increase the efficiency of homogenization. At the end of the blending, turn off the power strip switch connected to the TissueRuptor, remove the probe from the TissueRuptor, and return the tube (with probe in the tube) to ice.
   Note: The conical tube should be placed back immediately after homogenization to ensure the highest DNA quality.

8. Repeat steps 5-7 for all other samples. Up to 8 samples total.

9. Rinse each probe tip with 6 ml ice-cold Homogenization Buffer using a pipette, collecting in the same conical tube. Dispose of the probe properly (potential biohazard).

10. Decant homogenate through a 40 µm cell strainer on top of the labeled 50 ml conical tube that is set on ice. Retain conical tube for next step.

11. Add additional 6 ml ice-cold Homogenization Buffer to the 15 ml conical tube and swirl to rinse debris off sides of tube, and then pour over the cell strainer, collecting into the same 50 ml conical tube. Discard cell strainer properly (potential biohazard).

    Note: If the homogenate is not passing through the cell strainer, briefly lift and lower the strainer to aid in flow-through.

12. Pipet entire volume 2 times before transferring the homogenate to a new 15 ml conical tube and cap.

13. Centrifuge at 2,000 x g for 5 minutes at 4°C using a swinging bucket rotor (set acceleration and deceleration to 9).

14. Decant supernatant into TexQ waste (potential biohazard) immediately after centrifuge stops, set conical tube on ice for 30 seconds, and use a 1,000 µl pipette to remove as much residual liquid as possible while not disturbing the pellet (leaving < 200 µl volume).

15. Add 300 µl Wash Buffer A, resuspend the pellet with a 1,000 µl tip (set at 300 µl) by slowly pipetting up and down 5 times. Transfer the entire volume of suspension into previously labeled pre-chilled 1.5 ml Protein LoBind tube using a 1,000 µl tip. Retain conical tube for next step.

16. Add additional 700 µl Wash Buffer A to the 15 mL conical tube, gently pipette 2 times to mix, and transfer the entire volume into the same labeled pre-chilled 1.5 ml Protein LoBind tube using a 1,000 µl tip.
17. Centrifuge at 2,000 x g for 5 minutes at 4°C.
18. While not disturbing the pellet, aspirate supernatant to leave behind approximately 40 µl volume. Dispose of supernatant into TexQ waste (potential biohazard). Set tube on ice for 30 seconds.
19. Resuspend pellet in residual volume 10 times using a standard 200 µl tip. Residual volumes may differ.

Lyse and Digest Cells

20. Add 50 µl of Proteinase K to the Protein LoBind tube, cap the tube. DO NOT PIPET MIX.
21. Incubate at room temperature for 3 minutes.
22. Add 225 µl Buffer LBB, containing detergent, to sample with a 1,000 µl tip. Cap and invert tube 15 times to mix.

    Note: Buffer LBB with detergent is a viscous and foamy solution which will adhere to pipette tip. Dispense slowly and change tips between dispensing to ensure accuracy of dispense volume.
23. Rotate sample on HulaMixer for 15 minutes at room temperature at 10 rpm. No shaking/vibration.
24. Pulse spin tube for 2 seconds to collect liquid at the bottom of the tube.
25. Add 10 µl of 100 mM PMSF into the liquid portion of tube. Cap and invert tube 5 times to mix, pulse spin tube for 2 seconds to collect liquid at the bottom of the tube.
26. Incubate at room temperature for 10 minutes.

gDNA Bind, Wash and Elute

27. Add 85 µl Bionano Prep Salting Buffer to the tube, cap and invert 10 times, and pulse spin tube for 2 seconds.
28. Using forceps, carefully transfer a single 4 mm Nanobind Disk to the lysate.

    Note: Disks can sometimes stick together.
29. Add 400 µl 100% isopropanol to tube. Cap and invert tube 5 times to mix.
30. Rotate sample on HulaMixer for 15 minutes at room temperature at 10 rpm. No shaking/vibration.

    Note: Ensure that the Nanobind Disk does not remain in the lid of the tube during initial rotations. If it does, turn off rotator and invert microfuge tube until the Nanobind Disk goes back into the solution. Replace the tube on the HulaMixer and resume mixing.
31. Examine gDNA association with Nanobind Disk and invert to increase binding (See Training Video, 0:25):
    a. Place sample tubes into clear Dynamag tube rack and visually inspect all tubes in rack to ensure that gDNA is tethered to the Nanobind Disk.

b. If gDNA strands are visibly hanging low, quickly invert 180° to bring the gDNA into closer association with the Nanobind Disk.
c. 180° inversions can be done many times until the gDNA association with the Nanobind Disk appears unchanged.

32. Combine clear rack with the magnetic base as outlined below, making sure Nanobind Disk is secured by the magnet near the top of the liquid level. If not, re-rack (See Training Video, 0:50).

Note: The color of liquid in the pictures below was modified for illustrative purposes.

a. Invert clear Dynamag tube rack and place upside down with sample lids touching the work surface. The tubes will be on the same row of the rack, and in the row furthest from you.

b. Invert Dynamag magnetic base and lower onto clear rack.

c. Tilt combined apparatus slowly 90° towards you while it continues to rest on surface. The tubes will now be horizontal and visible to you.

d. Tilt combined apparatus slowly 90° towards you while it continues to rest on surface, so that it stands fully upright and tubes are facing you.

e. Make sure Nanobind Disk is held to the magnet near the top of the liquid level.

33. Set one 1,000 µl pipette to 1,000 µl and a second to 700 µl.
34. Remove supernatant as outlined below, careful not to aspirate the gDNA (See Training Video, 1:15):
    a. Angle entire rack at a 45° angle by holding in one hand (grasping the entire apparatus from below with tubes visible to you and lids towards your other hand).
    b. Wait 2 seconds for gDNA to lay on the Nanobind Disk.
    c. Slowly remove all liquid with a 1,000 µl extra-long tip angled away from the Nanobind Disk and/or gDNA to avoid disruption.
    d. Dispense supernatant into conical tube containing TexQ.

⚠ Ensure that the gDNA is not removed by visually inspecting the tip containing buffer before discarding. If gDNA is accidentally aspirated or becomes unbound from the disk, refer to Troubleshooting section below.

35. Perform Wash WB1 (See Training Video, 2:21):
    a. Dispense 700 µl of Buffer WB1 directly onto the disks in the tubes and cap tubes.
    b. Lift clear tube rack to separate from magnetic base.
    c. Invert clear rack with tubes 180° 4 times to wash.
    d. Re-rack clear tube rack and tubes with magnetic base as described in Step 32.
    e. Remove supernatant as described in Step 34.

⚠ Ensure that the gDNA is not removed by visually inspecting the tip containing buffer before discarding. If gDNA is accidentally aspirated or becomes unbound from the disk refer to Troubleshooting section below.

36. Repeat Wash WB1, Step 35.
37. Set the second pipette to 500 µl (previously at 700 µl).
38. Perform Wash WB2 (See Training Video, 4:10):
    a. Dispense 500 µl of Buffer WB2 directly onto the disks in the tubes and cap.
    b. Lift clear rack to separate from magnetic base.
    c. Invert clear rack 180° 10 times to wash.
    d. Re-rack clear tube rack and tubes with magnetic base as described in Step 32.

e. Remove supernatant as described in Step 34.

⚠ Ensure that the gDNA is not removed by visually inspecting the tip containing buffer before discarding. If gDNA is accidentally aspirated or becomes unbound from the disk refer to Troubleshooting section below.

39. Repeat Wash WB2, Step 38 (See Training Video, 5:50).

    Note: Remove buffer from 2 or 3 tubes at a time and process through Buffer EB incubation step in small batches to prevent the disk/gDNA from drying out.

40. Open tube lid fully (parallel to lab bench) and lift each tube apart from base.

41. In close proximity to a new Protein LoBind tube, transfer Nanobind Disk to a new Protein LoBind tube using Bionano Prep SP Magnetic Retriever (see Important Notes section for proper usage). Cap tube to prevent disk drying (See Training Video, 7:30).

42. Add 65 µl of Buffer EB to Protein LoBind tube.

43. Pulse spin the tube on benchtop microcentrifuge for 5 seconds.

44. Using a 10 µl standard tip, gently nudge Nanobind Disk towards the bottom of the tube, making sure that it is fully submerged in liquid. The disk should remain parallel to the bench surface (See Training Video, 8:20).

45. Incubate submerged Nanobind Disk in Buffer EB at room temperature for 20 minutes.

46. Collect extracted gDNA by transferring eluate to previously labeled 2.0 ml microfuge tube with a 200 µl standard tip.

47. Pulse spin the tube with the Nanobind Disk on benchtop microcentrifuge for 5 seconds and transfer all of the remaining eluate containing viscous gDNA to the same standard 2.0 ml microfuge tube as in previous step with a standard 200 µl tip. You may remove the disk before aspirating remaining elution buffer.

    Note: Almost all of the viscous gDNA comes off the Nanobind Disk during the pulse spin.

Homogenization of gDNA Solution (70 minutes)

Homogenization of gDNA Solution

48. Slowly pipette the entire gDNA volume into a standard bore 200 µl tip, then slowly dispense the gDNA. Avoid creating bubbles.

    - Repeat this process 3 times for a total of 4 strokes: (1 stroke = 1 aspiration and 1 dispense).

    Note: If gDNA uptake stalls due to high viscosity, it may be necessary to stir gently while slowly releasing the plunger to withdraw the gDNA.

49. Place standard 2.0 ml microfuge tube containing gDNA in rack of HulaMixer and rotate at room temperature for 1 hour at 15 rpm.

Note: During initial rotations, ensure that the gDNA gets drawn from the bottom of the microfuge tube to reside in the lid of the tube during rotations. If the DNA solution remains in the bottom of the tube during initial rotations, turn off HulaMixer and position rack so the microfuge tube is oriented upside down. Gently flick the bottom of the microfuge tube until the gDNA is drawn into the lid and resume mixing.

50. Remove microfuge tube from rack of HulaMixer and pulse spin tube on benchtop microcentrifuge for 2 seconds to bring the gDNA to the bottom of the tube. Allow the gDNA to equilibrate overnight at room temperature (25°C) to homogenize.

    Note: Most samples will become homogenous by the third day (from the start of the protocol), but samples may be labeled as soon as they become homogenous.

gDNA Quantitation (45 minutes)

Qubit Quantitation - BR dsDNA Assay

Refer to the Qubit dsDNA BR Assay Kit user manual for kit details and follow the methods described in the "Pipetting Viscous Genomic DNA" section, to ensure accurate pipetting of viscous gDNA.

1. Equilibrate Qubit BR Assay Kit Standards to room temperature.

   Note: If the gDNA has been stored at 4ºC, equilibrate at room temperature before moving to the next step.

2. Add Qubit BR Buffer to 0.5 ml Qubit Assay Tubes:
   a. For each sample, add 18 µl of Qubit BR Buffer to three separate Qubit Assay Tubes.
   b. For the Qubit Standards, add 10 µl Qubit BR Buffer to two separate Qubit Assay Tubes.
3. Using a 200 µl pipette with a wide bore tip, gently mix the entire gDNA sample volume by pipetting up and down 5 times, being careful not to generate bubbles.
4. Using a fresh standard bore pipette tip or positive displacement pipette tip for each draw:

   Remove 2 µl aliquots from the left side, middle, and right side of each sample and dispense into BR Buffer of corresponding Qubit Assay Tube, rinsing tip when dispensing. Place Assay Tubes in a floating rack and sonicate for 10 minutes. Perform Steps 5 and 6 during sonication.

   Note: If a bath sonicator is not available, vortex for at least 30 seconds at maximum speed, then pulse spin down briefly for 2 seconds.

5. Prepare Working Solution by diluting the Dye Assay Reagent into BR Dilution Buffer (1:200):
   a. 200 µl Working Solution for each of the two standards (400 µl total).
   b. 200 µl Working Solution for each sample aliquot (600 µl for each sample).
6. For the Qubit DNA standards, add 10 µl of Standards 1 and 2 to the Assay Tubes containing BR Buffer from Step 2b.
7. Once sonication is complete, retrieve assay tubes and pulse spin briefly. Vortex tubes for 5 seconds at maximum speed, then pulse spin again.

8. Add 180 µl of Working Solution to each sonicated DNA aliquot and Qubit DNA Standard aliquot. Vortex for 5 seconds, and pulse spin tubes.
9. Incubate samples for at least 2 minutes, then read on the Qubit Fluorometer.
10. Coefficient of Variation (CV = standard deviation/mean) from three readings should be < 0.30.

    Note: If CV > 0.30, gently pipette-mix the entire volume of gDNA with five strokes (1 stroke = 1 up stroke + 1 down stroke) using a wide bore tip. Let the gDNA rest at least overnight at room temperature before repeating quantitation.

    Note: Typical DNA concentrations range from 50-300 ng/µl. If concentration is > 150 ng/µl, refer to Important Notes of Bionano Prep Direct Label and Stain (DLS) Protocol (30206).

Sample ID	Left (ng/µl)	Middle (ng/µl)	Right (ng/µl)	Mean (ng/µl)	CV (stdev/mean)

Labeling

DNA is ready for Direct Label and Stain (DLS) labeling. See “Kits and Consumables” section at https://bionanogenomics.com/support/ for applicable kits and protocols.

Troubleshooting

The gDNA comes unbound from the Nanobind Disk.

Evidence: gDNA is aspirated or becomes detached from disk during binding or during washes.

Steps to follow if gDNA is aspirated:

1. Leaving the sample tube racked on the magnet, dispense gDNA-containing liquid back into tube containing disk.
2. Remove racked tube from magnet and invert rack multiple times by hand to re-establish binding.

Alternatively:

1. Leaving the sample tube racked on the magnet, dispense gDNA-containing liquid back into tube containing disk.
2. Aspirate liquid from tube such that a minimal volume (~50 µl) remains above unbound gDNA and discard supernatant leaving the DNA in a minimal volume at bottom of the tube.
3. Carefully aspirate unbound gDNA containing the minimal liquid into pipet tip and pipet directly onto racked disk on magnet to re-establish binding.

Steps to follow if gDNA is visually detached from the Nanobind Disk and not aspirated:

1. Remove the tube from the rack and hold horizontally.
2. Roll the tube between fingers until binding is re-established.

The gDNA is not homogeneous before labeling

Evidence: The gDNA quantitation CV of three measurements (top, middle and bottom) is > 0.30.

Steps to Follow:

1. Aspirate and dispense sample using a wide bore tip for a total of 5 times.
2. Incubate the gDNA at room temperature for 1 to 3 days.
3. After incubation, again aspirate and dispense the sample using a wide bore tip 5 times.
4. Quantitate with Qubit BR Assay.

The gDNA is not viscous

Evidence: Sample consistency is very thin and easily pipetted, but concentration is > 35 ng/µL.

The sample is likely not to have high molecular weight gDNA.

Check sample using pulse field gel electrophoresis before labeling to confirm presence of high molecular weight gDNA.

Evaluate sample prep method and input material quality/age and repeat DNA isolation from biological sample.

Frequently Asked Questions

What tissue types are compatible with this protocol?

- This protocol has been used to successfully process the following tissue types:
    - From Brown Norway Rat: liver, lung, kidney, colon, ovary, prostate, testes, and uterus.
    - From Human: bladder, lung, liver, kidney, colon, breast, prostate, brain, thyroid, and ovary.
    - From Mouse: spleen (2-3 mg input recommended)
- Skin, muscle, and non-vertebrate tissues are not yet fully supported.
- Normal tissue and tumor biopsies are recommended. This protocol has not been tested with fine needle aspirates.

What factors will influence gDNA quality?

- Storage and handling of tissues will influence gDNA quality. The following may negatively affect gDNA quality:
    - Tissues that have gone through a freeze thaw cycle after initial storage at -80C.
    - Frozen tissues exposed to room temperature for extended periods of time during cutting.
    - Necrotic tissue within the tissue sample.
    - Tissues with RIN (RNA Integrity Number) < 9.0.
- Too much starting material will lead to lower gDNA quality.

What factors will influence gDNA yield?

- Nuclei content relative to tissue mass will influence gDNA yield. Tissues that require a large tissue input weight due to low nuclei content may label poorly and have low throughput.

    Note: Tumor samples usually have higher gDNA yield per mg of tissue as compared to normal tissue.
- Tissues with high fat content may have low gDNA yield.

How many samples can be processed?

- This protocol can be used for batch sizes up to 8.
    - It will take up to 6 hours to process a batch of this size.
- Based on typical throughput on the Saphyr Instrument, data can be collected from at least 9 samples per week

What tissue preservatives are compatible with this protocol?

- While we have not currently tested preservatives for compatibility with this product, it is an area of ongoing research and we will update this section with new findings as they become available.

Appendix: Preparing Fresh Tissue or Tumor for Storage

Recommended input: 10 mg fresh tissue or tumor from lung, liver, kidney, uterus, ovary, colon, prostate, thyroid, testes, breast, and bladder. This protocol does not yet fully support muscle tissues.
Note: Tissue with low nuclei content relative to the tissue mass may not produce sufficient gDNA, and too much tissue may produce gDNA that is less pure and more difficult to become homogeneous.

1. Rinse tissue in ice-cold PBS and cut into smaller pieces (~10 mg per piece) on a sterilized ice-cold metal block.
    a. It is recommended to prepare multiple portions of each tissue.
2. Transfer tissue to a 1.5 ml tube with screw-cap, and snap freeze in liquid nitrogen for 3 minutes before transferring to -80ºC freezer for long term storage.
3. The frozen tissue is best used within 6 months storage at -80ºC.
4. If shipping frozen tissue, please follow the guidelines provided in Tissue and Tumor Shipping Instructions (30186).

Technical Assistance

For technical assistance, contact Bionano Genomics Technical Support.

You can retrieve documentation on Bionano products, SDS's, certificates of analysis, frequently asked questions, and other related documents from the Support website or by request through e-mail and telephone.

Type	Contact
Email	support@bionanogenomics.com
Phone	Hours of Operation: Monday through Friday, 9:00 a.m. to 5:00 p.m., PST US: +1 (858) 888-7663
Website	www.bionanogenomics.com/support

Bionano Genomics, Inc.
9540 Towne Centre Drive, Suite 100
San Diego, CA 92121

ADDENDUM N

Bionano Prep Direct Label and Stain (DLS) Protocol

Document Number: 30206

Document Revision: G

Table of Contents

Legal Notice

For Research Use Only. Not for use in diagnostic procedures.

Revision History

Revision	Notes
E	Decrease DTT in staining reaction
F	Include note indicating change in Staining Master Mix table. Update table formatting.
G	Update workflow diagram and user-supplied materials, modify membrane wetting step, edits to text for clarity.

Bionano Prep DLS Overview (750 ng)

DLS is a sequence-specific labeling of ultra-high molecular weight (UHMW) genomic DNA (gDNA) for Bionano Optical Genome Mapping (OGM) using a Direct Label Enzyme (e.g., DLE-1), followed by staining of the DNA backbone.

Workflow Overview – Label and Stain on Day 1; Quantify on Day 2, Load onto chip after quantification

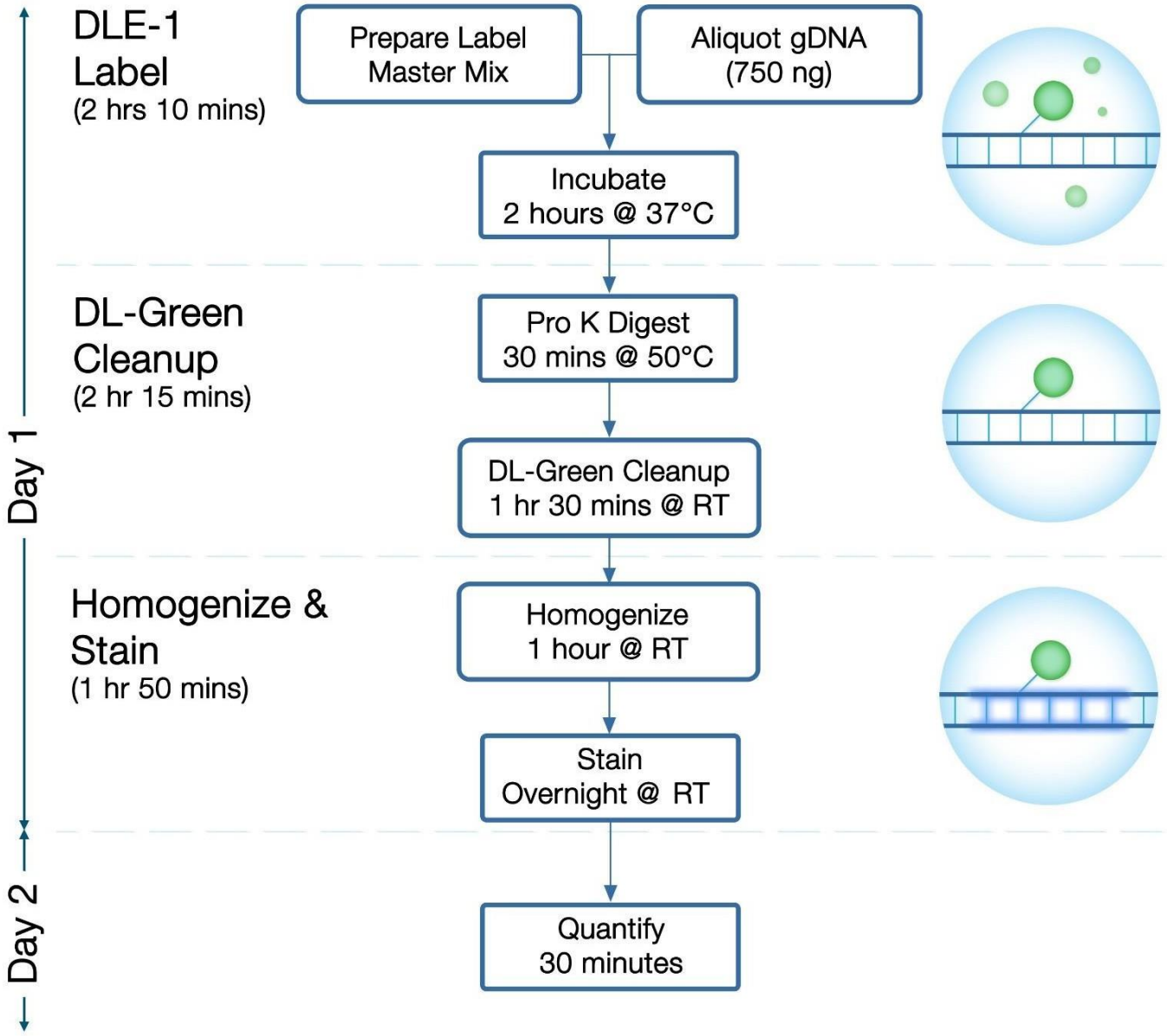

Note: Dashed lines (----------) denote potential pausing/stopping points.

Bionano Prep DLS Kit and User-Supplied Materials

Table 1: Bionano Prep DLS Kit Contents (Part # 80005)

Component	Part #	Amount	Storage	Handling Considerations
20x DLE-1	20351	18 µl	-20°C	Flick tube 3 times to mix, and centrifuge briefly. Keep in -20°C enzyme cooler until use.
20x DL-Green	20352	18 µl	-20°C	Thaw at room temperature (RT). Vortex and centrifuge briefly. Keep on pre-chilled aluminum block until use.
5x DLE-1 Buffer	20350	200 µl	-20°C	Thaw at room temperature. Vortex and centrifuge briefly. Keep at room temperature until use.
4x Flow Buffer	20353	190 µl	4°C	Vortex and centrifuge briefly. Keep at room temperature until use.
DNA Stain	20356	65 µl	-20°C	Thaw at room temperature. Vortex and centrifuge briefly. Keep at room temperature until use; DMSO in DNA Stain will crystalize on ice.
1M DTT	20354	75 µl	-20°C	
Ultra Pure Water	20355	900 µl	4°C	May keep at room temperature.
DLS 24 Well Plate	20357	1 plate	RT	Keep covered to avoid dust.
DLS Membranes (13 mm)	20358	25	RT	Avoid excess moisture.
DLS Plate Sealing Strips	20361	10	RT	
DLS Amber Tubes, Round Bottom	20362	12	RT	

Note: RT = 18 - 25°C

Table 2: User-Supplied Materials

Item	Description	Catalog #
HulaMixer Sample Mixer	Thermo Fisher	15920D
Thermocycler with heated lid	General lab supplier	
Puregene Proteinase K	Qiagen	158918 or 158920
PCR tubes, 0.2 ml, thin-walled, flat cap, nuclease-free	Thermo Fisher or equivalent	AM12225
Microcentrifuge tubes, 0.5 ml, Amber, nuclease-free	USA Scientific or equivalent	1605-0007
Pipet tips, unfiltered, 200 µl	USA Scientific or equivalent	1111-1810
Pipet tips, wide-bore, filtered, 200 µl	VWR or Rainin equivalent	46620-642
Pipet tips, standard, filtered; 2, 10, 20 and 200 µl	General lab supplier	
-20°C benchtop enzyme cooler	VWR or equivalent	414004-286
4°C aluminum cooling tube block	Sigma Aldrich or equivalent	Z740270
Forceps, pointed and curved	Electron Microscopy Sciences or	78141-01
Pipets (2, 10, 20 and 200 µl)	General lab supplier	
Ice bucket and Ice	General lab supplier	
Vortexer	General lab supplier	
Microcentrifuge for 0.2, 0.5, and 1.5 ml Tubes	General lab supplier	
Qubit Fluorometer	Thermo Fisher	Q33238
Qubit® Assay Tubes	Thermo Fisher	Q32856
Qubit® HS (High Sensitivity) dsDNA Assay Kit	Thermo Fisher	Q32851
Bath sonicator (recommended)	Branson or equivalent	CPX 952-119R
Positive-displacement pipet MR-10 (optional)	Rainin or equivalent	17008575
Pipet tips, 10 µl, C-10 for pos. displacement (optional)	Rainin or equivalent	17008604

Introduction and Important Notes

Introduction

This protocol describes an enzymatic labeling approach for direct fluorescent labeling of UHMW gDNA by the Direct Label Enzyme (DLE-1). The DLE-1 enzyme attaches the DL-Green fluorophore via covalent modification at a specific-sequence motif. This labeling process is non-damaging to the gDNA, allowing the generation of highly contiguous genome maps and providing high sensitivity to detection of structural variants. After sequence-specific labeling with DLE-1, the labeled DNA is stained for backbone visualization. When imaged on the Saphyr, the labeled samples are visualized as green dots on blue lines. The Bionano Prep Direct Label and Stain (DLS) kit (Catalog # 80005) provides the necessary reagents for this protocol.

DLE-1 Reaction Size (750 ng)

This protocol yields 60 µl of labeled DNA. This is sufficient to load on a single flowcell of a Saphyr Chip, with enough sample remaining for one additional flowcell in cases of low throughput or other failure. Starting material should be at least in the hundreds of kilobase in length; if necessary, this can be determined via pulsed-field gel electrophoresis (PFGE). Labeling metrics are determined on the Bionano Saphyr, measured in labels/100 kilobase pairs (kbp). Additional labeling metrics can be determined by supplying a reference and monitoring map rate, positive label variance (PLV), and negative label variance (NLV). See the “Important Notes” section below for additional details.

Details on expected metrics can be found in Document 30223, Saphyr Molecule Quality Report Guidelines.

Important Notes

General Considerations

- We recommend using an aluminum tube cooling block pre-chilled on ice to hold thawed reaction components and to assemble labeling reactions.
- Enzymes and buffers should be accurately pipetted out, with no droplets hanging on the outside of the pipet tip. The enzyme should be completely delivered into the reaction tube, and bubble formation should be carefully avoided to ensure reproducible reactions. This is best achieved by holding reagent tubes at eye level when aspirating or dispensing, to visualize the process.
- Slow and thorough pipet mixing of DLE-1 master mix with gDNA is a critical step and promotes DNA homogeneity and enzyme accessibility for efficient labeling of highly viscous DNA.
- This protocol involves the handling of light-sensitive fluorescent molecules. It is important to minimize the exposure to light of both the reactions and the light-sensitive reagents while working. Additionally, protect

from light the light-sensitive reagents during storage.

- Labeled DNA concentration is measured on Day 2, after labeling, cleanup, homogenization, and staining. DNA homogeneity is assessed by quantitating in duplicate (Coefficient of Variation (CV) < 0.30). Homogenous labeled DNA allows for an accurate estimate of concentration and more uniform loading of DNA onto the chip. The labeled DNA concentration should be between 4 and 12 ng/µl.

Batch Size

- Up to 12 samples can be processed at a time.
    - Each Bionano Prep DLS Kit contains reagents sufficient for 10 samples.

Requirements for Starting DNA

- The sample should contain megabase-length gDNA, typically determined by high viscosity and/or PFGE of the sample.
- gDNA concentration should be between 36 and 150 ng/µl.
    - gDNA samples > 150 ng/µl should be diluted with TE (pH 8.0) to 50 - 150 ng/µl, mixed 5 times with a wide-bore tip, and allowed to relax overnight at room temperature. Verify final DNA concentration and homogeneity before labeling.
    - For gDNA samples < 36 ng/µl, contact Technical Support at Support@bionanogenomics.com.

Determining Enzyme

- For non-human samples, before starting the DLS protocol, import the sequence data for your sample into either the In Silico Digestion feature of Bionano Access, or the standalone Label Density Calculator software, to ensure that DLS labeling is an appropriate choice for your sample. Your actual label density should be within ± 2 labels of predicted. Contact Technical Support at Support@bionanogenomics.com for guidance if uncertain.
- For non-human samples, current downstream analysis tools are most successful with genomes that have DLS label densities between 9 and 25 labels per 100 kbp.

Handling Genomic DNA

General:

- This protocol involves the handling of viscous genomic gDNA, which is difficult to pipet accurately. It is critical to follow all steps in this protocol carefully to ensure accurate sampling of DNA in order to achieve

proper enzyme-to-DNA and DNA-to-Stain ratio, and to minimize unnecessary handling of the gDNA, which can result in insufficiently long molecules for analysis.

Adding gDNA to Labeling Reaction:

- To ensure accurate sampling from the viscous gDNA stock, first maximize stock DNA homogeneity by gently pipet mixing the room temperature-equilibrated DNA solution with a wide-bore tip 5 times and follow guidelines below for proper pipetting into and out of a standard pipet tip, or positive displacement pipet tip, for complete delivery.

- Before drawing viscous gDNA into a standard tip, pipet an identical volume of water and mark the solution level on the tip with a fine tipped marker to serve as a guide when pipetting gDNA. Save the marked tip as the guide and use a new one for DNA retrieval. Alternatively, the use of a positive displacement pipet can improve consistency when pipetting viscous gDNA.

- To draw viscous gDNA into a standard tip, hold the stock DNA tube for close-up visualization, depress the pipet plunger until the first stop, submerge the pipet tip toward the middle of the viscous solution, and carefully release the plunger, as **slowly** as possible while moving the tip in a circular motion, to draw the viscous DNA into the tip while carefully monitoring DNA uptake. Keep the tip submerged even after the viscous DNA solution stops moving upward and levels off (use the marked tip as rough guide to see if viscous solution levels off at the appropriate level). Viscous DNA can take up to 30 seconds to fill the tip to the appropriate level. Releasing the plunger too quickly can produce a bubble in the tip, resulting in under-sampling (start over if this occurs). After the solution in the pipet tip has leveled off, and while the tip is still submerged in the DNA solution, scrape the tip against the bottom of the tube 5 times using a circular motion. Remove the tip from the DNA solution and visually inspect to confirm that it is filled to the appropriate level, by comparing to the marked tip. Removing the pipet tip from the gDNA solution too early, or improperly scraping the tip on the bottom of the tube, can produce a bubble at the end of the pipet tip, indicating under-sampling (start over if this happens). **Accurate pipetting of viscous gDNA is possible with practice and patience.**

- To deposit the entire volume of viscous gDNA into a tube or master mix, hold the reaction tube for close-up visualization and deliver the DNA by inserting the pipet tip in the solution and gently pressing the plunger until the first stop, then to the second stop, while monitoring DNA release, until the last bit of DNA has left the tip. Immediately remove the tip a3Ws soon as the last bit of DNA has left the pipet tip while maintaining a constant pressure to avoid uptake of fluid or introduction of air bubbles. Visually inspect the tip after removing from solution to confirm that it is empty.

Bionano DLS Labeling Protocol

Protocol Start, Day 1

See *Important Notes* section for proper handling of gDNA. gDNA concentration should be between 36 ng/µl and 150 ng/µl.

See *Kit Contents* and *User-Supplied Materials* sections for proper handling and storage of reagents.

Setup

1. Thaw 20x DL-Green. Vortex well and pulse spin. Hold on ice in 4°C aluminum block.
2. Thaw 5x DLE-1 Buffer. Vortex well and pulse spin. Hold at room temperature until use.
3. Flick 20x DLE-1 Enzyme three times and pulse spin. Hold on bench in -20°C enzyme block.
4. Remove Ultra Pure Water tube from 4°C (if necessary) and keep at room temperature.

DLE-1 Labeling (30 µl Reaction, 2 hours 10 minutes)

Dilute gDNA and Combine with Labeling Mix (10 minutes)

5. If gDNA quantitation has already been performed immediately prior to labeling, then proceed to Step 6. If not, pulse spin and then repeat quantitation prior to proceeding to Step 6.
6. In a thin wall PCR tube, add 750 ng gDNA (a) to Ultra Pure Water (b) to a total volume of 21 µl.
    a. 750 ng/ [gDNA concentration] = µl of gDNA
    b. 21 µl – (µl of gDNA) = µl of Ultra Pure Water.

	gDNA Concentration (ng/µl)	Volume of Ultra Pure Water (µl)	

7. If processing more than one sample, prepare a Labeling Master Mix in a 0.5 ml amber tube. Add the components in the order outlined in the table below. Pipet the entire volume of the Labeling Master Mix up and down with a standard pipet tip, five times, taking care not to generate bubbles. Pulse spin and keep in aluminum block on ice until use. Use within 30 minutes of mixing the components.

   Note: After making the master mix, leave 5x DLE-1 Buffer at room temperature to use in Step 12.

Labeling Master Mix Calculation Table

Labeling Reaction	1 Sample	# of Samples	Master Mix Excess	Master Mix Total
gDNA (750 ng) + Ultra Pure Water	21 µl			
5x DLE-1 Buffer	6.0 µl		× 1.2	µl
20x DL-Green	1.5 µl		× 1.2	µl
20x DLE-1	1.5 µl		× 1.2	µl
Final Reaction Volume	30 µl			µl

8. Using a standard pipet tip, add 9 µl Master Mix on top of the 21 µl gDNA + Ultra Pure Water, with no mixing. Then, using a new standard pipet tip, with pipet set to 28 µl, mix sample slowly up and down 5 times (1 up + 1 down = 1 time). Pulse-spin tube for 2 seconds. Protect from light.

   See the video titled DLS Master Mix Mixing under the DLS Labeling Kit section of the Support website.

   Note: A carefully and thoroughly mixed sample is necessary to efficiently label all molecules. Draw the sample from the bottom and dispense near the top (without touching pipette tip to the tube) to maximize the mixing.

Labeling (2 hours)

9. Incubate in a thermocycler using a heated lid set at 47°C (or "On" if no temperature choice is available):
   a. 2 hours at 37°C
   b. Hold at 4°C until next step. After removing from thermocycler, proceed quickly to the next step. Pulse spin briefly.

Proteinase K Digestion and DL-Green Cleanup (2 hours 15 minutes)

Proteinase K Digestion (35 minutes)

10. Dispense 5 µl Puregene Proteinase K (Qiagen) directly into the central bulk of the sample contained in the PCR tube. To avoid inadvertently removing DNA that may adhere to the tip, do not mix.

11. Incubate in a thermocycler using a heated lid set at 60°C (or "On" if no temperature choice is available):

a. 30 minutes at 50°C

b. Hold at 4°C until next step. After removing from thermocycler, proceed quickly to the next step. Pulse spin briefly.

Membrane Adsorption (1 hour, 40 minutes)

For Steps 12-18, please see the video titled DLS Membrane Demo under the DLS Labeling Kit section of the Support website.

12. For each sample, wet the underside of one DLS Membrane with 1x DLE-1 Buffer in the DLS 24 Well Plate:
    a. For each sample, prepare 60 µl of 1x DLE-1 Buffer (12 µl 5x DLE-1 Buffer + 48 µl Ultra Pure Water). Vortex to mix and pulse spin.
    b. Dispense 25 µl of 1x DLE-1 Buffer into the center of one well of the DLS 24 Well Plate.
    c. Use forceps to place a DLS Membrane on top of buffer.
    d. Seal wells immediately with a DLS Plate Sealing Strip to prevent evaporation. While holding the plate, apply pressure to secure the DLS Plate Sealing Strip to the top rim of the wells.
    e. Allow the membrane to fully wet for 10 minutes.

    Note: Membrane should change to a bluish color once fully wet. See around the 0:55 mark of the DLS Membrane Demo video. If membrane doesn't fully wet after 10 minutes, use a new membrane. Additional 1x DLE-1 buffer may need to be prepared for the new membrane.

13. Perform DL-Green cleanup by dispensing labeled DNA sample onto the center of the wetted membrane:
    a. Hold the plate securely and carefully remove the DLS Plate Sealing Strip. Using a standard pipet tip with the pipette set to 38 µl, aspirate the entire volume (~35 µl) of labeled DNA.
    b. Carefully dispense the labeled DNA onto the middle of the wetted DLS Membrane.
    c. Seal wells immediately with a DLS Plate Sealing Strip to prevent evaporation. While holding the plate, apply pressure to secure the DLS Plate Sealing Strip to the top rim of the wells.
    d. Protect the DLS 24 Well Plate from light (cover) and incubate at room temperature for 1 hour. Ensure that the plate stays undisturbed, with no inadvertent movement of the plate during incubation. ⚠
    e. 10 minutes before the incubation is complete, wet a second membrane in an unused well of the DLS 24 Well Plate, following steps 12b - 12e above.
    f. After 1 hour, hold the plate securely and carefully remove the DLS Plate Sealing Strip.
    g. Using an unfiltered standard pipette tip, with pipet set to 38 µl, slowly aspirate the entire labeled sample while making contact perpendicularly with the membrane and move the tip across the DNA area while aspirating to collect the DNA.

14. Repeat steps 13b - 13d, but dispense onto the second (unused) membrane prepared in Step 13e and incubate at room temperature for 30 minutes.

15. During the 30-minute incubation period, bring 1M DTT, 4x Flow Buffer, and DNA Stain to room temperature. Once thawed, vortex all tubes well, and pulse-spin briefly to collect contents. Keep all tubes at room

temperature until ready to use.

16. After 30 minutes, hold the plate securely and carefully remove the DLS Plate Sealing Strip.
17. Using an unfiltered standard pipette tip, with the pipet set to 35 µl, slowly aspirate the entire labeled sample while making contact perpendicularly with the membrane and move the tip across the DNA area while aspirating to collect the DNA. Transfer into a new PCR tube or 0.5 ml amber tube. Pulse spin for 2 seconds. Protect tubes from light. ⚠
18. Using a standard 200 µl pipette tip, aspirate 20 µl of the labeled sample from the PCR tube or 0.5 ml amber tube, and dispense into the bottom of the DLS Round Bottom Amber Tube (2 ml). Proceed to the next step (**DNA Staining and Homogenization**).
    a. If sample volume recovered is < 20 µl, bring the volume up to a total of 20 µl using 1x DLE-1 Buffer.

DNA Staining & Homogenization (1 hour 10 minutes)

Staining and Homogenization (1 hour, 10 minutes)

19. In a new 0.5 ml amber tube, prepare Staining Master Mix according to table below. Vortex to mix, then pulse-spin to collect contents.

Staining Master Mix Calculation Table

Staining Reaction	1 Sample	# of Samples	Master Mix Excess	Master Mix Total
Labeled Sample (Step 19)	20 µl			
4x Flow Buffer	15 µl		× 1.25	µl
1M DTT	6 µl		× 1.25	µl
DNA Stain	3.5 µl		× 1.25	µl
Ultra Pure Water	15.5 µl		× 1.25	µl
Total	**60 µl**			**µl**

Note: Flow Buffer is viscous, so pipet solutions containing it slowly to increase accuracy.

20. For each labeled DNA, add 40 µl Staining Master Mix on top of the labeled sample (20 µl) contained in the DLS Round Bottom Amber Tube (2 ml). Do not mix.

    Note: Master mix is dispensed on top of the labeled sample in order to avoid inadvertently drawing out DNA that may stick to the pipet tip.

21. Place DLS Round Bottom Amber Tubes containing samples into HulaMixer (Thermo Fisher) with speed set to 5 rpm. Tube holder surface should be flat and parallel to the work surface. Mix for 1 hour at room temperature with all options other than rotation turned off.

22. After 1 hour, remove samples from the HulaMixer. Pulse spin to collect contents.

    Note: Do not allow the rotation to proceed for longer than 1 hour, as this may decrease molecule N50.

23. Store overnight at room temperature, protected from light.

Protocol Start, Day 2

See list of User Supplied Consumables and Equipment to make sure they are all available.

Quantitation of Labeled and Stained DNA (30 minutes)

DNA Quantitation (30 minutes)

Determine the final concentration of the labeled and stained DNA. Best results will be obtained if the DNA concentration (average of two measurements) is between 4 and 12 ng/µl. Variation in the final concentration is due to the difficulties in accurately sampling the viscous starting gDNA and variation in gDNA recovery from DL-Green removal step. If your sample concentration does not fall within this range, see Troubleshooting section for recommendations.

Qubit dsDNA HS (High Sensitivity) Assay Kit & Qubit Fluorometer:

Note: The standard Qubit dsDNA HS Assay protocol will not provide accurate measurements of concentration due to the extremely long lengths of the labeled DNA. We have modified the Qubit protocol to include a sonication step to fragment an aliquot of the labeled DNA to ensure accurate concentration measurements. Refer to the Qubit dsDNA HS Assay Kit user manual for kit details.

1. Using a wide-bore tip on a 200 µl pipet set at 50 µl, mix labeled and stained DNA 5 times. Pulse-spin.
2. Let Qubit HS Standards and labeled DNA come to room temperature (at least 30 minutes).
3. Prepare 0.5 ml Qubit Assay Tubes:
    a. 2 separate Assay Tubes for the HS Standard measurement, each containing 10 µl of Qubit HS Buffer.
    b. 2 separate Assay Tubes per labeled sample, each containing 18 µl of Qubit HS Buffer.
4. Using a standard pipet tip or positive displacement pipet, remove two separate 2 µl aliquots from each sample and dispense into 18 µl HS Qubit buffer in Qubit Assay tube, rinsing tip. Place Qubit tubes in a floating rack and sonicate in a bath sonicator for 10 minutes. During sonication, prepare Working Solution as described below.

    Note: If a long string of DNA is attached to the tip when removing tip from tube, dispense sample back into tube and repeat aliquot removal with new tip.

    a. If a bath sonicator is not available, vortex for at least 30 seconds at maximum speed, then spin down briefly for 2 seconds.
5. Prepare Working Solution by diluting the Dye Assay Reagent into HS Dilution Buffer (1:200):
    a. Prepare 200 µl Working Solution for each of the two standards (400 µl total).
    b. Prepare 200 µl Working Solution for each sample aliquot (400 µl for each sample).
6. For the Qubit DNA standards, add 10 µl of Standards 1 and 2 to separate labeled Qubit Assay Tubes

containing 10 µl of Qubit HS Buffer from Step 3a.

7. Once sonication is complete, retrieve assay tubes and centrifuge briefly to collect solution at the bottom of the tubes. Vortex tubes for 5 seconds at maximum speed, then spin down tubes for 2 seconds.
8. Add 180 µl of Working Solution (prepared in step 5) to each tube of sonicated labeled DNA and Qubit DNA Standard plus HS Buffer. Vortex for 5 seconds, and centrifuge briefly to collect solution at the bottom of tubes.
9. Incubate samples in the dark for 2 minutes before quantitation on the Qubit Fluorometer.

   Note: The labeled DNA concentration should ideally fall between 4 - 12 ng/µl with a CV (standard deviation ÷ mean) between the samplings < 0.30. If both samplings are outside of 4 - 12 ng/µl, see **Troubleshooting** section below. If one sampling is between 4 - 12 ng/µl and the other is outside of this range, follow these guidelines:

   - If one sampling is between 4 - 12 ng/µl and the other is above 12 ng/µl, proceed to load chip.
   - If one sampling is between 4 - 12 ng/µl and the other is below 4 ng/µl, repeat HulaMixer mixing for 30 minutes and repeat the quantitation.

10. Record Qubit measurements in the table on the next page.
11. If you will not be running the samples on the same day, store in the dark at 4°C until use.

    Note: Labeled samples show no reduction in performance if used within one month.

gDNA Qubit Measurements

Sample ID	Measure 1 (ng/µl)	Measure 2 (ng/µl)	Average (ng/µl)	CV (stdev/mean)

Loading Bionano Chip (40 minutes; 30 minutes to bring chip to room temp and 10 minutes to load)

Refer to **Saphyr System User Guide** (for Saphyr P/N 60325 or 60239) for complete instructions on chip loading and instrument operation.

Note: When aspirating DLS-labeled sample for chip loading, draw from the middle of the tube.

Troubleshooting

Labeled sample should be stored at 4°C in a light-protected box when not in use. Labeled sample should be brought to room temperature prior to quantitation and/or chip loading.

Expected metrics based on internal experience at Bionano Genomics with human samples:

N50 (> 150 kbp)	Labels/ 100 kbp	Map Rate	Positive Label Variance	Negative Label Variance
> 230 kbp	14 - 17	> 70%	< 10%	< 15%

A. The gDNA is not homogeneous before labeling

Evidence: CV of the quantitation measurements does not meet requirements of the DNA isolation protocol (e.g., CV > 0.30 between left, middle, and right measurements in the SP protocols).

Steps to Follow:

1. Aspirate and dispense the sample slowly using a wide-bore tip 5 times.
2. Incubate the gDNA at room temperature for 1 to 3 days.
3. Aspirate and dispense the sample slowly using a wide-bore tip 5 times.
4. Quantitate with Qubit Broad Range Assay.

B. The gDNA is not viscous

Evidence: Sample consistency is very thin (non-viscous) and easily pipetted, but concentration is > 35 ng/µl.

It is likely that the sample does not contain high molecular weight gDNA.

Evaluate size of starting gDNA by pulsed-field gel electrophoresis (PFGE) before labeling.

Evaluate sample prep method and input material quality and age, and repeat DNA isolation from biological sample.

C. The gDNA concentration is < 36 ng/µl

Evidence: The concentration of gDNA measured at the end of the DNA isolation protocol is less than 36 ng/µl.

Contact Bionano Genomics Support at Support@bionanogenomics.com

D. The labeled sample is too viscous

Evidence: The sample takes an abnormally long time (greater than 30 seconds) to fill the fingers of the chip.

Contact Bionano Genomics Support at Support@bionanogenomics.com.

E. Label density is lower than expected

Evidence: The average detected label density will always be lower than the expected average site density. This is due to a combination of site clustering, DNA stretch, and optical resolution. For example, the average site density for DLE-1 in humans is 20.7 labels per 100 kbp, but the detected label density can vary from just above 14 to just below 17 labels per 100 kbp.

Low label density can be the result of suboptimal enzymatic labeling, photobleaching of fluorophores, or detection issues.

Potential causes of low label density during the protocol:

- Inhibitory substances in the DNA prep.
- Inadequate mixing of viscous gDNA and master mix.
- Mishandling of DLE-1 (exposure to elevated temperature, vortexing, etc.).
- Exposure of labeling reaction to light and photobleaching DL-Green.
- Prolonged exposure of DL-Green to the pH of the master mix (> 30 min).
- Hardware issue.

F. Labeled DNA is < 4 ng/µl for both measurements

Evidence: Both measurements are outside the concentration range of 4 -12 ng/µl using the Qubit High Sensitivity Assay Kit.

Steps to Follow:

1. Repeat quantitation of the starting DNA stock.
2. If the sample is 3 - 4 ng/µl, proceed to load at your own risk, but expected throughput will likely not be reached.
3. If the sample is < 3 ng/µl do not load. Check starting DNA concentration and repeat the labeling assay.

G. Labeled DNA is > 12 ng/µl for both measurements

Evidence: Both measurements are outside the concentration range of 4 -12 ng/µl using the Qubit High Sensitivity Assay Kit.

Steps to Follow:

1. If the sample is > 12 ng/µl, contact Bionano Customer Support (Support@bionanogenomics.com) for guidance.
2. You can proceed to load at your own risk, but the labeled sample may clog the chip and have reduced molecule N50.

H. The N50 (≥ 150 kbp) is less than 230 kbp, or the N50 (≥ 20 kbp) is less than 150 kbp

Evidence: The dashboard N50 metrics and Bionano Access Molecule Quality Report (MQR) results do not reach

the specifications listed above.

Steps to Follow:

1. Evaluate size of starting gDNA by pulsed-field gel electrophoresis (PFGE).
2. Evaluate sample prep method if there is no high molecular weight (megabase) gDNA present.
3. If starting gDNA size is large, relabel gDNA, making sure to avoid excessive pipetting or pipetting at high velocity.
4. Contact Bionano Customer Support (Support@bionanogenomics.com) for guidance as to whether you should rerun the sample on a different chip.

I. Map rate is low (human samples)

Evidence: The Bionano Access MQR map rate is < 70%

Steps to Follow:

1. Is the label density low (< 14 labels per 100 kbp)?
    a. If so, repeat quantitation of starting gDNA stock and repeat labeling after considering potential causes listed in Section D.
2. If the label density is within 14 – 17 labels per 100 kbp across all scans, contact Support.
3. Check N50 (≥ 20 kbp) value in the MQR. If this value is low (e.g., less than 100 kbp), it can cause issues with map rate

J. Effective throughput is less than 10 Gbp per scan

Evidence: The throughput after Scan 7 is still less than 10 Gbp per scan in the ICS or Access dashboard.

Steps to Follow:

1. Repeat quantitation of labeled sample.
2. Ensure flowcell is properly hydrated with nuclease-free water.

Potential Causes:

- Low N50 (≥ 20 kbp) and/or low N50 (≥ 150 kbp).
- Evaporation causing an increase in salt concentration, thus changing DNA migration.
    a. Were the Inlet and Outlet wells topped off (rehydrated) with nuclease-free water before placing chip plugs/clips?
- Non-homogenous DNA.
- DNA outside of the 4-12 ng/µl range.

Frequently Asked Questions

1. How far in advance can the membranes be wetted on the plate?

We recommend 10 minutes before adding sample to the membrane. It is possible to wet both membranes at the same time (10 minutes before first membrane use), but this is entirely dependent on the user's ability to create a tight seal with the sealing strip to prevent evaporation. Keep sealing strip on unless applying sample.

2. How long can labeling reaction sit at 4°C hold step?

Overnight, as long as it is protected from light.

3. How long can sample sit at 4°C after Pro K?

Overnight, as long as it is protected from light.

4. What is the impact of a DNA sample concentration being out of range?

We have not had problems loading samples with DNA concentration as high as 12 ng/ul, though samples above 12 ng/ul may clog the chip if homogeneity is poor, or may not be stained properly. In contrast we have found that samples with DNA concentration < 4 ng/ul may not collect enough data for effective throughput.

5. How long is the sample good for?

While we have found that stained DNA samples at optimal conditions can sit at 4°C protected from light for up to one month without degradation of sample metrics, we suggest running the samples within a week to reduce likelihood of sample quality issues that can develop over time.

6. The green background in DLS-labeled samples is higher than in NLRS-labeled samples. Is that a problem?

The leftover DL-Green often will show higher background in the images taken on the Saphyr than what is seen in NLRS-labeled samples. This is normal, and the membrane cleanup steps remove enough DL-Green to not impact data metrics. Positive label variance (PLV) from extra fluorophores occurs randomly and is not a problem if within expected metrics.

Technical Assistance

For technical assistance, contact Bionano Genomics Technical Support.

You can retrieve documentation on Bionano products, SDSs, certificates of analysis, frequently asked questions, and other related documents from the Support website or by request through e-mail and telephone.

Type	Contact
Email	support@bionanogenomics.com
Phone	Hours of Operation: Monday through Friday, 9:00 a.m. to 5:00 p.m., Pacific Time US: +1 (858) 888-7663
Website	www.bionanogenomics.com/support

Bionano Genomics, Inc.
9540 Towne Centre Drive, Suite 100
San Diego, CA 92121